UNIVERSIDADE FEDERAL DE MINAS GERAIS
FACULDADE DE FARMÁCIA
PROGRAMA DE PÓS-GRADUAÇÃO EM CIÊNCIAS FARMACÊUTICAS

LIZIANE OLIVEIRA FONSECA MONTEIRO

ENCAPSULAÇÃO DO PACLITAXEL EM LIPOSSOMAS RECOBERTOS COM FOLATO AUMENTA A CAPTAÇÃO CELULAR E O EFEITO ANTITUMORAL EM MODELO EXPERIMENTAL DE TUMOR DE MAMA

Belo Horizonte - MG
2018

LIZIANE OLIVEIRA FONSECA MONTEIRO

ENCAPSULAÇÃO DO PACLITAXEL EM LIPOSSOMAS RECOBERTOS COM FOLATO AUMENTA A CAPTAÇÃO CELULAR E O EFEITO ANTITUMORAL EM MODELO EXPERIMENTAL DE TUMOR DE MAMA

Tese apresentada ao Programa de Pós-Graduação em Ciências Farmacêuticas da Faculdade de Farmácia da Universidade Federal de Minas Gerais, como requisito parcial à obtenção do grau de Doutora em Ciências Farmacêuticas

Orientadora: Profa. Elaine Amaral Leite

Coorientadores: Prof. André Luis Branco de Barros

Profa. Mônica Cristina de Oliveira

Belo Horizonte - MG
2018

COLABORADORES

- Prof. Ângelo Malaquias - Departamento de Física, Instituto de Ciências Exatas, UFMG
- Prof. Adriano de P. Sabino - Departamento de Análises Clínicas, Faculdade de Farmácia, UFMG
- Prof. Geovanni Dantas Cassali – Departamento de Patologia Geral, Instituto de Ciências Biológicas, UFMG.
- Prof. Rogério Magalhães-Paniago - Departamento de Física, Instituto de Ciências Exatas, UFMG
- Prof. Valbert N. Cardoso - Departamento de Análises Clínicas, Faculdade de Farmácia, UFMG
- Prof. Vanessa Mosqueira - Laboratório de Desenvolvimento Galênico e Nanotecnologia, UFOP.
- Dra. Gwenaelle Pound-Lana - Laboratório de Desenvolvimento Galênico e Nanotecnologia, UFOP.
- MSc. Caroline Mari Oda – Programa de Pós-Graduação em Ciências Farmacêuticas, Faculdade de Farmácia, UFMG.
- MSc. Diego Carlos dos Reis - Departamento de Patologia Geral, Instituto de Ciências Biológicas, UFMG.
- MSc. Fernanda C. G. Evangelista - Programa de Pós-Graduação em Ciências Farmacêuticas, Faculdade de Farmácia, UFMG.
- MSc. Cristina Loures - Programa de Pós-Graduação em Ciências Farmacêuticas, Faculdade de Farmácia, UFMG.
- MSc. Renata S. Fernandes - Programa de Pós-Graduação em Ciências Farmacêuticas, Faculdade de Farmácia, UFMG.
- Luciano Cecílio de Castro – Faculdade de Fármacia, UFMG.

UNIVERSIDADE FEDERAL DE MINAS GERAIS

PROGRAMA DE PÓS-GRADUAÇÃO EM CIÊNCIAS FARMACÊUTICAS

FOLHA DE APROVAÇÃO

ENCAPSULAÇÃO DO PACLITAXEL EM LIPOSSOMAS RECOBERTOS COM FOLATO AUMENTA A CAPTAÇÃO CELULAR E O EFEITO ANTITUMORAL EM MODELO EXPERIMENTAL DE TUMOR DE MAMA

LIZIANE OLIVEIRA FONSECA MONTEIRO

Tese submetida à Banca Examinadora designada pelo Colegiado do Programa de Pós-Graduação em CIÊNCIAS FARMACÊUTICAS, como requisito para obtenção do grau de Doutora em CIÊNCIAS FARMACÊUTICAS, área de concentração CIÊNCIAS FARMACÊUTICAS.

Aprovada em 30 de outubro de 2018, pela banca constituída pelos membros:

Profa. Elaine Amaral Leite - Orientadora
UFMG

Prof. Ricardo Bentes de Azevedo
UnB

Prof. Helder Ferreira Teixeira
UFRGS

Profa. Marta Marques Gontijo de Aguiar
UFMG

Prof. Diego dos Santos Ferreira
UFMG

Prof. André Luís Branco de Barros - Coorientador
UFMG

Profa. Mônica Cristina de Oliveira - Coorientadora
UFMG

Belo Horizonte, 30 de outubro de 2018.

AGRADECIMENTOS

À Deus, por todas as bênçãos e por conceder força e persistência para concretizar esse trabalho.

Aos meus pais, Tânia e Alan, pelo exemplo, apoio e amor incondicional. Pelo incentivo de todos os dias, pelas orações e pela paciência, indispensáveis para a conclusão desse trabalho. É maravilhoso ter vocês comigo.

Ao meu irmão Lucas, pelo amor e parceria de sempre.

Ao meu marido Ricardo, por toda paciência e companheirismo ao longo dessa caminhada. Você foi essencial nessa conquista! Obrigada por todo apoio e por estar comigo em TODOS os momentos. Só tenho a agradecer por ser você, com toda sua dedicação em me fazer feliz, por cuidar sempre de mim e por me amar!

À Professora Elaine, mais uma vez, toda minha gratidão por ter confiado em mim a execução desse trabalho, apesar de todos obstáculos existentes. Agradeço por toda orientação, ensinamentos, disponibilidade e amizade oferecida ao longo desses anos! Só tenho a agradecer a Deus por colocar você no meu caminho, um exemplo de dedicação, profissionalismo e competência.

Ao Professor André, pela ajuda indispensável com os experimentos e pela eterna disponibilidade, além da competência e de toda dedicação em extrair o máximo de nós. Agradeço pela confiança e também por toda amizade e boas risadas.

À Professora Mônica, por ter me recebido com muito carinho em sua equipe, por compartilhar seu conhecimento, pela confiança transmitida e pelas palavras de conforto quando mais precisamos.

Ao Professor Lucas, pelo incentivo e amizade.

Ao Professor Ângelo Malaquias do Departamento de Física – UFMG, pela disponibilidade e disposição em ajudar nas análises dos estudos de SAXS.

À Prof. Vanessa Mosqueira e Dra. Gwenaelle Pound-Lana pela colaboração com os experimentos de caracterização físico-química.

Ao Prof. Adriano de Paula Sabino e a Msc. Fernanda Cristina Gontijo Evangelista pela colaboração nos experimentos de citometria de fluxo.

Ao Prof. Geovanni Dantas Cassali e ao Dr Diego Carlos dos Reis pela colaboração com as análises histomorfometricas e imunohistoquimicas.

Ao Luciano, pela disponibilidade e ajuda no laboratório.

Ao José Batista e Adelaide, pela simpatia e disponibilidade.

Aos amigos do LTF pelos bons momentos compartilhados dentro e fora do laboratório.

Às meninas, Ju, Renata e Pequena por toda amizade e companheirismo, pelas risadas, almoços, festas e viagens, fazendo tudo ficar mais divertido! E por toda ajuda com os experimentos, é claro!

À Aina, por toda amizade e pelos ótimos momentos compartilhados, principalmente os longos cafés no shopping que deixavam meu dia melhor.

À Carol, agradeço por todo companheirismo e amizade. Obrigada, a você e ao Fa, por estarem sempre disponíveis, com todo carinho do mundo, em me receber sempre que precisei. Você foi essencial nessa conquista, uma grande amiga que o mestrado/doutorado me deu.

Aos meus familiares, em especial, meus avós, por todas as orações e carinho.

Aos amigos queridos, que tornaram todos os momentos mais fáceis e leves.

À FAPEMIG, CAPES, CNPQ e LNLS pelo apoio financeiro.

RESUMO

O paclitaxel (PTX) é um fármaco utilizado no tratamento do câncer de mama, contudo, seu uso é limitado devido a sua baixa solubilidade aquosa e aos efeitos tóxicos apresentados pelas formulações comercialmente disponíveis. A fim de contornar esses problemas, lipossomas pH-sensíveis, recobertos com polietilenoglicol (PEG) e funcionalizados com folato contendo PTX (LpHS-folato-PTX) foram desenvolvidos por nosso grupo e caracterizados do ponto de vista físico-químico e avaliados em relação ao comportamento biológico *in vitro* e *in vivo* frente a linhagem tumoral MDA-MB-231(mama humano). Estudos de SAXS em condições de alta hidratação evidenciaram alterações na organização supramolecular das moléculas de dioleoifosfatidiletanolamina (DOPE) após a inclusão da PTX na bicamada lipídica, sem mudanças significativas na pH-sensibilidade do sistema. Análises morfológicas e físico-químicas demonstraram um sistema lipossomal com tamanho nanométrico com características adequadas para uso intravenoso. Elevada captação no fígado, baço e rins, em camundongos Balb/C sadios bem como uma captação tumoral maior que o músculo contralateral em animais Balb/C nude portadores de tumor MDA-MB-231 em todos os tempos avaliados foi observada nos estudos de biodistribuição, sendo a relação tumor-músculo maior para o grupo tratado LpHS-folato-PTX. A análise *in vitro* de captação celular demonstrou a superioridade do sistema LpHS-folato-PTX na entrega celular de PTX, o que culminou em maior citotoxicidade contra células MDA-MB-231, sendo apoptose a principal via de morte celular. Na avaliação do ciclo celular, um aumento expressivo de células em G0/G1 foi observado após o tratamento com LpHS-folato-PTX comparado ao PTX disperso em Cremophor EL® e etanol (PTX:Cr+Et) e LpHS-PTX, onde a maior parte das células encontravam-se em G2/M. O tratamento *in vivo* com LpHS-folato-PTX reduziu o crescimento tumoral e a captação do radiofármaco ^{99m}Tc-BNN em comparação aos tratamentos com PTX:Cr+Et e lipossomas pH-sensíveis, recobertos com PEG contendo PTX (LpHS-PTX). Análises histomorfométricas demonstraram aumento nas áreas de necrose e inflamação nos tumores dos animais tratados com LpHS-folato-PTX. Redução significativa na contagem de células proliferativas e aumento na porcentagem de células apoptóticas foi observada na avaliação imunohistoquímica para esse mesmo grupo. Em conjunto, os resultados do presente estudo demonstraram a maior eficácia da formulação LpHS-folato-PTX, tornando-a uma alternativa potencial no tratamento de tumor de mama.

Palavras-chave: Câncer. Paclitaxel. Lipossomas. pH-sensibilidade. Folato. Biodistribuição. Apoptose. Atividade antitumoral. MDA-MB-231.

ABSTRACT

Paclitaxel (PTX) is an effective chemotherapeutic agent widely used in breast cancer treatment. Nevertheless, the low solubility of the drug and the side effects of commercialformulations available limit their clinic use. In other to overcome this drawback, PTX-loaded folate-coated long circulating and pH-sensitive liposomes (SpHL-folate-PTX) were developed by our group. Then, in this study, the physicochemical characterization and *in vitro* and *in vivo* biological behavior of this formulation against tumor line MDA-MB-231 (human breast) were evaluated. SAXS studies under high hydration conditions evidenced that the PTX inclusion in the lipidic bilayer leads to shifts in the supramolecular organization of the dioleylphosphatidylethanolamine (DOPE) molecules, however, it did not affect the pH-sensitivity of the liposomal formulation. The morphological and physicochemical analysis of the system demonstrated a nanometric dispersion suitable for intravenous administration. Biodistribution studies showed high uptake in liver, spleen, and kidneys, as a greater tumor uptake compared to contralateral muscle in all timeframes with a higher tumor-muscle ratio observed for the group treated with SpHL-folate-PTX. Cellular uptake assay, *in vitro,* showed a higher delivery of PTX into the cells by SpHLF-PTX which leads to a superior cytotoxicity whit apoptosis process the main cell death pathway. The cell cycle evaluation showed an expressive increase of cells with a stop at G0/G1 phase after treatment SpHL-folate-PTX when compared to PTX prepared in Cremophor and ethanol (PTX:Cr+Et) and SpHL-PTX, that present the most of cells at G2/M phase. Antitumor activity *in vivo* showed a significant reduction in the tumor growth and a lower uptake by ^{99m}Tc-BBN in scintigraphic images for SpHL-folate-PTX group compared to PTX:Cr+Et e SpHL-PTX, which suggest a higher efficacy of this formulation. Histomorphometric analyzes demonstrated an increase in the necrosis and inflammation areas in the animals treated with SpHL-folate-PTX. A decreasing in the proliferative cells and a higher percentage of apoptotic cells were observed by immunohistochemical analyses after the treatment with SpHL-folate-PTX. Therefore, the presented data confirmed the potential of SpHL-folate-PTX as an alternative antitumor therapy, especially for breast cancer.

Key-words: Cancer. Paclitaxel. Liposomes. pH-sensitivity. Folate. Biodistribution. Apoptosis. Antitumor activity. MDA-MB-231.

LISTA DE FIGURAS

REVISÃO BIBLIOGRÁFICA

<u>ARTIGO 1 - Paclitaxel-loaded pH-sensitive liposome: new insights on structural and physicochemical characterization</u>

LISTA DE TABELAS

REVISÃO BIBLIOGRÁFICA

ARTIGO 1 - Paclitaxel-loaded pH-sensitive liposome: new insights on structural and physicochemical characterization

ARTIGO 2 - Paclitaxel-loaded folate-coated long circulating and pH-sensitive liposomes as a potential drug delivery system: a biodistrution study

ARTIGO 3 - Paclitaxel-loaded folate-coated pH-sensitive liposomes enhance cellular uptake and antitumor activity

LISTA DE ABREVIATURAS E SIGLAS

CHEMS	Hemisuccinato de Colesterila
CR+Et	Cremophor EL® + etanol
DLS	Espalhamento dinâmico da luz
DOPE	Dioleoifosfatidiletanolamina
DP	Desvio Padrão
DSC	Calorimetria Exploratória Diferencial
DSPE-PEG_{2000}	Diestearoilfosfatidiletanolamina acoplado ao polietilenoglicol 2000
DSPE-PEG_{2000}-DTPA	Diestearoilfosfatidiletanolamina acoplado ao polietilenoglicol 2000 e ao ácido dietilenotriaminopentacético
DSPE-PEG_{2000}-folato	Diestearoilfosfatidiletanolamina acoplado ao polietilenoglicol e folato
EPR	Enhanced Permeability Retention
H_{II}	Hexagonal invertida
HER2	Receptor tipo 2 do fator de crescimento epidérmico humano
HFS	Solução fluorocrômica hipotônica
IC50	50% de inibição da viabilidade celular
IP	Iodeto de propídeo
IP	Índice de polidispersão
LpHS	Lipossomas pH-sensíveis de circulação prolongada
LpHS-PTX	Lipossoma pH-sensível de circulação prolongada carreando o paclitaxel
LpHS-folato	Lipossomas pH-sensíveis de circulação prolongada funcionalizados com folato
LpHS-folato-PTX	Lipossoma pH-sensível de circulação prolongada funcionalizada com folato carreando o paclitaxel
LUV	Vesículas unilamelares grandes
MET	Microscopia Eletrônica de Transmissão
MLV	Vesículas multilamelares
NaCl	Cloreto de Sódio
NaOH	Hidróxido de sódio
PE	Fosfatidiletanolamina
PTX	Paclitaxel
RE	Receptores de estrógeno
RF	Receptores para folato
RP	Receptores de progesterona
SAXS	Espalhamento de raios-X a baixo ângulo
SFM	Sistema fagocitário mononuclear
SRB	Sulforodmanina B
SUV	Vesículas unilamelares pequenas
^{99m}Tc	Tecnécio-99-metaestável
TNBC	Câncer de mama triplo negativo

SUMÁRIO

INTRODUÇÃO

1. INTRODUÇÃO

Atualmente, o câncer é um problema de saúde pública mundial, devido a sua alta prevalência e elevada mortalidade. A identificação de novas estratégias para prevenir e tratar essa grave doença é de extrema importância (SIEGEL, MILLER, JEMAL, 2016). Os tumores de mama figuram entre os tumores malignos mais comuns em pacientes do sexo feminino. Estima-se, a ocorrência de cerca de 1,3 milhões de casos de câncer de mama anualmente, sendo este responsável por cerca de 15% de todas as mortes relacionadas ao câncer. No Brasil, o câncer de mama é o tipo mais incidente em mulheres com estimativa de aproximadamente 60 mil casos em 2018 (SHAJAHAN-HAQ, CHEEMA, CLARKE, 2015; INCA, 2018). Dentre os diversos subtipos de câncer de mama, pode-se destacar o câncer de mama triplo negativo (TNBC) que consiste em tumores mamários caracterizados por ensaios imuno-histoquímicos negativos para receptores de estrógeno (RE), receptores de progesterona (RP) e receptores tipo 2 do fator de crescimento epidérmico humano (HER2) (PRAT *et al.*, 2013; TURNER, REIS-FILHO, 2013; JIAO *et al.*, 2014; TONG *et al.*, 2018).

Embora a quimioterapia seja a principal alternativa terapêutica, a utilização de agentes antitumorais no tratamento do TNBC é ainda um desafio devido à dificuldade de se estabelecer alvos terapêuticos específicos. Dentre os antitumorais mais usados, podemos destacar o paclitaxel (PTX). Esse fármaco apresenta elevada atividade, no entanto, as principais formulações utilizadas na clínica, Taxol® (dispersão micelar de PTX) e Abraxane® (nanopartículas de albumina contendo PTX) apresentam diversos efeitos tóxicos como reações de hipersensibilidade, neuropatia periférica, mielossupressão, alterações cardíacas, mucosite, estomatite, alterações gastrointestinais, náuseas e alopecia (HOYER, 2000; DONYAI, SEWELL, 2006; SURAPANENI, DAS, DAS, 2012; ZHANG *et al.*, 2014; BARBOSA *et al.*, 2015; MONTEIRO *et al.*, 2016; WOZNIAK *et al.*, 2016, MONTEIRO *et al.*, 2018a).

Recentemente, nosso grupo desenvolveu uma formulação lipossomal pH-sensível de circulação prolongada funcionalizada com folato carreando o PTX (LpHSF-PTX) a qual demonstrou ganhos importantes em termos de estabilidade e citotoxicidade *in vitro* em linhagens celulares de câncer de mama (BARBOSA *et al.*, 2015). No intuito de verificar o potencial terapêutico desse novo sistema no tratamento de câncer de mama, estudos físico-químicos e biológicos (*in vitro* e *in vivo)* em modelos experimentais de tumor de mama TNBC foram realizados no presente estudo.

Nesse contexto, a presente tese encontra-se dividida em duas partes: a primeira apresenta uma revisão da literatura com a fundamentação teórica do trabalho e a segunda parte da tese, subdividida em três etapas, descreve o trabalho experimental desenvolvido, com métodos e resultados detalhadamente apresentados.

REVISÃO DE LITERATURA

2. REVISÃO DE LITERATURA

2.1 Câncer

O câncer é uma doença caracterizada pelo crescimento e proliferação descontrolado de células transformadas devido a alterações de seu DNA (PAUWELS *et al.*, 1998; ALMEIDA *et al*., 2005; SAFARZADEH, SHOTORBANI, BARADARAN, 2014). Os processos de crescimento e diferenciação são essenciais para a formação e recomposição dos tecidos com diversas funções específicas e vitais para os seres vivos. Eles são regulados por um ciclo celular complexo com diversos mecanismos intrínsecos regulatórios em pontos estratégicos do processo, que permitem verificar a viabilidade de continuar ou bloquear o ciclo. Diante disso, defeitos nesse sistema de checagem são a principal causa de instabilidade genômica, configurando uma situação crítica para o desenvolvimento do câncer (KENNY, ABOAGYE, PRICE, 2004; ROBBINS, COTRAN, 2005; BRASILEIRO-FILHO, 2006; PFLAUM, SCHLOSSER, MULLER, 2014; MINCHOM, AVERSA, LOPEZ, 2018). Dentre as principais mutações relacionadas ao aparecimento de câncer pode-se destacar as alterações no oncogene *ras*, que culminam na produção excessiva de proteínas envolvidas em vias sinalizadoras do crescimento celular. Além disso, mutações no gene supressor p53, também são importantes uma vez que impedem a síntese de proteínas de reparo do DNA e indutoras de apoptose, permitindo a proliferação descontrolada de células malignas (PAUWELS *et al.*, 1998; PRIOR, LEWIS, MATTOS, 2012; PFLAUM, SCHLOSSER, MULLER, 2014; UEHARA, TANAKA, 2018).

Desta forma, o processo de carcinogênese é um acontecimento multifatorial, caracterizado por três estágios principais, os quais conduzem à transformação progressiva de células saudáveis em células malignas. O primeiro estágio da doença é o processo de iniciação, no qual as células sofrem o efeito de um agente carcinogênico e passam a apresentar alterações genéticas, contudo, o tumor ainda não é detectável clinicamente. No estágio de promoção, as células geneticamente alteradas pela ação de oncopromotores transformam-se em células malignas. Finalmente, o processo de progressão é caracterizado pela multiplicação celular descontrolada com surgimento das primeiras manifestações clínicas da doença (ALMEIDA *et al.*, 2005; HLATKY, HAHNFELDT, 2014). Nesse contexto, características importantes das células tumorais podem ser destacadas, tais como a insensibilidade a sinais inibitórios de crescimento, a evasão à morte celular programada (apoptose), o potencial ilimitado de replicação, a

angiogênese sustentada, a invasão tecidual e a metástase (HANAHAN, WEINBERG, 2011; JENA, 2012; SAFARZADEH, SHOTORBANI, BARADARAN, 2014; FOUAD, AANEI, 2017).

2.2 Câncer de mama

Dentre os diversos tipos de tumores sólidos, o câncer de mama figura como um dos tumores malignos mais comuns em pacientes do sexo feminino em todo o mundo. A progressão da idade, pré-disposição genética (cerca de 25% dos pacientes com câncer de mama têm uma história familiar positiva) e fatores ambientais são fatores associados ao risco aumentado de desenvolvimento do câncer de mama (SHAH, ROSSO, NATHANSON, 2014; TONG *et al*., 2018). O desenvolvimento e a progressão da doença estão ligados ao acúmulo de diversas alterações genéticas nas células epiteliais do tecido mamário e à presença de um microambiente favorável para a proliferação, a invasão e, até mesmo, a metastização das células neoplásicas (ANDÒ *et al*, 2014; GOUBRAN *et al*, 2014; FOUAD, AANEI, 2017).

O câncer de mama é uma doença heterogênea com múltiplos subtipos identificados, os quais apresentam diferentes características morfológicas, celulares e moleculares bem como diferentes comportamentos clínicos, resposta terapêutica e evolução (SHAJAHAN-HAQ, CHEEMA, CLARKE, 2015; TOMAO *et al*., 2015; ZHANG *et al.*, 2015). Baseado em análise da expressão gênica global dos tumores, estudos recentes têm fornecido dados para a classificação do câncer de mama em subtipos distintos permitindo determinar tratamentos quimioterápicos mais específicos para cada modalidade de carcinoma mamário (YERSAL e BARUTCA, 2014; TELES, MORALLES, COMINETTI, 2018).

Os tumores de mama podem ser divididos em receptores de estrogênio (RE) positivos e negativos. Cerca de 75% desses tumores são classificados com RE positivos, que podem ser divididos em subtipos Luminal A e Luminal B, que, em geral, também são positivos para receptores de progesterona (RP) e não apresentam superexpressão do receptor tipo 2 do fator de crescimento epidérmico humano (HER2). Os tumores mamários negativos para ER podem ser divididos em dois subtipos: HER2+ e basal. No subtipo HER2+, esse protooncogene encontra-se suprexpresso e no subtipo basal observa-se a presença de diversos genes característicos das células epiteliais basais da mama e o HER2 não é superexpresso, podendo mesmo estar ausente (YERSAL e BARUTCA, 2014).

O TNBC corresponde ao subtipo basal, sendo caracterizado por ensaios imuno-histoquímicos negativos para RE, RP e HER2). Esse tipo de carcinoma apresenta um grau histológico elevado, com menor proporção de arranjos tubulares, alto grau de pleomorfismo nuclear e elevado índice mitótico, além do rápido comprometimento dos linfonodos, o que está associado ao mau prognóstico da doença (PRAT *et al.*, 2013; TURNER, REIS-FILHO, 2013; JIAO *et al.*, 2014; AHN *et al.*, 2016). Além disso, o TNBC consiste em um tumor altamente vascularizado, apresentando elevados níveis de fator de crescimento vascular endotelial (VEGF), que favorecem a nutrição das células neoplásicas e possível migração destas para outros locais (BENDER, GABHANN, 2013; ALLURI, NEWMAN, 2014), sendo os principais sítios de metástase os pulmões e o cérebro (FOULKES, SMITH, REIS-FILHO, 2010; MANCINI *et al.*, 2014).

O uso de fármacos antitumorais no tratamento do TNBC é um desafio devido à dificuldade de se determinar alvos terapêuticos específicos bem como à ausência de diretrizes estabelecidas para o tratamento desse carcinoma. Neste tipo de câncer, os agentes quimioterápicos mais utilizados são as antraciclinas (doxorrubicina e epirubicina), os taxanos (docetaxel e PTX), os antimetabólitos (5-fluorouracil, gencitabina) e a ciclofosfamida (WESTBROOK, STEARNS, 2013; YADAV *et al*, 2014; TELES, MORALLES, COMINETTI, 2018; LEBERT *et al*, 2018).

2.3 Paclitaxel

O PTX, foi isolado pela primeira vez em 1971 por Wall & Wani, no Instituto Nacional do Câncer dos Estados Unidos, a partir do extrato das cascas da *Taxus brevifolia* (GUCHELAAR *et al*., 1994; ZHANG, *et al.*, 2014; YANG, HORWITZ, 2017). Esse fármaco (**Figura 1**) é um alcaloide diterpeno quimicamente conhecido como (2α, 5β, 7β, 10β,13α)-4,10-Diaceoxi-13-{[2R,3S)-3-(benzoil-amino)-2-hidroxi-3-fenilpropanoil]oxi}-1,7-di-hidroxi-9-oxo-5,20-epoxi-tax-11-em-2-ilo, sendo sua estrutura formada por um núcleo rígido e complexo constituído por quatro anéis fundidos e quatro cadeias laterais hidrofóbicas que tornam a molécula altamente lipofílica (log P próximo de 4,0) e praticamente insolúvel em água (0,3 a 1,0 μg/mL) (LIU, ZHANG, YAN, 2011; SURAPANENI, DAS, DAS, 2012; ZHANG, *et al.*, 2014).

Figura 1 - Estrutura química do PTX.

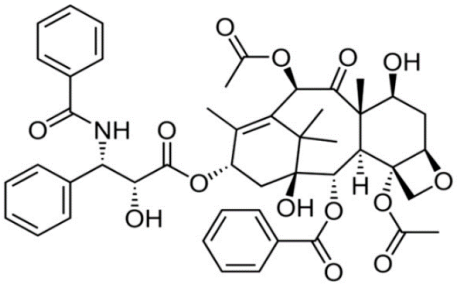

O PTX pertence à classe dos taxanos e atua por meio da estabilização dos microtúbulos, estruturas essenciais no processo de divisão celular, uma vez que permitem a formação do fuso mitótico e garantem a separação dos cromossomas duplicados em dois conjuntos idênticos antes da clivagem da célula. Estruturalmente, os microtúbulos são constituídos por treze protofilamentos formados por heterodímeros de α e β tubulina alinhados longitudinalmente em forma de tubo, apresentando duas extremidades distintas: uma positiva finalizada com uma subunidade de β-tubulina e outra negativa que termina com uma subunidade α-tubulina (SCHIFF, FANT, HORWITZ, 1979; ALTMANN, GERTSH, 2007; YANG, HORWITZ, 2017).

A ligação do PTX à subunidade β-tubulina no lúmen dos microtúbulos provoca um distúrbio na formação dessas estruturas que passam a apresentar doze protofilamentos, ocasionando estabilização irreversível dos microtúbulos e supressão da dinâmica microtubular (**Figura 2**). Nesse processo ocorre a perda da funcionalidade dos microtúbulos e a inibição da mitose das células em divisão na fase G2, impedindo a proliferação das células neoplásicas (SCHIFF, FANT, HORWITZ, 1979; GUCHELAAR *et al.*, 1994; JORDAN, WILSON, 2004; ALTMANN, GERTSH, 2007; SURAPANENI, DAS, DAS, 2012; BARBUTI, CHEN, 2015; YANG, HORWITZ, 2017).

Figura 2 - Mecanismo de ação do PTX. A molécula de PTX se liga a subunidade β-tubulina no lúmen dos microtúbulos impedindo sua despolimerização e interrompendo a proliferação celular.

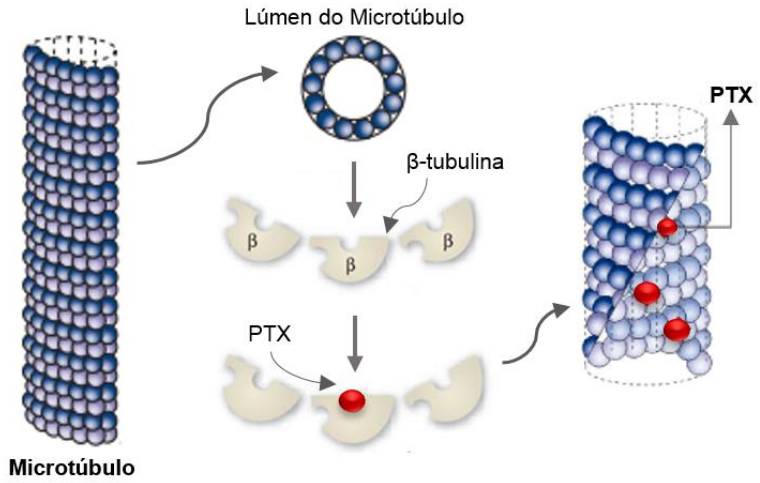

Adaptado de JORDAN e WILSON, 2004; SNYDER, 2007.

O uso do PTX foi aprovado no início da década de 90 pelo *Food and Drug Administration* (FDA). Atualmente, esse fármaco figura entre os agentes antitumorais mais importantes na clínica para o tratamento de diferentes tipos de tumores sólidos como mama, ovário, próstata, câncer de células não-pequenas de pulmão, colón, sarcoma de Kaposi relacionado à síndrome da imunodeficiência adquirida (SIDA) e cabeça e pescoço (GUCHELAAR *et al*., 1994; LIU, ZHANG, YAN, 2011; ZHAN, *et al.*, 2014; MONTEIRO *et al*., 2016). Devido a sua baixa solubilidade em água, entre 0,3 e 1,0 µg/mL, a companhia norte-americana Bristol-Meyer Squibb comercializou pela primeira vez uma dispersão micelar do PTX em etanol desidratado e Cremophor® EL, um derivado polietoxilado do óleo de rícino, na proporção 1:1 (v/v), conhecida como Taxol®. Contudo, esse medicamento apresenta alguns problemas farmacotécnicos como a instabilidade da formulação após a diluição, uma vez que a reconstituição resulta em uma solução com concentração consideravelmente superior (0,3 - 1,2 mg/mL) a solubilidade aquosa do PTX, podendo ocasionar problemas de precipitação do fármaco após a diluição (DONYAI, SEWELL, 2006; SURAPANENI, DAS, DAS, 2012; MONTEIRO *et al*., 2017). Além disso, o Cremophor EL® presente no Taxol® tem a capacidade de lixiviar agentes plastificantes como o di(2-etilhexil)ftalato (DEHP) das embalagens e de cateteres padrões constituídos de cloreto de polivinila (PVC) o que pode induzir quadros de hepatotoxidade grave (GELDERBLOM *et al.*, 2001; DONYAI, SEWELL, 2006). A aplicação do Taxol® na terapia oncológica está ainda relacionada a diversos efeitos adversos. Dentre eles

destacam-se as reações de hipersensibilidade aguda caracterizadas principalmente por dispneia com broncoespasmo, urticária e hipotensão, e em quadros mais graves, paradas cardiorrespiratórias e colapso cardíaco (ROWINSKY e DONEHOWER, 1995; MARKMAN, 2003; MIELKE, SPARREBOOM, MROSS, 2006; SURAPANENI, DAS, DAS, 2012; KOUDELKA e TURÁNEK, 2012; BERTRAND *et al*, 2014; BARBOSA *et al*, 2015; MONTEIRO *et al*, 2018a).

A neuropatia periférica sensorial também é uma manifestação clínica decorrente do tratamento com Taxol®, sendo a ausência de mecanismos de efluxo o provável fator relacionado a esse efeito. Estudos mostram que este efeito está relacionado tanto ao fármaco quanto ao veículo (GORNSTEIN e SCHWARZ, 2014; WOZNIAK *et al.*, 2016). Entre os sintomas causados pode-se citar a neuropatia motora, com paralisação e dormência dos membros, hipotensão ortostática e perda sensorial periférica (GELDERBLOM *et al.*, 2001; MIELKE, SPARREBOOM, MROSS, 2006). O tratamento com o Taxol® pode ocasionar, também, mielossupressão, principalmente, sob a forma de neutropenia grave de curta duração, cardiotoxicidade, mucosite, estomatite, náuseas e alopecia (HOYER, 2000; MARKMAN, 2003; SHAH *et al*., 2012).

Em virtude disso, o emprego de sistemas nanoestruturados para vetorização e liberação de agentes antineoplásicos vem ganhando destaque no âmbito farmacêutico, uma vez que possibilitam uma liberação controlada e localizada do fármaco, aumentando a biodisponibilidade nos tecidos-alvo, melhorando, assim, sua eficácia terapêutica e reduzindo a toxicidade associada ao tratamento (LOPES *et al.*, 2013; BARBOSA *et al.*, 2015; MONTEIRO *et al.*, 2016; MONTEIRO *et al.*, 2018a; MONTEIRO *et al.*, 2018b). Como é possível observar na **Tabela 1,** existem três formulações nanoestruturadas contendo PTX disponíveis no mercado farmacêutico mundial para uso clínico, contudo essas apresentam alguns inconvenientes e limitações que demonstram a necessidade de buscar novos sistemas que permitam aumentar a especificidade e reduzir a toxicidade do tratamento utilizando o PTX.

Tabela 1 – Sistemas nanoestruturados contendo PTX disponíveis no mercado farmacêutico.

Formulação Comercial	País de Comercialização	Constituição	Indicação	Estudos clínicos*	Referências
Abraxane®	Estados Unidos	Nanopartículas de albumina	Mama metastático	Redução da toxicidade Aumento da dose máxima tolerada Dispensa administração prévia de corticosteroides e anti-histamínicos Aumento da ocorrência de neurotoxicidade.	FADER, ROSE, 2009; PAIK *et al*., 2011; YAMASHITA *et al*., 2011; YARED, TKACZUK, 2012; FENG, MUMPER, 2013.
Genexol-PM®	Coréia do Sul	Micelas - PEG e poli-(D,L-latico)	Mama e pulmão	Redução da toxicidade Aumento da dose máxima tolerada. Eficácia in vivo três vezes superior. Reações de hipersensibilidade, neuropatia e neutropenia,	HENNENFENT, GOVINDAN, 2006; LIM *et al*., 2010; YARED, TKACZUK, 2012; WERNER *et al*., 2013.
Lipusu®	China	Lipossomas convencionais - PC e PG	Pulmão, ovário e mama	Atividade antitumoral semelhante Redução da toxicidade Baixa seletividade pelo tecido tumoral	CHEN *et al*., 2003; YANG, LI, XU, 2006; WANG *et al*., 2013; XU *et al*., 2013.

***Nos estudos clínicos, os resultados foram comparados ao uso do Taxol®. PC – fosfatidilcolina; PG – fosfatidilglicerol; PEG – polietilenoglicol.**

2.4 Lipossomas

Dentre os sistemas nanoestruturados de transporte e liberação de fármacos, os lipossomas ocupam um lugar de destaque uma vez que são constituídos por moléculas com elevada biocompatibilidade e biodegradabilidade. Além disso, são estruturas versáteis, pois suas características como tamanho, lamelaridade, superfície, fluidez e composição podem ser modificadas de acordo com os requisitos farmacotécnicos e farmacológicos necessários para veicular a substância de interesse (ULRICH, 2002; FRÉZARD *et al*., 2005; BATISTA, CARVALHO, MAGALHÃES, 2007; SAWANT, TORCHILLIN, 2012; NOGUEIRA *et al*., 2015). Em virtude disso, o emprego de sistemas lipossomais para a vetorização de agentes antitumorais tornou-se uma estratégia farmacotécnica importante na terapia do câncer. A utilização de lipossomas para veicular esses agentes pode ocasionar a liberação lenta e específica dos fármacos no tecido tumoral, levando ao aumento na eficácia terapêutica e redução da toxicidade inerente ao tratamento (SAWANT, TORCHILLIN, 2012; VANNEMAN, DRANOFF, 2012; IWAMOTO, 2013; ZHAO, RODRIGUEZ, 2013; OLUSANYA *et al*., 2018).

Lipossomas são vesículas esféricas constituídas basicamente por fosfolípides (sintéticos ou naturais) que, em solução aquosa, se organizam, espontaneamente, em uma ou várias bicamadas lipídicas, orientadas concentricamente em torno de um compartimento aquoso (**Figura 3**). Devido às características anfifílicas das estruturas lipossomais, esses sistemas possibilitam encapsular substâncias hidrofílicas, em sua cavidade interna, lipofílicas, na região apolar da bicamada lipídica, e anfifílicas, na interface entre a região polar e apolar (BANGHAM et al. 1965; LASIC, 1998; FRÉZARD *et al*., 2005; BATISTA, CARVALHO, MAGALHÃES, 2007; SHAILESH *et al*., 2009; LAOUINI *et al*., 2012; LOPES *et al*., 2013; MADNI *et al*., 2014; OLUSANYA *et al*., 2018). De acordo com seu tamanho e com o número de bicamadas presentes, as vesículas lipossomais podem ser classificadas em vesículas unilamelares pequenas (SUV), com diâmetro entre 25-100 nm, vesículas unilamelares grandes (LUV), com diâmetro médio maior que 100nm e, bicamadas múltiplas são classificadas como vesículas multilamelares (MLV) com diâmetro superior a 1000nm (VEMURI, RHODES, 1995; LASIC, 1998; LAOUINI *et al*., 2012, NOGUEIRA *et al*., 2015).

Figura 3 – Representação esquemática da formação e estrutura dos lipossomas a partir de moléculas de fosfolípides em solução aquosa.

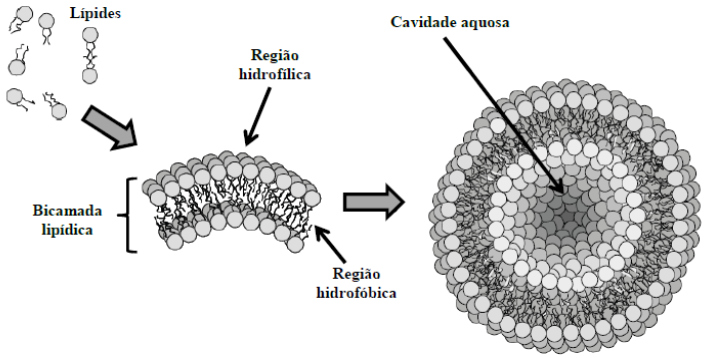

Adaptado de BALAZN e GODBEY, 2011.

Com o intuito de promover um aumento da eficácia antitumoral, aumento da seletividade e redução de efeitos tóxicos, as formulações lipossomais têm sido delineadas por meio da combinação de diferentes propriedades/funções para a obtenção de sistemas multifuncionalizados. É possível, por exemplo, (a) prolongar seu tempo de permanência na circulação sanguínea; (b) promover maior acúmulo no sítio desejado; (c) obter responsividade a um estímulo local, como pH ou temperatura; (d) permitir a entrega eficaz do fármaco às células ou organelas específicas; (e) carrear agentes de contrastes para acompanhamento em tempo real da acumulação no sítio desejado e (f) carrear simultaneamente dois ou mais agentes quimioterápicos, o que pode resultar em sinergismo de citotoxicidade (**Figura 4**) (MAYER, JANOFF, 2007; TORCHILIN, 2012; PERCHE, TORCHILIN, 2013; OLUSANYA *et al*., 2018; RIAZ *et al*., 2018).

Figura 4: Representação esquemática de um carreador lipossomal multifuncional.

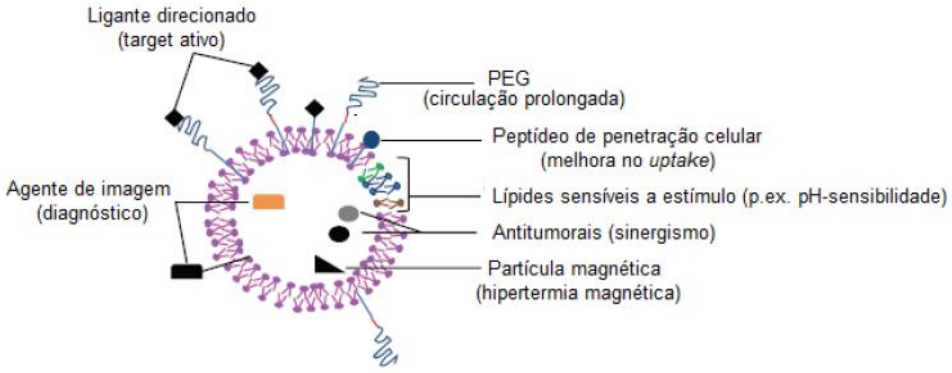

Adaptado de Perche, Torchilin, 2013.

O maior obstáculo relativo aos lipossomas convencionais é sua rápida captura *in vivo* por células do sistema mononuclear fagocitário (SMF). Desta forma, diversas estratégias foram desenvolvidas na tentativa de contornar esse problema, dentre elas destaca-se a incorporação de um polímero hidrofílico na superfície da bicamada lipídica, como o polietilenoglicol (PEG) (VEMURI, RHODES, 1995; MUFAMANDI *et al*, 2011; PERCHE, TORCHILIN, 2013, MADNI, 2014). A presença dos grupos volumosos hidrofílicos do PEG pode aumentar o tempo de circulação dos lipossomas, uma vez que estas moléculas ocasionam a formação de uma barreira estérica na superfície lipossomal que reduz as interações hidrofóbicas entre as vesículas e as opsoninas, minimizando a captação pelas células do SFM. Portanto, o distearoilfosfatidiletanolamina acoplada ao polietilenoglicol 2000 (DSPE-PEG_{2000}), **Figura 5**, vem sendo extensamente utilizado em formulações lipossomais com esse propósito (KLIBANOV *et al*., 1990; GABIZON *et al*., 1997; FERREIRA *et al*., 2013; BARBOSA *et al*., 2015; MONTEIRO *et al*., 2016).

Figura 5 - Estrutura química da distearoilfosfatidiletanolamina acoplada ao polietilenoglicol 2000 (DSPE-PEG_{2000}).

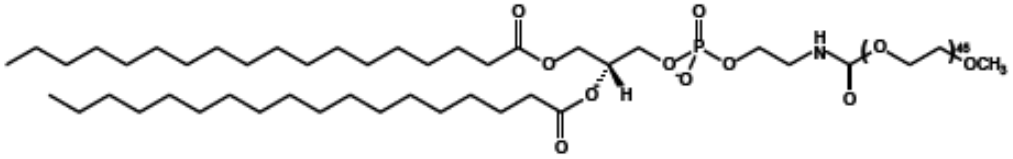

Uma vez que os fármacos antitumorais são veiculados em lipossomas "peguilados" esses podem ter seus efeitos antitumorais significativamente aumentados, pois permite um maior número de passagens do sistema pela região tumoral o que favorece o acúmulo das vesículas neste local, em função do efeito de permeabilidade e retenção (EPR) aumentados neste tecido (**Figura 6**). Este efeito é resultado do intenso processo de angiogênese relacionado às altas concentrações de fatores de crescimento endotelial presentes nas células neoplásicas. O rápido desenvolvimento desses novos vasos ocasiona a formação de fenestrações no revestimento endotelial do tecido tumoral que favorece a passagem e acúmulo dos lipossomas nessa região (**Figura 7**). Além disso, a ausência de drenagem linfática adequada nesta região, resulta em aumento da pressão intersticial e retardo do extravasamento das macromoléculas acumuladas. Esses dois processos associados resultam no mecanismo conhecido como EPR (MAEDA *et al*., 2000; SAWANT, TORCHILIN, 2012; FERREIRA *et al*., 2013; ZYLBERBERG, MATOSEVIC, 2016; MONTEIRO *et al.*, 2017; RIAZ *et al*., 2018).

Figura 6 – Representação esquemática do efeito da modificação da superfície de nanopartículas pela incorporação de PEG na adsorção de proteínas plasmáticas e na biodistribuição.

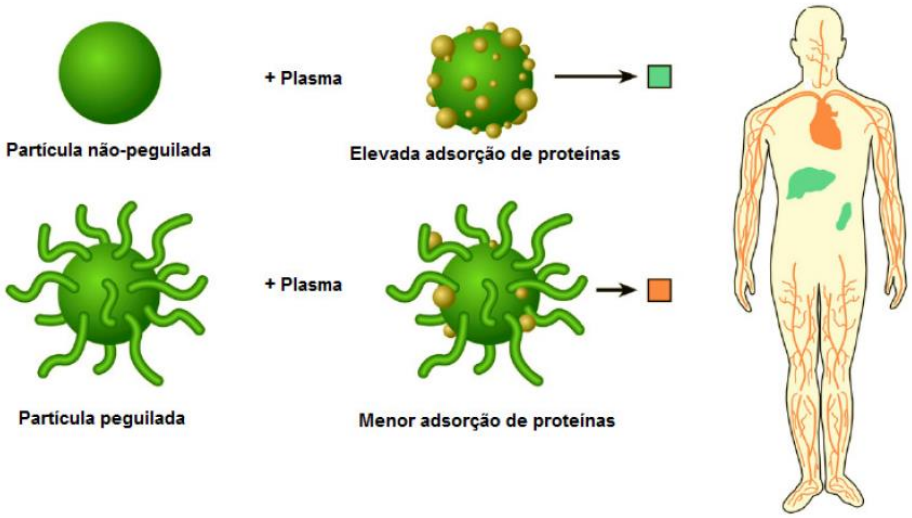

Adaptado de AGGARWAL *et al*., 2009.

Figura 7 – Representação esquemática do efeito EPR. Vasculatura do tecido tumoral com fenestrações, permitindo o extravasamento dos lipossomas nessa região.

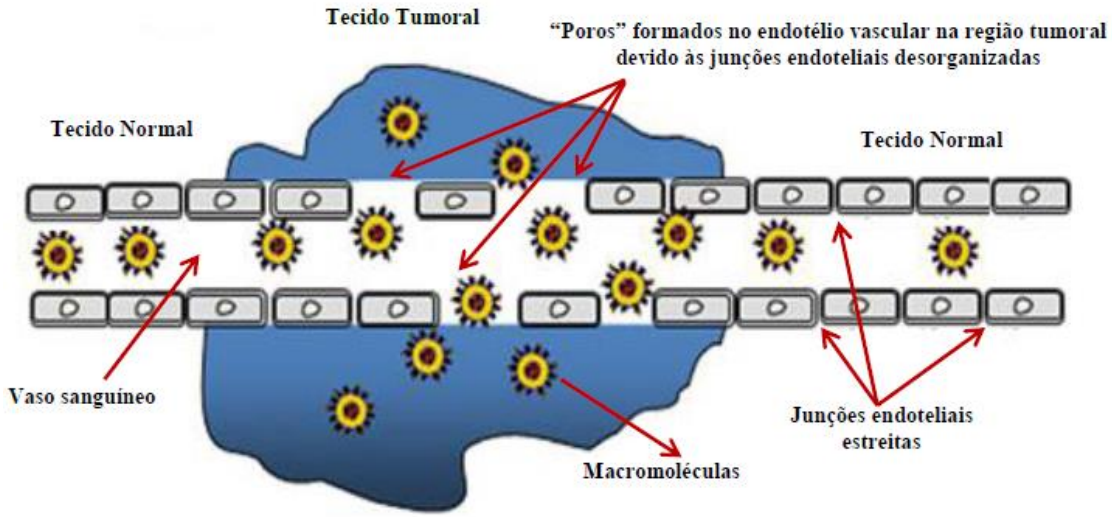

Adaptado de SAWANT e TORCHILIN, 2012.

Após atingir a região tumoral, a liberação do fármaco no citoplasma das células neoplásicas é essencial para a obtenção do efeito antitumoral. Nesse contexto, a modificação da composição estrutural das vesículas lipossomais usando fosfolípides sensíveis às condições biológicas

específicas da região tumoral vem sendo adotada como estratégia para melhorar o desempenho do sistema. Assim, lipossomas pH-sensíveis têm sido extensamente estudados como alternativa para o acúmulo de agentes antineoplásicos no tecido tumoral, uma vez que exploram as condições de pH reduzido existente nestes locais (LOOMIS, MCNEELEY, BELLAMKONDA, 2011; MUFAMANDI *et al*., 2011; FERREIRA *et al.*, 2013; GENTILE *et al*., 2013; NOGUEIRA *et al.*, 2015).

Sabe-se que o meio extracelular do tecido tumoral é mais ácido (pH próximo de 6,5) do que nos tecidos normais (pH em torno de 7,4). Esse fato é decorrente da vascularização heterogênea do tecido tumoral que contribui para a ineficiência do *clearance* dos metabólitos ácidos resultantes da glicólise aeróbica intensa que ocorre nas células tumorais. Portanto, a presença de um sistema pH-sensível nesse ambiente ácido, resulta na desestabilização e liberação do conteúdo encapsulado. Além disso, após internalização dos sistemas lipossomais por via endocítica, o contato desses com meio ácido presente no endossoma tardio (pH próximo de 5,0) também induz a desestabilização das vesículas e liberação do seu conteúdo diretamente no citoplasma da célula tumoral. Esse segundo processo tem sido a hipótese mais aceita em relação a liberação do conteúdo encapsulado nos lipossomas pH-sensíveis (FERREIRA *et al.*, 2013; GOUBRAN *et al.*, 2014; BARBOSA *et al.*, 2015; MONTEIRO *et al*., 2018a).

As hipóteses que explicam a interação entre vesícula lipossomal e endossomal estão representadas na **FIGURA 8**. A primeira, representada na **FIGURA 8-A**, propõe que após a endocitose, ocorre a desestabilização da membrana lipossomal em meio ácido dos endossomas, ocasionando a interação entre os componentes lipossomais e a membrana endossomal liberando o material veiculado no citoplasma. Outra possibilidade é que após a desestabilização dos lipossomas, o fármaco encapsulado sofre difusão pela membrana endossomal para o citoplasma (**FIGURA 8-B)**. Por fim, sugere-se que a desestabilização lipossomal ocasione o início da desestabilização endossomal, formando poros em sua superfície que permitem a passagem do fármaco para o citoplasma, como representado na **FIGURA 8-C** (FERREIRA *et al.*, 2013).

Figura 8 – Mecanismos propostos para a liberação intracitoplasmática do material incorporado aos lipossomas pH-sensíveis.

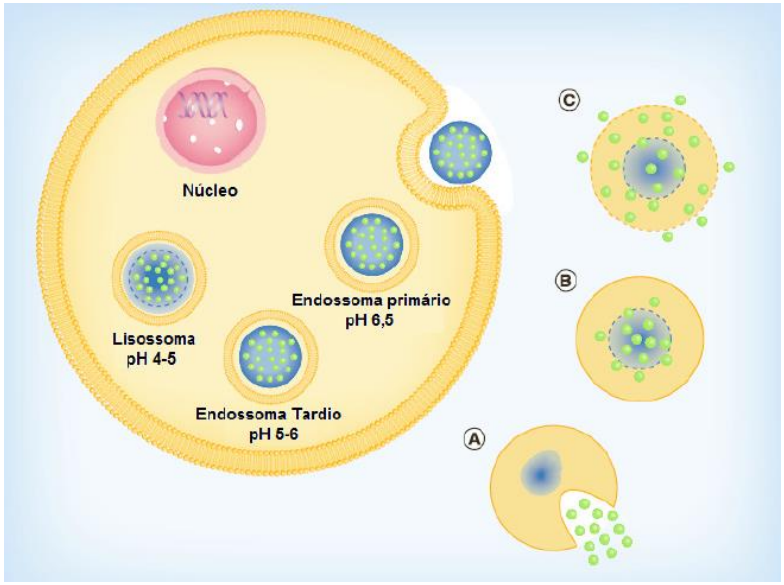

Adaptado de FERREIRA *et al.*, 2013.

Os lipossomas pH-sensíveis são constituídos por lípides insaturados, como os derivados da fosfatidiletanolamina (PE), entre eles a dioleoilfosfatidiletanolamina (DOPE) (**FIGURA 9-B)**, associados com compostos carboxilados como o hemisuccinato de colesterila (CHEMS) (**FIGURA 9-A**) (CARVALHO- JÚNIOR *et al*., 2007; FERREIRA *et al*., 2013; LOPES *et al*., 2015; MONTEIRO *et al*., 2016; MONTEIRO *et al*., 2018a; MONTEIRO *et al*., 2018b).

Figura 9 - Estruturas químicas do hemisuccinato de colesterila (A) e da dioleilfosfatidiletanolamina (B).

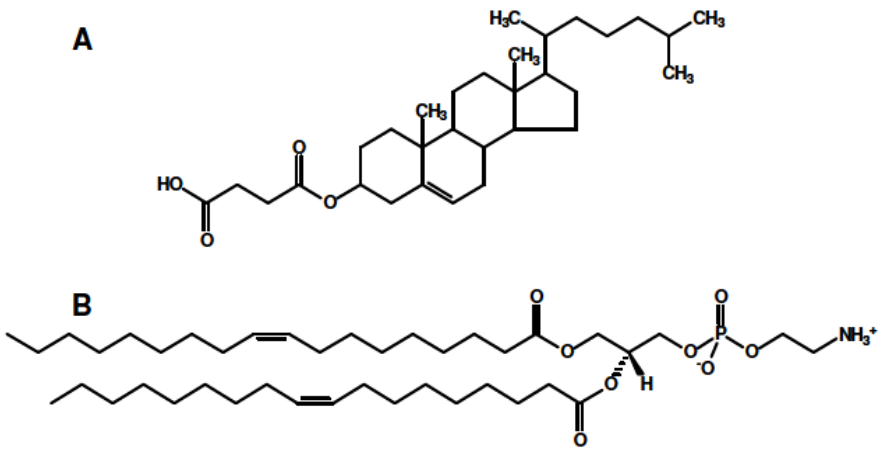

A geometria cônica apresentada pelos derivados da PE, como a DOPE, caracterizada por uma cabeça polar pequena e pouco hidratada ocupando um pequeno volume quando comparado ao volume das cadeias hidrocarbônicas, impede que este fosfolípide se organize espontaneamente na forma de bicamadas, quando em meio aquoso. Isso favorece sua organização sob a forma hexagonal invertida (H_{II}) devido às fortes interações intermoleculares entre os grupos amino e fosfato da sua porção polar (**FIGURA 10A**). Quando agentes estabilizantes possuindo um grupo acídico protonável, como CHEMS, são adicionados ao sistema, suas moléculas se inserem entre as moléculas da DOPE provocando repulsão eletrostática pela proximidade com o grupo fosfato da DOPE, o que favorece a organização lamelar do sistema (**FIGURA 10B**). Em meio ácido, as moléculas de CHEMS são protonadas desestabilizando a bicamada lipídica e as moléculas de DOPE retornam para a fase H_{II}, com consequente liberação do conteúdo lipossomal (SIEGEL, 1986; DE OLIVEIRA *et al.*, 1998; DE OLIVEIRA *et al.*, 2000; FERREIRA *et al*., 2013; LOPES *et al*., 2015; MONTEIRO *et al*., 2016; MONTEIRO *et al*., 2018a).

Figura 10 - Representação esquemática da organização estrutural de derivados da PE na ausência (A) e na presença (B) de CHEMS.

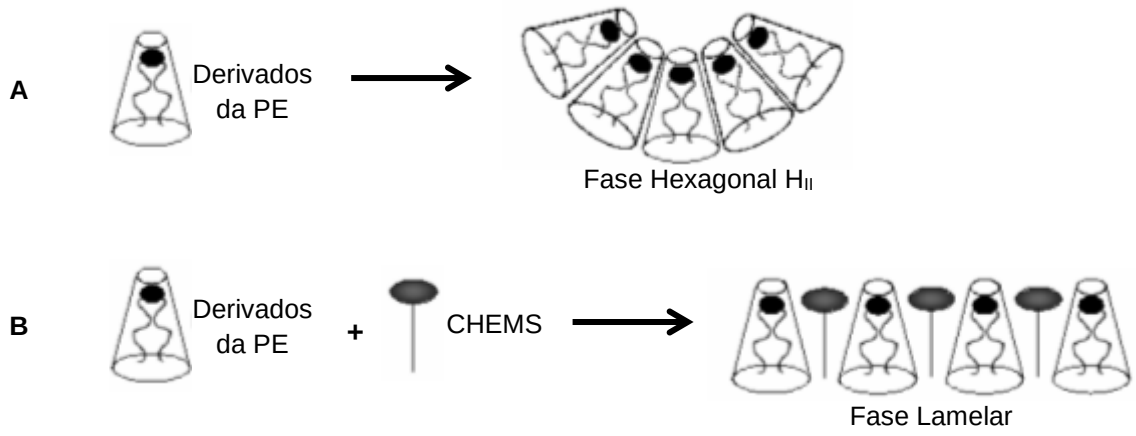

Com objetivo de aumentar a especificidade da interação entre os lipossomas e as células-alvo, e garantir o direcionamento das formulações antitumorais especificamente para o tecido neoplásico, a utilização de ligantes sítio-específicos acoplados na superfície lipossomal tem sido investigada. Esses ligantes são reconhecidos de forma seletiva por moléculas ou receptores superexpressos na superfície das células acometidas por determinada doença, aumentado assim a internalização dos nanossistemas. Dentre os principais ligantes utilizados para a modificação da superfície lipossomal podemos citar peptídeos, oligossacarídeos, anticorpos, ácidos

nucléicos e moléculas pequenas, tais como vitaminas (WANG, THANOU, 2010; PERCHE, TORCHILIN, 2013; BERTRAND *et al.*, 2014; BARBOSA *et al.*, 2015; MONTEIRO *et al.*, 2018a; OLUSANYA *et al.*, 2018).

Sabe-se que uma ampla variedade de linhagens tumorais, como melanoma, cabeça e pescoço, ovário, pulmão, mama, endométrio, rim e cérebro, superexpressam receptores para folato (RF) em sua superfície. Por outro lado, o nível de expressão de RF em tecidos normais é muito mais baixo ou ausente. Assim, o padrão distinto de expressão de RF entre tecidos normais e neoplásicos tornam estas estruturas alvos ideais para entrega sítio-específica de fármacos (REDDY, ALLAGADDA, LEAMON, *et al.*, 2005; HUANG *et al.*, 2014; LIU, FANG, XU, 2014, BARBOSA *et al.*, 2015). Portanto, a incorporação do ácido fólico, ligante natural e seletivo dos RF, conjugado a outras moléculas como PEG, na superfície das vesículas lipossomais, mostra-se uma alternativa promissora para favorecer o processo de internalização lipossomal por via endocítica, aumentando a liberação do fármaco especificamente no citoplasma das células tumorais (SAPRA, ALLEN, 2003; REDDY, ALLAGADDA, LEAMON, 2005; SAWANT, TORCHILIN, 2012; WATANABE, KANEKO, MAITANI, 2012; HUANG *et al.*, 2014).

Nesse sentido, Barbosa e colaboradores (2015b) desenvolveram uma formulação lipossomal pH-sensível de circulação prolongada composta por DOPE:CHEMS:DPSE-PEG_{2000}:DSPE-PEG-folato (5,7:3,8;0,45:0,05, respectivamente) para o carreamento do PTX (LpHS-folato-PTX). Esse sistema foi avaliado durante 150 dias de armazenamento a 4 °C, mostrando estabilidade adequada até o centésimo dia de avaliação, sem alteração significativa nos parâmetros estudados (diâmetro médio, índice de polidispersão, potencial zeta, teor de encapsulação e pH). Além disso, o estudo de citotoxicidade mostrou elevada atividade citotóxica dessa formulação contra linhagens celulares de câncer de mama (MDA-MB-231 e MCF-7) e reduzida toxicidade para a linhagem de células normais (L929) quando comparada ao PTX livre. Observou-se também um índice de seletividade da formulação LpHS-folato-PTX superior para a linhagem MDA-MB-231, indicando uma maior sensibilidade desta linhagem tumoral ao tratamento. No intuito de elucidar o comportamento termodinâmico das moléculas de DOPE na presença do PTX, e consequentemente, possíveis alterações na pH-sensibilidade, essa formulação lipossomal foi também avaliada em condições de baixa hidratação mediante associação das técnicas de Calorimetria Exploratória Diferencial (DSC) e Espalhamento de raios-X a baixo ângulo (SAXS). Os resultados demonstraram que a inclusão do PTX na

bicamada não altera as transições de fase lamelar para não-lamelar das moléculas da DOPE, processo indispensável para a desestabilização do sistema lipossomal e liberação do material encapsulado no tecido tumoral (MONTEIRO *et al*, 2016). Nesse sentido, esse conjunto de dados nos estimularam a conduzir estudos mais detalhados em relação a caracterização físico-química e ao comportamento biológico (*in vitro e in vivo*) dessa nova formulação, a fim de demonstrar o seu potencial na terapia antitumoral, mais especificamente, no tratamento do TNBC.

OBJETIVOS

3. OBJETIVOS

3.1 Objetivo Geral

Avaliar o potencial de lipossomas pH-sensível de circulação prolongada recobertos com folato como estratégia para tratamento do tumor de mama humano MDA-MB-231.

3.2 Objetivos Específicos

- Preparar lipossomas pH-sensíveis de circulação prolongada contendo PTX, funcionalizados ou não com folato (LpHS-folato-PTX e LpHS-PTX, respectivamente).
- Caracterizar as formulações lipossomais quanto ao diâmetro médio, índice de polidispersão, potencial zeta e teor de encapsulação do PTX.
- Avaliar a organização supramolecular das formulações lipossomais pela técnica de SAXS.
- Avaliar a biodistribuição dos LpHS-folato-PTX em animais sadios e em modelo experimental tumoral de mama MDA-MB-231, comparando com a dispersão micelar (PTX:Cr+Et) e LpHS-PTX.
- Avaliar comparativamente a captação *in vitro* das vesículas lipossomais e do PTX:CR+Et pelas células MDA-MB-231, por meio das técnicas de radiomarcação isotópica com ^{99m}Tc e por CLAE.
- Avaliar o ciclo celular e quantificar o índice de apoptose nas células da linhagem MDA-MB-231 após tratamento com LpHS-folato-PTX, LpHS-PTX e PTX:CR+Et.
- Avaliar a hemocompatibilidade do LpHS-folato-PTX, LpHS-PTX e PTX:CR+Et.
- Avaliar da atividade antitumoral dos LpHS-folato-PTX em modelo experimental tumoral de mama MDA-MB-231, comparando com PTX:CR+Et e LpHS.

PARTE EXPERIMENTAL, RESULTADOS E DISCUSSÃO

4. PARTE EXPERIMENTAL, RESULTADOS E DISCUSSÃO

4.1 Artigo 1: Paclitaxel-loaded pH-sensitive liposome: new insights on structural and physicochemical characterization

Autores: Liziane Monteiro, Angelo Malachias, Gwenaelle Pound-Lana, Rogerio Magalhães-Paniago, Vanessa Mosqueira, Mônica de Oliveira, André Luis de Barros, Elaine Leite.

Artigo publicado no periódico **Langmuir, v. 34, n. 20, p 5728-5737, 2018**.

ABSTRACT

A long-circulating and pH-sensitive liposome containing PTX (SpHL-PTX) was recently developed by our group. Once at an acidic environment, e.g. tumor, these liposomes undergo destabilization releasing the encapsulated drug. In this way, the aim of this study was evaluate the molecular and supramolecular interactions between the lipid bilayer and PTX in similar biological environment conditions. High sensitivity analyses of SpHL-PTX structures were obtained by small angle X-ray scattering (SAXS) technique combined with other techniques such as DLS, AF4, TEM and HPLC. The results showed that PTX incorporation in the liposomal bilayer clearly leads to changes in supramolecular organization of DOPE molecules inducing the formation of more ordered structures. Changes in supramolecular organization were observed at lower pH, indicating that pH-sensitivity was preserved even in the presence of FBS proteins. Furthermore, morphological and physicochemical characterization of SpHL-PTX evidenced the formation of nanosized dispersion suitable for intravenous administration. In conclusion, a stable nanosized dispersion of PTX was obtained at pH 7.4 with suitable parameters for intravenous administration. At lower pH conditions, the pH-sensitivity of the system was clearly evidenced by changes in the supramolecular organization of DOPE molecules, which is crucial for the delivery of PTX into the cytoplasm of the targeted cells. In this way, results obtained by different techniques confirm the feasibility of SpHL as a promising tool to PTX delivery in acidic environments, such as tumors.

Keywords: Liposomes, pH-sensitivity, Small angle X-ray scattering, Asymmetric flow field-flow fractionation, drug delivery

1 Introduction

Chemotherapy is the most common treatment for many types of cancer. To achieve an optimal anticancer efficacy, high doses of drugs are required as well as the maintenance of high levels for a prolonged time in the blood circulation, which often results in systemic side effects[1,2]. Among drugs commonly used in cancer therapy, paclitaxel (PTX) has shown high activity against a wide range of solid tumors. However, intravenous administration of PTX is challenging due to its low aqueous solubility[3-5]. Therefore, novel approaches to optimize the administration of PTX are encouraged. In this sense, liposomes are versatile spherical structures composed of phospholipids surrounding an aqueous compartment, which have been extensively used to encapsulate hydrophilic, hydrophobic and amphiphilic molecules[6-8].

Recently, our group developed a long-circulating and pH-sensitive liposome containing PTX (SpHL-PTX), composed of dioleylphosphatidylethanolamine (DOPE), cholesterylhemisuccinate (CHEMS), and distearoylphosphatidylethanolamine-polyethylene glycol$_{2000}$ (DSPE-PEG$_{2000}$)[9]. The design of this system takes advantage of the polymorphic phase behavior of DOPE. The small volume of its polar head compared to the hydrocarbon chain promotes strong intermolecular interactions between amine and phosphate groups, inducing the H_{II} organization[10-16]. At neutral pH, the insertion of titrable amphiphilic acid molecules, such as CHEMS, causes an electrostatic repulsion between carboxylate and phosphate groups favoring the formation of lamellar phases. The contact of these liposomes with an acidic environment, either in endosomal vesicles or in the extracellular tumor matrix, leads to the protonation of the carboxylate groups triggering a transition from lamellar to hexagonal phase and the encapsulated drug is released[10, 11, 14-17].

However, hydrophobic molecules inserted in the lipid bilayer, such as PTX, might compromise the lamellar to non-lamellar phase transition of DOPE, affecting the pH-sensitivity of the system. In this sense, we investigated the changes in the DOPE phase behavior in the presence of PTX under quasi-anhydrous conditions. The results showed that the presence of CHEMS led to stabilization of DOPE in a lamellar structure, while the heat of this system promoted DOPE organization in H_{II} phase and consequently, liposome destabilization. The inclusion of PTX in the liposomal bilayer did not alter the supramolecular organization or phase transition of the structural lipid[11]. However, once into the endosomal vesicles, an aqueous environment, pH-sensitivity might be impaired by a different behavior of DOPE[10,11,17-20]. In this context, the aim of this study was to prepare and characterize SpHL-PTX under hydrated conditions in

order to evaluate the molecular and supramolecular interactions between the lipid bilayer and PTX in similar biological environment conditions.

2 Experimental Section

2.1 Materials

Paclitaxel was supplied by Quiral Quimica do Brasil S.A (Juiz de Fora, Brazil). Dioleoylphosphatidylethanolamine (DOPE) and distearoylphosphatidyl-ethanolaminepolyethyleneglycol$_{2000}$ (DSPE-PEG$_{2000}$) were purchased from LipoidGmbH (Ludwigshafen, Germany). Cholesterylhemisuccinate (CHEMS), fetal bovine serum (FBS), phosphorus standard solution (0.65 nM), perchloric acid, ammonium molybdate solution and 4-amino-2-naphthyl-4-sulfonic reagent were acquired from Sigma Chemical Company (St. Louis, USA). Sodium chloride (NaCl) was obtained from Merck (Rio de Janeiro, Brazil). HPLC grade acetonitrile was purchased from Fischer Scientific (New Jersey, USA). Dulbecco's modified Eagle's medium (DMEM) was supplied by Gibco Life Technologies (Carlsbad, USA). Water was purified using a Milli-Q apparatus (Millipore, Billerica, USA). All other chemicals and reagents used in this study were of analytical grade without further purification.

2.2 Liposome Preparation

The liposomes were prepared by the lipid hydration method, as previously described [9]. Liposomes composition was DOPE, CHEMS, and DSPE-PEG$_{2000}$ at lipid concentration of 10 mmol/L (molar ratio of 5.7:3.8:0.5, respectively). Firstly, chloroform aliquots of the lipids and PTX were transferred to round bottom flask and the organic solvent was removed by evaporation under reduced pressure until a formation of a thin lipid film. Next, a solution of NaOH at a CHEMS/NaOH (mol/mol) ratio of 1:1 was added, and the film was hydrated with NaCl solution (0.9% w/v), followed by vigorous shaking in a vortex. Finally, the obtained multilamellar vesicles were immediately submitted to the high-intensity probe sonication (20% amplitude) for 5 minutes, in an ice bath, using a high-intensity ultrasonic processor (R2D091109 model; Unique® Instruments, Indaiatuba, Brazil). Free PTX was removed by centrifugation (Heraeus Multifage X1R Centrifuge, Germany) at 3000 rpm at 4ºC for 10 minutes. The empty liposomes (without drug) were also prepared as described above. All products were stored at 4ºC.

2.3 Evaluation of Supramolecular Interactions by SAXS Analysis

SpHL and SpHL-PTX were submitted to ultracentrifugation for two hours at 150,000 g at 4°C (OPTIMA^{TM} L-80XP, Beckman Coulter – Fullerton, CA, USA). The pellet containing the vesicles was re-suspended using three different solutions: NaCl 0.9% (w/v), DMEM and DMEM containing 10% (v/v) FBS. All solutions were prepared at pH 7.4, 6.8 or 5.0. Then, the samples were again submitted to ultracentrifugation, and the pellet obtained was analyzed by small-angle X-ray scattering (SAXS).

SAXS analysis was performed on a beamline D1B-SAXS1 instrument at the Brazilian Synchrotron Light Laboratory (LNLS, Campinas, Brazil), at a fixed X-ray wavelength of 0.1488 nm. SAXS measurements of the samples were detected using a 300K Pilatus detector providing a range of 0.15 - 4.0 nm^{-1}, where $q = (4\pi/\lambda) \sin \theta$ and θ is the scattering angle. Liposomes were deposited on metal rings, which were sealed by a polyimide film (Kapton®). A sample holder with a DSC-linkam heating system was also used in the analyses. The lattice parameter (a) was calculated using the formula $a = 2\pi/q$, which is valid for the first-order peaks of all packing structure types analyzed in this work.

2.4 Physicochemical characterization

2.4.1 Particle Diameter, Polydispersity Index and Zeta Potential Analysis

Dynamic Light Scattering (DLS) using the Zetasizer NanoZS90 equipment (Malvern Instruments, England), equipped with a He-Ne Laser emitting at 633nm wavelength, was carried out to determine the mean particle diameter and polydispersity index of SpHL and SpHL-PTX. Samples were analyzed by unimodal analysis at 25°C and at a fixed angle of 90° after appropriate dilution (1:10) in ultra-pure water.

Zeta potential measurements were determined by DLS associated with electrophoretic mobility on the same equipment as used for diameter analyses. The measurements were performed after diluting the samples in a filtered (0.45 μm, Millipore) 0.9% w/v NaCl solution (1:10). All data sets were expressed in terms of the mean (±) standard deviation of at least three different liposomal formulations.

2.4.2 Asymmetric Flow Field Flow Fractionation (AF4-MALS-DLS)

Liposome fractionation was carried out on a Postnova analytics (Landberg, Germany) AF2000 MT AF4 system equipped with a PN7520 solvent degasser, two PN1130 HPLC pumps (tip and focus pumps) and an AF2000 module (crossflow pump), PN5300 auto sampler thermostated at 15°C, PN4020 Channel oven set at 25°C, a separation channel fitted with a Postnova AF2000 MT Series Nova RC AQU 5 kDa cut-off regenerated cellulose membrane and a 350 µm spacer. Fractionated sample characterization was performed with a set of three detectors in series, namely, a PN3211 UV absorption set for detection of absorbance at 254 nm, a PN3621 multi-angle laser light scattering (MALS) detector with a 532 nm laser (12°-164°, 20 angles) at 35°C and a Malvern PN3702 Zetasizer NanoZS (Malvern Instruments, UK) DLS detector with a 633 nm laser. The system uses a Hellma Analytics Suprasil® 3 mm light path quartz flow cell, for 173° back scattered light detection, recorded at 5 s time intervals, at 25°C. The carrier liquid used was a 10 mmol/L NaCl in Milli-Q water filtered on 0.1 µm. The detector flow rate was kept at 0.5 mL/min. The liposome formulations were diluted in the carrier liquid (150 µL in 850 µL of 10 mmol/L NaCl) and 20 µL were injected. The injection flow was 0.2 mL/min with an injection time of 3.0 min. The crossflow rate was set to decrease exponentially after a transition time of 1 min from its initial value to 0.05 mL/min over a period of 15 min, kept at 0.05 mL/min for 31 min followed by 5 min at 0 mL/min. Particle radii of gyration (R_g) were determined in flow mode using the angular variation of the scattered light intensity at angles spanning from 12° to 164°, recorded on the MALS detector using the Postnova AF2000 software calculation for spherical shape model. The UV signal intensity was used as a measure of the relative frequency of each fraction. D_{10}, D_{50}, and D_{90}, were obtained from the cumulative distribution of gyration diameters obtained by integrating the whole sample peak, and D_n, D_w and D_z, the intensity-, weight- and Z-average, respectively, of the gyration diameter distribution for values between D_{10} and D_{90}. Values outside these parameters were discarded due to their intrinsically large error. The hydrodynamic diameters in flow mode were determined using the Malvern Zetasizer 7.11 data analysis software.

2.4.3 Transmission Electron Microscopy (TEM)

Transmission electron microscopy images on the SpHL and SpHL-PTX systems were carried out using a negative staining method that provided a complementary morphological evaluation. Briefly, the liposomal formulations were placed on a formvar-coated copper grid and stained

with 2% (w/v) phosphotungstic acid solution containing 0.5% (w/v) bovine serum albumin and 0.5% (w/v) saccharose[21]. The stained samples were observed using a FEI Tecnai G2-12 Spirit Biotwin microscope at 120 kV (Centro de Microscopia, Universidade Federal de Minas Gerais, Belo Horizonte, Brazil).

2.4.4 Drug Encapsulation Percentage

Drug encapsulation was determined by measuring the PTX concentration in the non-purified liposomes and purified liposomes[9]. In brief, SpHL-PTX were disrupted using isopropanol at a volume ratio of 1:10 and later diluted in a mixture of acetonitrile:water 55:45 (v/v). This dispersion was filtered through a 0.45 µm Millex HV filter (Millipore, Billerica, MA, USA) and analyzed by high performance liquid chromatography (HPLC)[20]. The encapsulation percentage (EP) was calculated using the following equation:

$$EP = \frac{[PTX]purified\ liposomes}{[PTX]non\ purified\ liposomes} \text{x } 100. \quad (1)$$

The data reported were expressed as the mean (±) standard deviation of at least three different liposomal formulation measurements.

2.4.5 Phospholipid Quantification

The phospholipid concentration was determined by measuring phosphorus concentration using the Bartlett method [22] with some modifications. Aliquots of 25, 50, 100, 150 and 200 µL of phosphorus standard solution (0.65 nmol/L) and an appropriate amount of the liposome samples (containing about 30 nmol phospholipids) were transferred to glass tubes. Next, 0.4 mL of perchloric acid 70% (v/v) was added, and the tubes were incubated for 30 min at 180°C in a pre-heated heating block. Thereafter, the tubes were cooled to room temperature, and 0.2 mL of ammonium molybdate solution 5.0% (w/v) and 50 µL of 4-amino-2-naphthyl-4-sulfonic reagent were added. The tubes were vigorously vortex-mixed and heated again at 90 °C for 7 min. Finally, the intensity of the blue color was analyzed on a spectrophotometer (Evolution 201 UV-Visible Spectrophotometer Thermo Scientific, USA) at a wavelength of 830 nm. A standard curve was constructed by plotting mass (0.5, 1.0, 2.0, 3.0, and 4.0 µg) *vs.* absorbance.

The linear regression equation was $y = 0{,}2559x + 0{,}043$ (r = 0.9977), where y is the absorbance of phosphorus standard solution and x is the mass of phosphorus present.

3 Results

3.1 SAXS Analysis

In order to evaluate the effect of the pH on the phase behavior of DOPE, SAXS analyses of SpHL and SpHL-PTX were conducted at 25°C after resuspension in NaCl 0.9% (w/v) or DMEM culture medium at pH 7.4, 6.8 and 5.0 (Figure 1).

Figure 1 - SAXS patterns of liposomal formulations prepared at 25°C in NaCl 0.9% (w/v) and DMEM at pH 7.4, 6.8 and 5.0. The indexes (peak labels) represent phases that can be identified by the periodicity of the Bragg reflections. Red and blue indexes are related to a lamellar phase while green and pink indexes (which include square-root labeled peaks) represent the hexagonal phase.

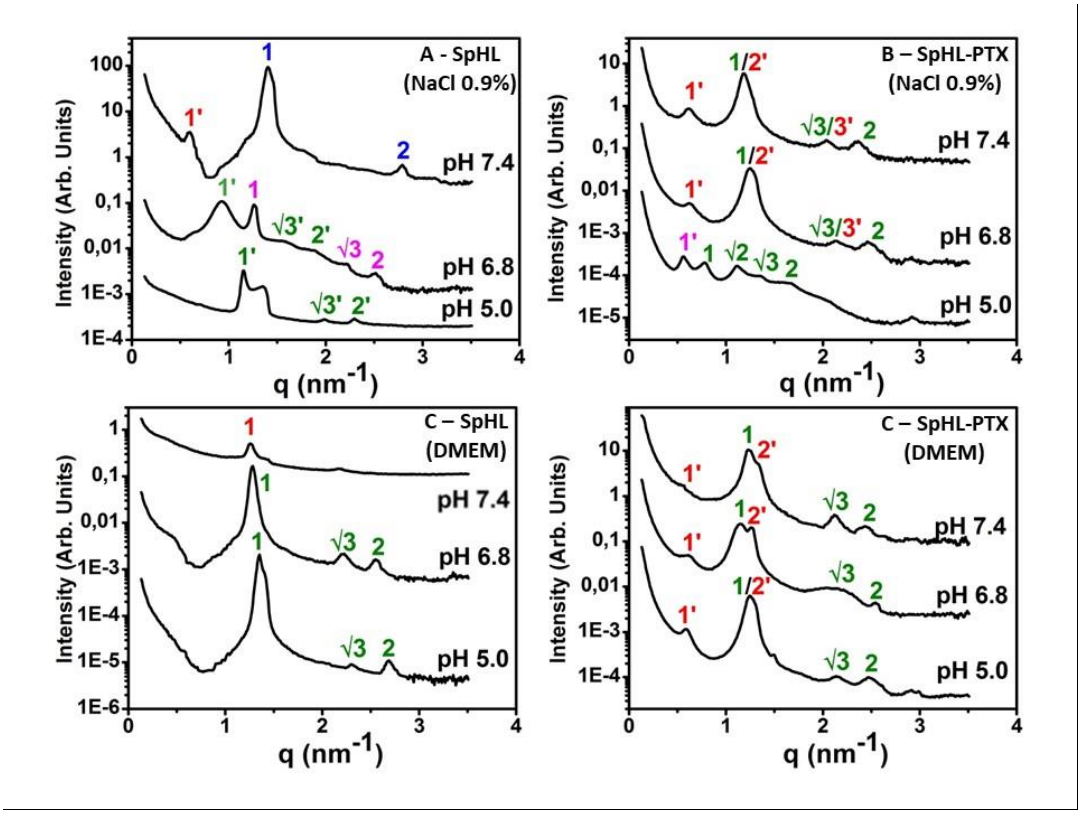

At pH 7.4, the coexistence of two lamellar domains could be observed in the diffraction patterns of SpHL prepared in NaCl (0.9%, w/v) (Figure 1A). The first type of order (red index) exhibits

a peak at q = 0.6 nm−1, for which it could not be attributed to highest-order Bragg indices, but points a lattice spacing value of 10.47 nm, characteristic of lamellar regions enriched with DSPE−PEG2000. The second sequence of SAXS peaks (blue indexes) presented q = 1.40 and 2.79 nm−1, with Bragg indices of nearly 1 and 2, respectively, and lattice parameter equals to 4.49 nm, showing a lamellar phase organization of DOPE molecules. On the other hand, at pH 6.8, the coexistence of two ordered structure types, both in hexagonal phases, could be verified. The first nonlamellar order presented SAXS peaks at q = 0.93, 1.56, and 1.88 nm−1, whereas q values for the second sequence of peaks were found at q = 1.26, 2.21, and 2.51 nm−1. Both sequences show a periodicity of Bragg reflections with ratios close to 1, √3, and 2 and retrieved lattice spacings of 6.76 and 4.99 nm. This result showed the occurrence of a lamellar−hexagonal DOPE phase transition after pH reduction. SAXS measurements acquired at pH 5.0 revealed significant changes in the sample diffraction pattern. A single sequence of peaks, located at q = 1.15, 1.99, and 2.30 nm−1, with Bragg index ratios close to 1, √3, and 2, respectively, was observed. This also suggests a hexagonal phase organization of DOPE with a lattice spacing of 5.46 nm.

Figure 1B shows the results from SAXS of SpHL-PTX prepared in NaCl 0.9% (w/v) at different pH. At pH 7.4, the occurrence of two different ordered structures in the system was detected. The first type of order (red indexes) presented a sequence of peaks with q = 0.63, 1.18, and 2.00 nm^{-1} (Bragg index ratios of approximately 1, 2, and 3), and correspond to a lamellar lattice spacing of 9.97 nm, probably related to a region with high concentration of DSPE-PEG_{2000}. The second order type (green indexes) is found to present hexagonal order, exhibiting Bragg index ratios of approximately 1, √3 and 2 (q values at 1.18, 2.00 and 2.36 nm^{-1}) and a lattice parameter of 5.32 nm. The two SAXS peaks identified at q values of 1.18 nm^{-1} and 2.00 nm^{-1} are a superposition of peaks from both ordered structures (they are larger and present humps or shoulders). Interestingly, peaks representing the lamellar phase (red indexes) exhibit higher intensity – known to be proportional to the ordered volume – than the hexagonal ones, suggesting that lamellar is the dominant ordered structure type. No significant change in the phase organization of the systems could be identified at pH 6.8, but a shift on q positions to higher values was observed in comparison to pH 7.4. At pH 5.0, SAXS revealed a peak sequence located at q = 0.55, and 1,1 nm^{-1}, which could be attributed to a lamellar phase. The lattice parameter for this region was found to be of 11.22nm, suggesting again the presence of DSPE-PEG_{2000} molecules in high concentration. Another sequence of peaks identified at q = 0.78, 1.35, and 1.64 nm^{-1} with Bragg index ratios of nearly 1, √3, and 2 was found in this sample, pointing out to the formation of a hexagonal-ordered DOPE molecules. Since changes

in the q position and the shape of the peaks were observed, the data showed again that the presence of PTX did not modify the pH-sensitivity of the liposomes.

Diffraction patterns of SpHL and SpHL-PTX re-suspended with culture medium (DMEM) are shown in Figures 1C and 1D, respectively. In this case, SAXS measurements were obtained at 25°C and 37°C. The analysis carried out on SpHL at pH 7.4 revealed the presence of only one peak with q = 1.35 nm^{-1} and a correspondent lattice spacing of 4.65 nm. This result, compared to those for SpHL in NaCl at pH 7.4 (Figure 1A), suggests interactions between SpHL and DMEM constituents that could driving the system into a short-range ordered state. At acidic pH (6.8 and 5.0), a sequence of peaks suggesting a hexagonal organization, with q= 1.28, 2.21, and 2.55 nm^{-1}(ratio of Bragg reflection positions equals to 1, √3, and 2), and lattice spacing equivalent to 4.90 nm were observed. Although lipid bilayer and culture medium showed some interaction, the pH-sensitivity was not impaired in the presence of DMEM. For the SpHL-PTX condition, a coexistence of lamellar and non-lamellar organization was also verified at pH 7.4 (Figure 1D). The lamellar phase was identified at q = 0.61 and 1.30 nm^{-1} with Bragg indexes of 1' and 2', while a second order type revealed peaks located at q = 1.23, 2.13, and 2.47 nm^{-1}, corresponding to Bragg reflection position ratios close to 1, √3, and 2, characteristic of a hexagonal organization of DOPE. In this condition the hexagonal order showed higher intensity (volume of ordered material) than those observed in Figure 1 B, at pH 7.4. The lattice spacing obtained for the first and the second order types (that correspond to lamellar and hexagonal phases) were 10.30 nm and 5.11 nm, respectively. This difference can be a consequence of a heterogeneous distribution of lipid components within the lipid bilayer. Similar scattering patterns were obtained at pH 6.8 and 5.0, although a discrete shifts and peak width changes were noted, suggesting a slight modification in domain size and lattice spacing in the supramolecular organization of DOPE (which, nevertheless, keeps the packing symmetry).

In addition, SpHL-PTX samples were heated at 37.0 °C to simulate *in vivo* conditions (data not showed). The same Bragg reflections and supramolecular organization were observed as those obtained at 25.0 °C at the three pH evaluated. Therefore, an increase in the temperature did not modify the characteristics of SpHL-PTX, especially pH-sensitivity.

Figure 2 - Schematic analysis of SAXS peaks from Figure 1. The data depicted here is obtained from the analysis of peaks 1' and 2 from Figures 1 B and 1 D, and peak 1 from Figure 1 C. Figures A and B are related to SpHL-PTX in NaCl 0,9% (Figure 1B), showing lattice spacing and domain size values, respectively, for the lamellar (left panels) and hexagonal phases (right panels). Figure C refers to SpHL in DMEM (Figure 1C), showing lattice spacing (left panel) and domain size (right panel) for the lamellar phase. Figures D and E refer to data from SAXS on SpHL-PTX in DMEM (Figure 1D), showing lattice spacing and domain size values, respectively, for the lamellar (left panels) and hexagonal phases (right panels).

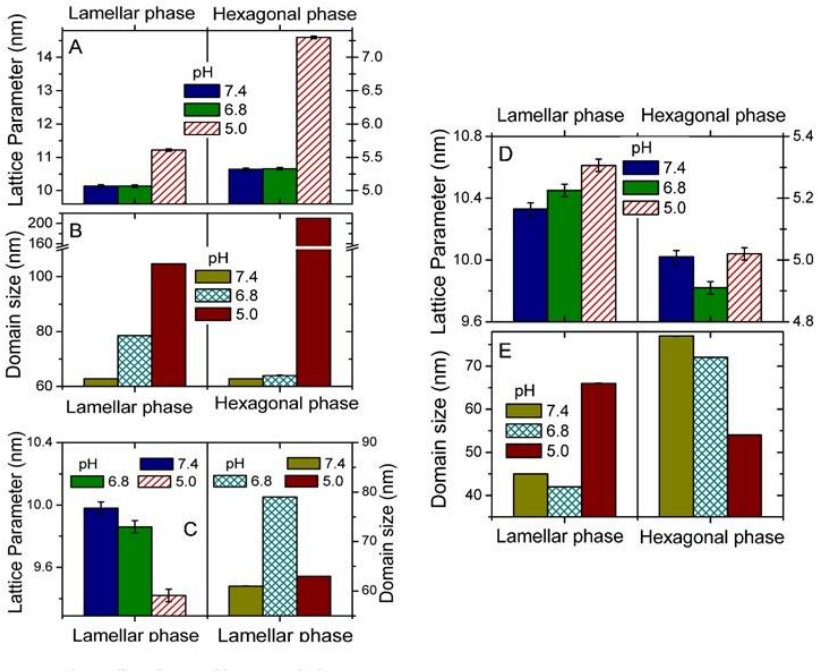

An overview of lattice spacing and domain size information extracted from SAXS peak position and width, respectively, is shown in Figure 2 (see discussion section for details). Here the dataset of Figure 1(a) was not graphically explored since distinct phases appear in the SpHL (NaCl 0.9%) formulation. Among the other datasets results on lamellar and hexagonal phases were compared. The evaluation of SAXS data from Figure 1(b) [SpHL-PTX (NaCl 0.9%)] is graphically summarized in Figure 2 (a) and 2(b), while the analysis of the data of Figure 1(c) [SpHL (DMEM)] is shown in Figure 2 (c). Finally, the SAXS results of Figure 1(d) [SpHL-PTX (DMEM)] is shown in Figures 2 (d) and 2(e).

It is already reported that the presence of serum proteins might influence the stability of liposomes[26]. Therefore, we evaluated supramolecular changes in SpHL and SpHL-PTX prepared in FBS-supplemented DMEM at three pH (7.4, 6.8 and 5.0) and two temperatures (25°C and 37°C). At 25°C (pH 7.4, 6.8 or 5.0), both liposomes showed a unique broad peak

with low intensity and no high-order Bragg indexes could be attributed to these systems. Nevertheless, a shift in the *q* position and shape of the peaks suggestive of with interactions FBS proteins, can clearly be observed in Figure 3 (see discussion section). Similar results were obtained at 37°C (data not shown here).

Figure 3 - SAXS patterns of SpHL and SpHL-PTX prepared in culture medium DMEM FBS-supplemented at pH 7.4, 6.8 and 5.0, obtained at 25°C.

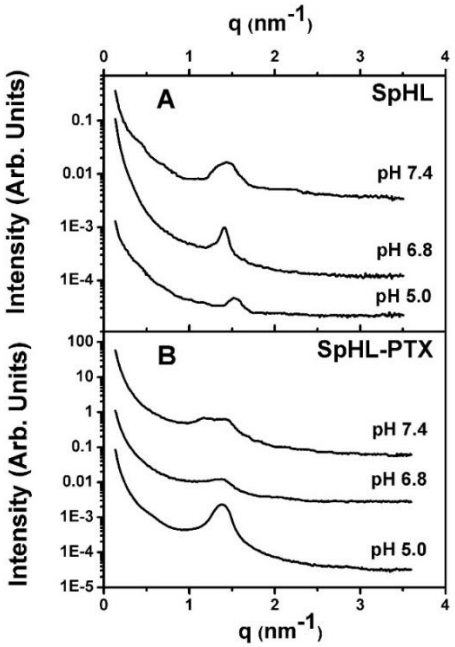

Finally, we evaluated the effects of the temperature on phase transitions of DOPE. The SAXS patterns were obtained in a temperature range from 0° C to 50°C by heating SpHL-PTX (NaCl 0.9% (w/v) at pH 7.4) at a rate of 5°C/min (Figure 4).

One notices here that the coexistence of lamellar and hexagonal phases is observed throughout the whole temperature ramp. The presence of peaks at *q* values equal to 0.56, 1.16, and 1.90 nm^{-1} (Bragg index ratios of 1, 2, and 3), and *q* = 1.13, 1.90 and 2.33 nm^{-1} (Bragg index ratios of nearly 1, √3 and 2), characterize the lamellar and hexagonal phases, respectively. The lattice parameter obtained was equivalent to 11.22 nm and 5.56 nm, which characterize domains with high and low density of DSPE-PEG_{2000}, respectively. As previously described, the peak at *q* values of 1.16 nm^{-1} and 1.90 nm^{-1} (red and blue indexes) consists of two overlapped peaks (better observed at the 1/2' peak, where a hump is observed for higher q values with respect to the peak apex), implying the concurrence of two domains. The intensity of peaks, proportional to the volume o ordered structures in a given phase, indicates that hexagonal and lamellar phases present roughly similar volumetric content in these samples. No phase transition of the

structural lipid from lamellar and hexagonal phases into other supra-molecular organization was observed.

Figure 4 - (A) SAXS patterns of SpHL-PTX prepared in NaCl 0.9% (w/v) at pH 7.4 obtained at different temperatures. The indexes (peak labels) represent phases, which can be identified by the periodicity of the Bragg reflections. Red indexes are related to a lamellar phase and blue indexes are related to the hexagonal phase. Arrows indicate intensity increase (↑), intensity decrease (↓) and peak narrowing (→←). (B) Normalized order parameter (relative phase content) for the lamellar (solid dots) and hexagonal (open dots) phases, using the integrated area below the 1' (lamellar) and 2 (hexagonal) peaks of Figure A. (C) Lattice spacing as a function of the temperature, extracted from measured positions of peaks 1' (lamellar phase, solid dots) and 2 (hexagonal phase, open dots) of figure A. (D) Ordered domain size obtained from peaks 1' (lamellar phase, solid dots) and 2 (hexagonal phase, open dots) of Figure A. In panels (B), (C) and (D) the solid lines are guides to the eyes only.

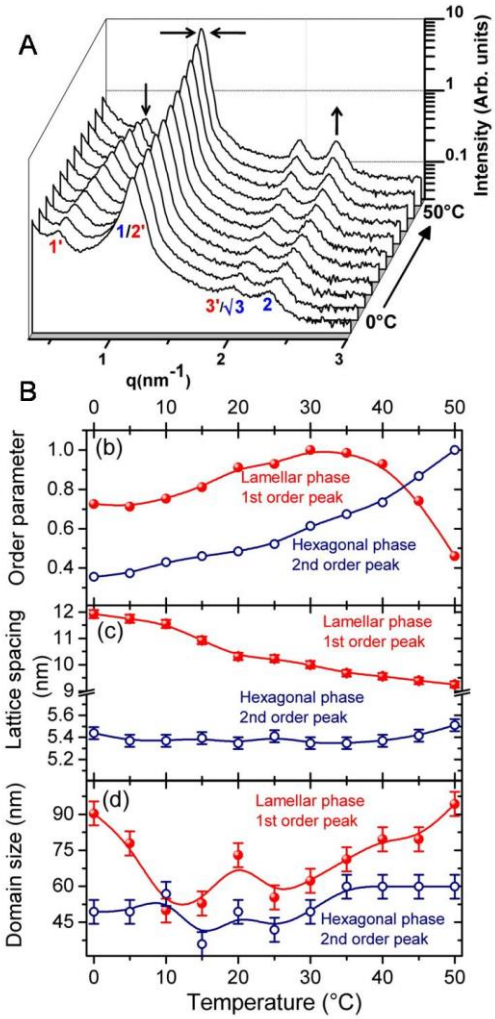

A relative order parameter analysis, consisting of plots of the normalized area of the first lamellar peak and the second (√3) hexagonal peak is shown in Figure 4B. This plot quantitatively shows the evolution of a phase volume as temperature shifts, relative to its volume in a reference temperature (the maximum peak area is normalized to unity). One observes that the maximum volume of lamellar phase is retrieved close to 31°C, followed by a rapid decrease in the temperature interval between 40°C and 50°C. Otherwise, the hexagonal order parameter increases monotonically in the temperature range as the temperature increases. Although a high order hexagonal phase peak was used here its intensity behavior is compatible with the first peak of hexagonal packing, which becomes narrower and more intense in Figure 4 A near 50°C due to the shrink the intensity hump that corresponds to the second order lamellar peak (labeled 2'). Figure 4 C depicts the lattice spacing extracted from the first-order lamellar phase (1') and the second-order hexagonal phase (2) peak positions. One observes a 15 % decrease in the lamellar phase lattice spacing from the low to the high temperature range probed, while the hexagonal phase lattice does not vary considerably (fluctuations within the error bar). This can be an indication that intra-lamellar material in the lamellar phase is expelled or re-organized at large temperature values. The ordered domain size, evaluated in Figure 4 D also remains mostly unchanged for the hexagonal phase, exhibiting large values for the lamellar phase at the lowes and highest probed temperatures. In this last case, the results may be explained by a change in the size distribution as temperatures span from 0°C to 30°C (favoring smaller structures). In this interval the order parameter of lamellar phase (Figure 4 B) increases, indicating the system is driven towards the formation of a larger number of small liposomes. From 30°C to 50°C, the lamellar phase order parameter decreases (Figure 4 B), indicating that lamellar order becomes less favorable. In such condition, small liposomes cease to form and only large liposomes with lamellar order are stable (Figure 4 D).

3.2 Physicochemical properties of SpHL and SpHL-PTX

The physicochemical properties of SpHL and SpHL-PTX are summarized in Table 1. The mean diameter of SpHL-PTX was significantly higher than SpHL, leading to a 20% increase in diameter after PTX incorporation. The low PDI values, near 0.2, are consistent with homogeneously dispersed systems. Zeta potential values near to neutral range were verified for SpHL and SpHL-PTX. In addition, high encapsulation efficiency of PTX (~ 90%) was obtained. This finding could be explained by a strong interaction between PTX and hydrocarbon chains of the lipids due to the well-known lipophilic nature of PTX[3,9-11]. No significant loss in

phospholipids was observed for SpHL-PTX (98.1 ± 2.2) and the drug-to-lipid molar ratio in SpHL-PTX was 0.09 ± 0.003.

Table 1 - Physicochemical characterization of liposomal systems.

Parameters	SpHL	SpHL-PTX
Diameter ± SD (nm)	129 ± 6	156 ± 5[a]
PDI ± SD	0.21 ± 0.01	0.23 ± 0.01
Zeta Potential ± SD (mV)	-3.1 ± 0.3	-4.1 ± 1.4
Encapsulation Percentage (%)	-	89 ± 2
Drug-to-lipid molar ratio	-	0.090 ± 0.003

[a]represents significant difference as compared with liposomal formulation without PTX. Data expressed as the mean ± standard deviation (SD) of three batches. *P*-values less than 0.05 were set as the level of significance (Tukey's test). PDI, polydispersity index

Table 2 - Asymmetric flow field flow fractionation data of the liposomes.

Technique	Parameter	SpHL (Mean± SD)	SpHL-PTX (Mean±SD)
MALS (nm)	Peak D_g[b](nm)	98 ± 3	117 ± 2
	D_{10} (nm)	45 ± 3	40 ± 4
	D_{50} (nm)	117 ± 3	142 ± 1
	D_{90} (nm)	276 ± 3	311 ± 5
	D_n (nm)	97 ± 2	106 ± 2
	D_w (nm)	127 ± 2	149 ± 6
	D_z(nm)	166 ± 3	198 ± 11
	PdI (D_w/D_n)	1.3	1.4
DLS (nm)	Peak D_h[b] (nm)	127 ± 7	151 ± 4
Form Factor	D_g/D_h[b]	0.77 ± 0.06	0.77 ± 0.01

[a] Gyration diameters determined by multi-angle light scattering (MALS) in flow mode.
[b] calculated at peak maximum.
D_n, D_w, D_z, number, weight and Z-average gyration diameters.PDI,polydispersity index,
D_{10}, D_{50}, D_{90}, gyration diameters corresponding to 10, 50 and 90% of the intensity-weighted distributions.
Data expressed as mean ± standard deviation (SD) of three measurements.

SpHL and SpHL-PTX were also submitted to fractionation by AF4, whereby the nanometer-sized particles eluted as a function of their hydrodynamic diameter (Figures 5 A and B). Absolute particle diameter determination was achieved with hyphenated MALS and DLS

characterization in flow mode (Table 2). An increase in hydrodynamic diameter upon PTX loading from 127 to 151 nm was also determined. A slight widening of the diameter-distribution was observed in the PTX-loaded liposome (Figure 5 C), corresponding to an increase in the proportion of larger liposomes.

Figure 5 - Asymmetric flow field flow fractionation results. Fractograms with UV detector signal (black line), gyration diameters (blue solid dots) and hydrodynamic diameters (blue open circles) for SpHL (A) and SpHL-PTX (B). Comparison between gyration diameter distributions (C) of the SpHL (black line) and SpHL-PTX (grey line). Dg: gyration diameter, by multi-angle light scattering; Dh: hydrodynamic diameter, by dynamic scattering.

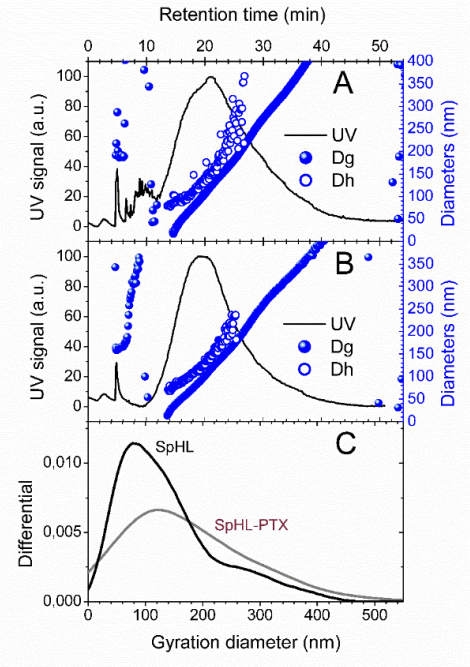

Nonetheless, the size distribution remained monomodal and relatively narrow with polydispersity index of 1.3 and 1.4 for SpHL and SpHL-PTX, respectively (Table 2). The shape factor value was 0.77 for both liposomal formulations. The images of SpHL and SpHL-PTX obtained by TEM are shown in Figure 6. Both liposome systems are observed as quasi-spherical vesicles (some of them are slightly elongated). Although TEM measurements without cryogenic capabilities (cryo-TEM) do not allow for a reliable reproduction of the liposome morphology in a liquid environment, they unambiguously and directly provide the type of lamellar configuration (single- or multi-lamellar) in the studied systems. Among our samples all liposomes exhibited multilamellar structure with observed diameters smaller than 200 nm, which is consistent with the results obtained by DLS and AF4-MALS-DLS (Tables 1 and 2).

Figure 6 - TEM photomicrographs obtained for SpHL (A and B) and SpHL-PTX (C and D) in different fields. The black arrows indicate multilamellar liposomes.

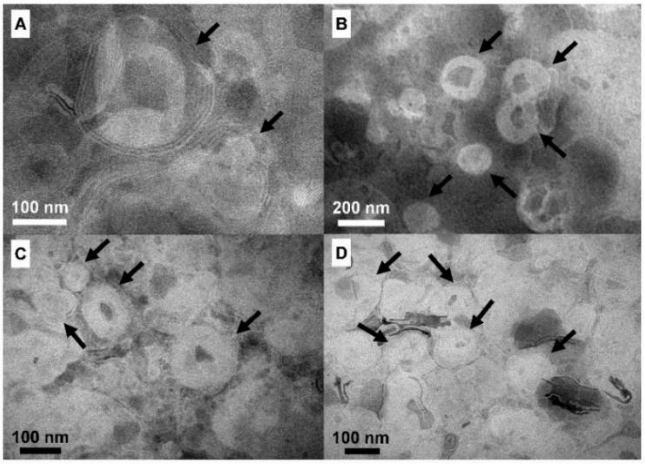

4 Discussion

pH-sensitive liposomes have emerged as an interesting approach to improve therapeutic efficacy of many antitumor drugs. These nanosystems are designed to explore the acidification process that occurs in the tumor extracellular matrix as well as within the endosomes. It is well described that liposomes are internalized through the endocytic pathway and, once into endosomes, exposed to lower pH (~5.0). At such an acidic pH, liposomes may fuse with or destabilize the endosome membrane, releasing the entrapped drug into the cytoplasm[13,16,19,21]. Additionally, the extracellular tumor area is, typically, characterized by a slightly acidic environment. Previous studies have demonstrated a significant release of PTX from SpHL at pH 6.8[9,16,23,24]. On the other hand, in order to reach the tumor site, pH-sensitive liposomes must be stable in biological fluids at a physiological pH. In this context, changes in the supramolecular organization of structural lipid such as transition from lamellar to non-lamellar phases after exposure to an acidic condition has a pivotal role in the antitumor activity[11,13,17,19]. Based on these findings, possible disturbances in the supramolecular organization of DOPE should be addressed in order to attain substantial information of a new formulation for tumor therapy. Therefore, physicochemical characteristics and supramolecular analyses of the pH-sensitive liposomes were deeply studied after incubation with different media (NaCl 0.9% w/v, DMEM, and DMEM with 10% FBS) at three different pH (7.4, 6.8 and 5.0).

Data obtained for liposomes in NaCl 0.9% clearly demonstrated that SpHL and SpHL-PTX are stable at physiological pH (pH 7.4), but undergo destabilization under acidic conditions (Figure 1A and B). At pH 7.4, the coexistence of lamellar and hexagonal domains may be due to a heterogeneous distribution of CHEMS molecules inside the bilayer. These domain structure types are found in similar volume in our formulation. These findings can be confirmed by the presence of liposomal vesicles in the microscopy analysis and DLS. Previous studies also showed the same event in mixtures of DOPE:CHEMS:DSPE-PEG_{2000}[10,11]. In addition, DOPE transition from lamellar to non-lamellar (hexagonal) phases at pH 5.0 suggests that pH-sensitivity was not troubled by PTX incorporation. These results are in agreement with previous studies, which showed the ability of SpHL- to release about 75.0% of their content under an acid environment[9].

An important issue for *in vitro* and *in vivo* application of pH-sensitive liposomes is the interaction of the liposome bilayer with biological fluid components, which may disturb the pH-sensitivity properties [14]. As afore mentioned, the presence of one peak for SpHL at pH 7.4 suggests a possible interaction between SpHL and culture medium components (Figure 1C); but the alterations observed in the SAXS peaks at pH 6.8 and 5.0 indicate that the absence of a direct modification of expected phase transitions of the DOPE molecules. On the other hand, the coexistence of lamellar and non-lamellar phase could be observed at all pH conditions, suggesting higher membrane stability for SpHL-PTX. This finding might indicate the stability of SpHL-PTX subjected to in-vivo blood circulation, which assure the integrity of liposomes from the injected site to the therapeutic target.

The SAXS data evaluation shown in Figure 2 (a) indicates that the lattice spacing of SpHL-PTX (NaCl 0.9%) liposomes considerably increases for a pH value of 5.0 for both lamellar and hexagonal phases, while values retrieved at pH 7.4 and 6.8 are similar. This trend is followed by an increase in liposome ordered domain size for both phases in low pH values, if compared to pH 7.4 and 6.8. Although the overall order of the hexagonal phase is reduced at pH 5.0 (lower intensity observed in the hexagonal peaks), this may indicate that the population of small liposomes (size < 80 nm) is reduced at this condition with respect to larger liposomes (size > 80 nm) or that a coalescence of small liposomes into larger ones take place. These larger structures would then present the observed distinct lattice spacing.

Lattice spacing and domain size remain similar for all pH conditions of liposomes in the SpHL (DMEM) formulation, as shown in Figure 2(c). In such condition the values retrieved from SAXS analysis vary less than 10% and 20% for lattice spacing and ordered domain size, respectively.

At the SpHL-PTX (DMEM) formulation, reduced changes are observed in the lattice spacing of lamellar and hexagonal phases [Figure 2(d)]. However, larger ordered domain sizes are favored for the hexagonally packed structures at pH values of 7.4 and 6.8. This tendency is inverted for pH 5.0, where liposomes in lamellar phase clearly exhibit larger domain sizes [see Figure 2(e)]. One must notice here that the volume of ordered material in a given phase depends only on the area below a SAXS peak ascribed to this phase. On the other hand, domain size is inversely proportional to the peak width. The interplay between both variables is only evaluated through the experimental data analysis. Here, in pH 5.0, the SpHL-PTX (DMEM) formulation presents a lower volume of lamellar ordered phase. This is indicated from the fact that the lamellar peak 2' merges into the hexagonal peak 1 [Figure 1D], without a clear hump as observed in higher pHs (which denotes its lower intensity compared to peak 1). Nevertheless, in this condition the domain size is larger, which can be understood in a scenario where only large liposomes are stable, alhtouh they exist in an overall smaller volume.

The addition of FBS in the dispersion medium leads to less ordered DOPE molecules (Figure 3) compared to dispersions in NaCl 0.9% w/v (Figure 1 A and B). Similar results were previously reported for liposomes composed of DOPE:CHEMS [15]. The short-range order, which arises from a chemically more complex multi-component system is experimentally evidenced by the presence of the first-order SAXS peaks solely (large order peaks vanish). The large entropy of mixing in such conditions takes place since a larger amount of molecular species compete for the interaction with the surface of liposomes. The long-range spatial registry of multi-lamellar systems is then scrambled with respect to the same system in a less complex environment. In our particular case, interaction between liposomes and serum proteins may result in changes in their membrane fluidity, stability, and pharmacokinetic profile, which may reduce the drug concentration at the target tumor sites [25-27]. Despite the presence of PEG (a molecule that should limit the adsorption of proteins) our observations indicate that probably a small fraction of the liposomal surface may loose its polymer coverage (see SAXS results). In this sense, the interaction with proteins cannot be ruled out. Nevertheless, a shift in the q position and in the shape of the peaks suggest that pH-sensibility was not completely disturbed.

SpHL and SpHL-PTX showed mean diameters smaller than 200 nm by batch DLS and AF4-MALS-DLS, which is suitable for intravenous administration[28]. Although an increase in diameter of about 20 nm was observed upon PTX loading, it is important to mention that the size distribution remained similar (Tables 1 and 2). In addition, for SpHL-PTX, 90 % of the

liposome sample weight-averaged distribution corresponded to diameters lower than 310 nm (by DLS in flow mode) and no large liposomes or aggregates (D_h > 500 nm) could be detected. Small particles may favor passive targeting of liposomes to tumor tissues through the enhanced permeability and retention (EPR) effect, due to the overexpression of fenestrations in the neovasculature[7,16,29-31]. Eventhought, a number of studies have shown that small liposomes (diameter < 200 nm) are more stable in serum than larger ones (diameter > 600 nm) due to differences in lipid packing that determines surface pressure in the membrane [13,17,28]. Furthermore, zeta potential is another important parameter to guarantee the adequate stability of colloidal systems. Although high zeta potential is reported as more adequate for vesicle stability, in this specific case, values near to neutral range observed for both liposomes might be attributed the presence of DSPE-PEG_{2000} which leads to low electrophoretic mobility due to the great hydrodynamic resistance[9,21,32-34]. The presence of PEG generates a hydrophilic layer at the liposomes that protects them from fusion, aggregation, and opsonin adhesion. This might contribute to an extended circulation of the liposomes *in vivo* that would consequently favor their accumulation in the tumor[9,35-39].

Additional morphological information could be drawn from the simultaneous determination of diameters by MALS and DLS in flow mode, by determining the D_g/D_h ratio, called shape factor. For both SpHL and SpHL-PTX, the shape factor value was 0.77, very close to the theoretical value of 0.775, which is characteristic of spherical particles with uniform density distribution[40]. Other authors reported shape factor values close to 1.0, characteristic of hollow spherical vesicles, for liposomes with different compositions and unilamellar structure[41-43]. The lower value obtained in our case indicates that the vesicles, whether they contained PTX or not, presented light scattering centers evenly distributed throughout the nanostructure volume, and therefore were not likely to be unilamellar. This result was confirmed by TEM analysis (Figure 6). Images obtained for SpHL and SpHL-PTX were consistent with the particle diameters measured by DLS and MALS, showing mostly multilamellar spherical vesicles with diameters lower than 200 nm.

The scheme shown in Figure 7 summarizes the essential results obtained in this study: 1) A stable nanosized dispersion of PTX in water and in isotonic medium was obtained, with the predominance of multilamellar structures; 2) At pH 7.4 stability in the different media was achieved, suggesting that the system may be able to resist changes in the blood circulation and maintain the formulation integrity to the therapeutic target; 3) Under pH conditions mimicking the endosome environment (pH 5.0), the pH-sensitivity of the system was clearly evidenced by changes in the supramolecular organization of DOPE molecules under conditions of excess

water. This change is crucial for the delivery of PTX into the cytoplasm of the targeted cancer cells, which could enhance the concentration and consequently the antitumor activity of this drug.

Figure 7 - Sketch of a possible scenario for liposomal compounds organization in a multilamellar structure with nanometric size and high encapsulation percentage of PTX. When in the presence of different media (NaCl 0.9% w/v, DMEM, and DMEM with 10% FBS) at different pH (7.4, 6.8 and 5.0), our data analysis points to changes in the supramolecular organization of the DOPE. The size of liposomes in the illustration are merely illustrative.

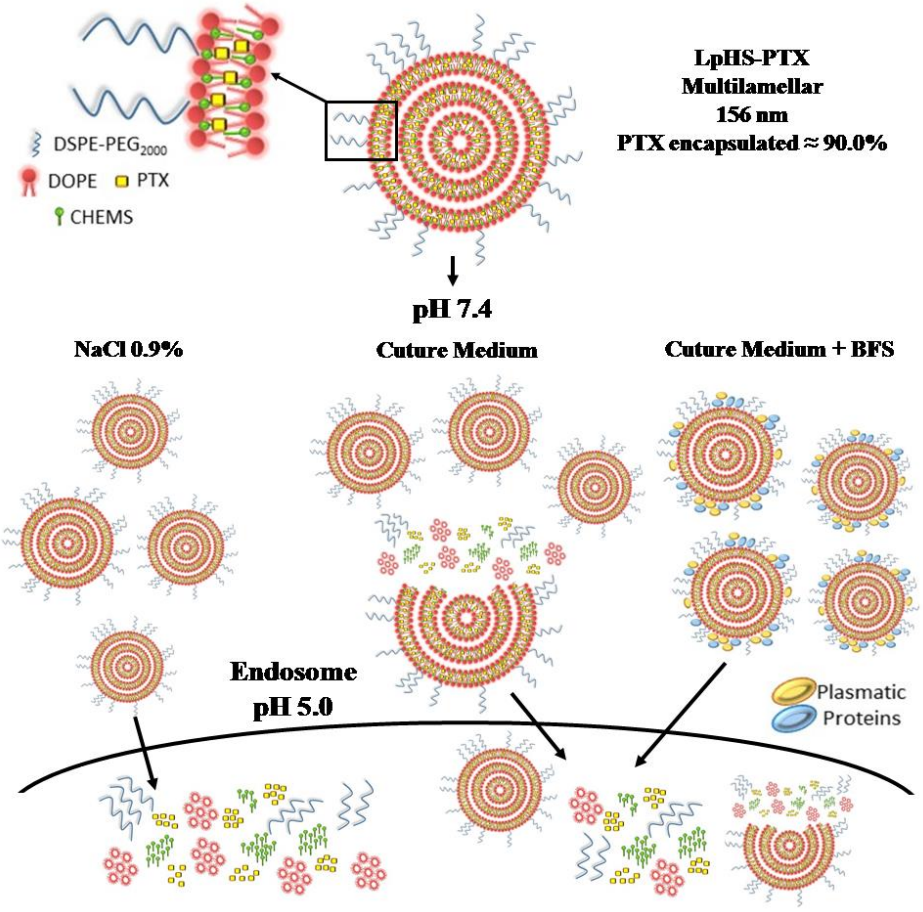

5 Conclusion

The present study demonstrates that the inclusion of PTX in the liposomal bilayer clearly leads to changes in the supramolecular organization of DOPE molecules in fully hydrated conditions.

The formation of more ordered structures did not affect the pH-sensitivity of the SpHL-PTX since changes in supramolecular organization were observed at lower pH, even in the presence of FBS proteins. Moreover, morphological and physicochemical characterization of SpHL-PTX indicate suitable parameters for intravenous administration.

Acknowledgement

The authors would like to thank FAPEMIG, CAPES, CNPq and LNLS (Campinas, Brazil) for their financial support. In addition, Liziane O. F. Monteiro is grateful to CAPES for providing a scholarship.

References

1. Peer, D.; Karp, J. M.; Hong, S.; FaroKHzad, O. C.; Margalit, R.; Langer, R. Nanocarriers as an ememerging platform for cancer therapy. Nat. Nanotechnol. 2007, 2, 751-760.
2. Joo, K.; Xiao, L.; Liu, L.; Liu, S.; Lee, Y.; Conti, C.; Wong, P. S.; Li, M. K.; Wang, Z.P. Crosslinked Multilamellar Liposomes for controlled delivery of anticancer drugs. Biomaterials 2013, 34, 3098-3109.
3. Koudelka, S.; Turánek, S. Liposomal paclitaxel formulations. J. Control. Release 2012, 163, 322-334.
4. Iwamoto, T. Clinical application of drug delivery systems in cancer chemotherapy: review of the efficacy and side effects of approved drugs. Biol. Pharm. Bull. 2013, 36, 715-718.
5. Chan, J. K.; Brady, M. F.; Penson, R. T.; Huang, H.; Birrer, M. J.; Walker, J. L.; DiSilvestro, P. A.; Rubin, S. C.; Martin, L. P.; Davidson, S. A.; Huh, W. K.; O'Malley, D. M.; Boente, M. P.; Michael, H.; Monk, B. J. Weekly vs. every-3-week paclitaxel and carboplatin for ovarian cancer. N. Engl. J. Med. 2016, 374, 738-748.
6. Laouini, A.; Jaafar-Maalej, C.; Limayem-Blouza I.; Sfar, S.; Charcosset, C.; Fessi, H. Preparation, Characterization and applications o liposomes: state of the art. J. Colloid Sci. Biotechnol. 2012, 1, 147-168.
7. Sawant, R. R.; Torchilin, V. P. Challenges in development of targeted liposomal therapeutics. AAPS 2012, 14, 303-315.
8. Nogueira, E.; Gomes, A. C; Preto. A.; Cavaco-Paulo, A. Design of liposomal formulation for cell targeting. Coll. Surf. B. 2015, 136, 514-426.
9. Barbosa, M. V.; Monteiro, L. O. F.; Carneiro, G.; Malagutti, A. R.; Vilela, J. M. C.; Andrade, M. S.; Oliveira, M. C.; Carvalho-Junior, A. D.; Leite, E. A. Experimental design of a liposomal lipid system: a potential strategy for paclitaxel-based breast cancer treatment. Coll. Surf. B. 2015, 136, 553-561.
10. Lopes, S. C. A.; Novais, M. V. M.; Ferreira, D. S.; Braga, F. C.; Magalhães-Paniago, R.; Malachias, A.; M.C. Oliveira, Ursolic Acid Incorporation Does Not Prevent the Formation of a Non-lamellar Phase in pH-Sensitive and Long-Circulating Liposomes. Langmuir 2014, 30, 15083 –15090.

11. Monteiro, L. O. F.; Lopes, S. C. A.; Barros, A. L. B.; Magalhães-Paniago, R.; Malachias, A.; de Oliveira, M. C.; Leite, E. A. Phase behavior of dioleyphosphatidylethanolamine molecules in the presence of componentes of pH-sensitive liposomes and paclitaxel. Coll. Surf. B. 2016, 144, 276-283.
12. Siegel, D. Inverted micellar intermediates and the transitions between lamellar, cubic, and inverted hexagonal lipid phases. II. Implications for membrane-membrane interactions and membrane fusion. Biophys. J. 1986, 49, 1171-1183.
13. de Oliveira, M. C.; Fattal, E.; Couvreur, P.; Lesieur, P.; Bourgaux, C.; Ollivon, M.; Dubernet, C. pH-sensitive liposomes as a carrier for oligonucleotides: a physic-chemical study of the interaction between DOPE and 15-mer oligonucleotide in quasI-anhydrous samples. Biochim. Biophys. Acta 1998, 1372, 301-310.
14. Simões, S.; Moreira, J. M.; Fonseca, C.; Duzgunesand, N.; Lima, M. C. P. On the formulation of pH-sensitive liposomes with long circulation times. Adv. Drug. Deliv. Rev. 2004, 56, 947-965.
15. Silva, S. M. L.; Coelho, L.; Malachias, A.; Perez, C. A.; Pesquero, J. L.; Paniago, R. M.; de Oliveira, M. C. Study of the structural organization of cyclodextrin-DNA complex loaded anionic and pH-sensitive liposomes. Chem. Phys. Lett. 2011, 506, 66-70.
16. Ferreira, D. S.; Lopes, S. C. A.; Franco, M. S.; de Oliviera, M. C. pH-sensitive liposomes for drug delivery in cancer treatment. Ther. Deliv. 2013, 4, 1-24.
17. De Oliveira, M. C.; Rosilio, V.; Lesieur, P.; Bourgaux, C.; Couvreur, P.; Ollivon, M.; Dubernet, C. pH-sensitive liposomes as a carrier for oligonucleotide in excess water. Biophys. Chem. 2000, 87, 127-137.
18. Gentile, E.; Cilurzo, F.; Marzio, L. D.; Carafa, M.; Ventura, C. A.; Wolfram, J.; Paolino, D.; Celia, C. Liposomal chemotherapeutics. Future Oncol. 2013, 9, 1849–1859.
19. Mallick, S.; Choi, J. S. J. Liposomes: Versatile and Biocompatible Nanovesicles for Efficient Biomolecules Delivery. Nanosci. Nanotechnol. 2014, 14, 755-765.
20. Barbosa, M. V.; Monteiro, L. O. F.; Malagutti, A. R.; Oliveira, M. C.; Carvalho-Júnior, A. D.; Leite, E. A. Comparative study of first-derivate spectrophotometry and high performance liquid chromatography methods for quantification of paclitaxel in liposomal formulation. J. Braz. Chem. Soc. 2015, 26, 1338-1343.
21. Lopes, S. C. A.; Novais, M. V. M.; Teixeira, C. S.; Honorato-Sampaio, K.; Pereira, A. M. T.; Ferreira, L. A. M.; Braga, F. C.; Oliveira, M. C. Preparation, physicochemical characterization and cell viability evaluation of long-circulating and pH-sensitive liposomes containing ursolic acid. BioMed Res. Intern. 2013, 1-7.
22. Barlett, G. R. Phosphorus assay in column chromatography. J. Biol. Chem. 1959, 234, 466-468.
23. Stubbs, M.; Mc Sheehy, P. M. J.; Griffiths, R. Causes and consequences of acidic pH in tumors: a magnetic resonance study. Adv. Enzyme Regul. 1999, 39, 13-30.
24. Goubran, H. A.; Kotb, R. R.; Stakiw, J.; Emara, M. E.; Burnouf, T. Regulation of tumor growth and metastasis: the role of tumor microenvironment. Cancer Growth Metastasis 2014, 7, 9-18.
25. Thakur, R.; Das, A.; Chakraborty, A. The fate of anticancer drug, ellipticine in DPPC e DMPC liposomes upon interaction with HAS: A photophysical approach. J. Potochem. Photobiol. B 2014, 130, 122-131.
26. Richards, R. L.; Gewurz, H.; Osmand, A. P.; Alving, C. R. Interactions of C-reactive protein and complement with liposomes. Immunology 1977, 74, 5672-5676.
27. Diakowski, W.; Ozimek, L.; Bielska, E.; Bem, S.; Langner, M.; Sikorski, A. F. Cholesterol affects spectrin-phospholipid interactions in a manner different from changes resulting from alterations in membrane fluidity due to fatty acyl chain composition. BBA 2006, 1758, 4-12.

28. Liu, D.; Huang, L. pH-Sensitive, plasma-stable liposomes with relatively prolonged residence in circulation. BBA 1990, 1022, 348-354.
29. USP 36-NF 34. *The United States Pharmacopoeia National Formulary*. Rockville: United States Pharmacopoeial Convention Inc.; 2016.
30. Matsumura, Y.; Maeda. H. A new concept for macromolecular therapeutics in cancer chemotherapy: mechanism of tumoritropic accumulation of proteins and the antitumor agent smancs. Cancer Res. 1986, 46, 6387-6392.
31. Meng, S.; Su, B.; Li, W.; Ding, Y.; Tang, L.; Zhou, W.; Song, Y.; Li, H.; Zhou, C.; Enhanced antitumor effect of novel dual-targeted paclitaxel liposomes. Nanotechnology 2010, 21.
32. Woodle, M. C.; Collins, L. R.; Sponsler, E.; Kossovsky, N.; Papahadjopoulos, D.; Martin, F. J. Sterically stabilized liposomes: reduction in electrophorectic mobility but not electrostatic surface potencial. Biophys. J. 1992, 61, 902-910.
33. Leite, E. A.; Souza, C. M.; Carvalho-Júnior, A. D.; Coelho, L. G. V.; Lana, A. M. Q.; Cassali, G. D.; de Oliveira, M. C. Encapsulation of cisplatin in long-circulating and pH-sensitive liposomes improves its antitumor effect and reduces acute toxicity. Int. J. Nanomed. 2012, 7, 5259-5269.
34. de Barros, A. L. B.; Mota, L. G.; Ferreira, C. A.; Corrêa, N. C. R.; Góes, A. M.; de Oliveira, M. C. 99mTc-labeled bombesin analog for breast cancer identification. J. Radioanal. Nucl. Chem. 2013, 295, 2083–2090.
35. Soares, D. C. F.; de Oliveira, M. C.; De Barros, A. L. B.; Cardoso, V. N.; Ramaldes, G. A. Liposomes radiolabeled with ^{159}Gd: in vitro cytotoxic antitumoral activity, biodistribution study and scintigraphic image in Ehrlich tumor bearing mice. Eur. J. Pharm. Sci. 2011, 43, 290-296.
36. Miyata, K.; Christi, R. J.; Kataoka, K. Polymeric micelles for nano-scale drug delivery. React. Funct. Polym. 2011, 71, 227–234.
37. Wolfram, J.; Suri, J.; Yang, Y.; Shen, J.; Celia, C.; Fresta, M.; Ferrari, M. Shrinkage of pegylated and non-pegylated liposomes in serum. Coll. Surf. B. 2014, 114, 1-15.
38. Frézard, F.; Schettini, D. A.; Rocha, O. G. F.; Demicheli, C. Lipossomas: propriedades físico-químicas e farmacológicas, aplicações na quimioterapia à base de antimônio. Quím. Nova 2005, 28, 511-518.
39. Koudelka, S.; Turánek, P.; Masek, J.; Korvasová, Z.; Skrbalová, M.; Plocková, J.; Bartheldyová, E.; Turánek, J. Liposomes with high encapsulation capacity for paclitaxel: preparation, characterization and in vivo anticancer effect. J. Pharm. Sci. 2009, 99, 2309-2319.
40. Kunz, D.; Thurn, A.; Burchard, W. Dynamic light scattering from spherical particles. Colloid. Polym. Sci. 1983, 261, 635-644.
41. Stauch, O.; Schubert, R.; Savin, G.; Burchard, W. Structure of artificial cytoskeleton containing liposomes in aqueous solution studied by static and dynamic light scattering.Biomacromolecules 2002, 3, 565-78.
42. Hinna, A.; Steiniger, F.; Hupfeld, S.; Brandl, M.; Kuntsche, J. Asymmetrical flow field-flow fractionation with on-line detection for drug transfer studies: a feasibility study. Anal Bioanal. Chem. 2014, 406, 7827–7839.
43. Vezočnik, V.; Rebolj, K.; Sitar, S.; Ota, K.; Tušek-Žnidarič, M.; Štrus, J.; Sepčić, K.; Pahovnik, D.; Maček, P.; Žagar, E. Size fractionation and size characterization of nanoemulsions of lipid droplets and large unilamellar lipid vesicles by asymmetric-flow field-flow fractionation/multi-angle light scattering and dynamic light scattering. J. Chromatogr. A. 2015, 30, 185-191.

4.2 Artigo 2: Paclitaxel-loaded folate-coated long circulating and pH-sensitive liposomes as a potential drug delivery system: a biodistrution study.

Autores: Liziane Monteiro, Renata Fernandes, Caroline Mari Oda, Sávia Lopes, Danyelle Townsend, Valbert Cardoso, Mônica Oliveira, Domenico Rubello, André Luis de Barros, Elaine Leite.

Artigo publicado no periódico **Biomedicine & Pharmacotherapy, v. 97, p. 489–495, 2018.**

ABSTRACT

A range of antitumor agents for cancer treatment is available; however, they show low specificity, which often limit their use. Recently, we have reported the preparation of folate-coated long-circulating and pH-sensitive liposomes (SpHL-folate-PTX) loaded with paclitaxel (PTX), an effective drug for the treatment of solid tumors, including breast cancer. The purpose of this study was to prepare and characterize SpHL-PTX and SpHL-folate-PTX radiolabeled with technetium-99m (^{99m}Tc). Biodistribution studies and scintigraphic images were performed after intravenous administration of ^{99m}Tc-PTX, ^{99m}Tc-SpHL-PTX and ^{99m}Tc-SpHL-folate-PTX into healthy and tumor-bearing mice. High radiochemical purity (>98%) and *in vitro* stability (>90%) were achieved for both liposome formulations. The pharmacokinetic properties of ^{99m}Tc-SpHL-DTPA-PTX and ^{99m}Tc-SpHL-folate-DTPA-PTX decreased in a monophasic manner showing half-life of 400.1 and 541.8 min, respectively. **S**cintigraphic images and biodistribution studies showed a significant uptake in liver, spleen and kidneys, demonstrating these routes as way for excretion. At 8h post-injection, the liposomal tumor uptake was higher than ^{99m}Tc-PTX. Interesting, 4h after administration, the liposome folate coated showed higher tumor-to-muscle ratio than ^{99m}Tc-SpHL-DTPA-PTX and ^{99m}Tc-PTX. In conclusion, the liposomal systems, showed high tumor uptake by scintigraphic images, especially the ^{99m}Tc-SpHL-folate-DTPA-PTX that showed a sustained and higher tumor-to-muscle ratio than non-functionalized liposome, which indicate its feasibility as a PTX delivery system to folate positive tumors.

Key words: breast cancer; scintigraphic images; MDA-MB-231 tumor; paclitaxel; pH-sensitive liposomes; folate.

1 Introduction

Cancer is a public health worldwide problem, due to its high prevalence and mortality. A range of antineoplastic agents is available for clinical applications; however, their low specificity leads to toxic effects in healthy tissues, which, in many cases, could limit their use [1-5]. Among the chemotherapeutic agents, paclitaxel (PTX) is one of the most effective and potent drugs used in the treatment of several solid tumors including, breast, ovarian, non-small cell lung cancer, head and neck tumors [3,6-8]. PTX is poorly soluble in water, therefore, it is commercially available as a micellar dispersion in Cremophor EL® (polyethoxylated castor oil) and dehydrated ethanol (1:1 v/v), which allows its administration by the intravenous route. Nevertheless, several drawbacks have been related to their clinical application, such as hypersensitivity reactions, peripheral sensory neuropathy, and myelosuppression, besides development of drug resistance [3,6,9-12]. To overcome these problems, liposomes have emerged as an interesting platform for effective drug delivery since they are biocompatible, biodegradable and nontoxic nanosystems. In addition, encapsulation into liposomes might prevent drug degradation, improve drug solubility and reduce drug distribution to undesired tissues [3,6,13,14]. Nowadays, some formulations with PTX into different nanosystems have been reported and approved for clinical applications. Among them, a conventional liposomal preparation made up of phospatidylcholine and phosphatidylglycerol (in a 9:1 molar ratio, respectively) containing PTX, Lipusu®, was approved in China, in 2006 for the treatment of ovarian, breast, head and neck cancer, gastric and non-small cell lung carcinoma [3,6,15-17]. In South Korea, a polymeric micelle formulation, Genexol-PM®, another PTX-nanosystem, has been approved for breast cancer treatment, and, in 2005 FDA approved the Abraxane®, a PTX albumin-bound nanoparticle formulation, for the treatment of metastatic cancer [18-22]. In general, these nanosystems demonstrated *in vivo* efficacy similar to Taxol®, however some studies have demonstrated their similar toxicity as well low selectivity to tumor tissue, after intravenous injection [11,15-22]. In other to overcome this drawback, we reported the preparation of PTX-loaded folate-coated long circulating and pH-sensitive liposomes (SpHL-folate-PTX). The liposomal formulation is composed by dioleylphosphatidylethanolamine (DOPE), cholesteryl hemisuccinate (CHEMS), distearoylphosphatidylethanolamine-polyethylene $glycol_{2000}$ ($DSPE\text{-}PEG_{2000}$) and distearoylphosphatidyl-ethanolaminepolyethyleneglycol$_{2000}$-folate ($DSPE\text{-}PEG_{2000}$-folate) in the molar ratio of 5.7:3.8:0.45:0.05, respectively [3]. Previous studies using small angle X-ray diffraction clearly

demonstrated the pH-sensitive of SpHL-PTX showing that the presence of CHEMS led to the stabilization of DOPE molecules in a lamellar structure at pH 7.4. Nonetheless, at lower pH, i.e. at tumor tissues, CHEMS is protonated leading to a hexagonal phase, which is essential to release the drug from liposomes [14]. SpHL-PTX revealed a high level of PTX leakage when in contact with an acid medium. Significant difference in PTX leakage was obtained from pH 6.8, and a release around 30% higher were observed. At pH 5.0 a release next to 70.0% were achieved which confirms the pH-sensitivity of the system. *In vitro* studies on MDA-MB-231 cells, a human breast tumor line, showed a higher cytotoxic activity for liposomal formulation in comparison to the free drug. Worth mentioning was the improved cytotoxicity of folate-coated formulation which suggests a higher uptake of the vesicles explained by superexpression of folate receptors in this cell line [3]. Due to these promising results, it is essential to evaluate the biodistribution profile of these nanoparticles in order to determine the real potential of these formulations as PTX delivery systems. As such, the purpose of this study was to prepare and characterize SpHL-PTX and SpHL-folate-PTX, radiolabeled with technetium-99m (^{99m}Tc). Biodistribution studies and scintigraphic images were performed after intravenous administration of ^{99m}Tc-PTX, ^{99m}Tc-SpHL-PTX and ^{99m}Tc-SpHL-folate-PTX into healthy and tumor-bearing mice.

2 Materials and methods

2.1 Materials

Paclitaxel was supplied by Quiral Quimica do Brasil S.A (Juiz de Fora, Brazil). Cremophor EL® and $SnCl_2.2H_2O$ were purchased from Sigma-Aldrich (São Paulo, Brazil). Dioleoylphosphatidylethanolamine (DOPE) and distearoylphosphatidyl-ethanolaminepolyethyleneglycol$_{2000}$ (DSPE-PEG$_{2000}$) were acquired from Lipoid GmbH (Ludwigshafen, Germany). Cholesteryl hemisuccinate (CHEMS) was supplied from Sigma Chemical Company (St. Louis, USA). Sodium chloride (NaCl) was obtained from Merck (Rio de Janeiro, Brazil). Acetonitrile HPLC grade was purchased from Fischer Scientific (New Jersey, USA).^{99m}Tc was obtained from an alumina-based ^{99}Mo/^{99m}Tc generator. Water was purified using a Milli-Q apparatus (Millipore, Billerica, USA). All other chemicals and reagents used in this study were of analytical grade. MDA-MB-231 (human breast adenocarcinoma) cell line was purchased from American Type Culture Collection (ATCC® HTB-26™) (Manassas, USA). Dulbecco's modified Eagle's medium (DMEM), fetal bovine serum, penicillin and

streptomycin were supplied by Gibco Life Technologies (Carlsbad, USA). Trypsin-EDTA solution (0.5%) and trypan blue were purchased from Sigma-Aldrich (São Paulo, Brazil). Matrigel was acquired from BD Biosciences (Bedford, MA). Female BALB/c mice (6–8-week-old) were obtained from CEBIO-UFMG (Belo Horizonte, Brazil) and BALB/c nude mice (6–8-week-old) were supplied from IPEN-SP (São Paulo, Brazil). All animal studies were approved by the local Ethics Committee for Animal Experiments (CEUA/UFMG) under the protocol number 409/2013.

2.2 Synthesis of distearoylphosphatidyl-ethanolaminepolyethyleneglycol$_{2000}$-Diethylene-triaminepentaacetic acid (DSPE-PEG$_{2000}$-DTPA)

The DSPE-PEG$_{2000}$-DTPA was synthetized as previously described [15]. Briefly, a solution of DSPE-PEG$_{2000}$-NH_2 in DMSO (40.0 mg/ml) was added to DTPA dianhydride in DMSO:pyridine 7:3 (v/v) (32.0 mg/ml). The mixture was heated in an oil bath under constant stirring for 90 min at 100°C. Then, ultrapure water was added to the reaction and mixture was maintained at 100°C, for 90 min. The solvent was evaporated and the product was re-suspended in water and purified by dialysis using a Spectrapore® membrane with a 1.0 kDa cut-off, at room temperature for 36 h. The final product was lyophilized in a 24 h cycle and stored at −20°C.

2.3 Liposomes preparation

Liposomes composed of DOPE, CHEMS e DSPE-PEG$_{2000}$ and DSPE-PEG$_{2000}$-DTPA (SpHL-DTPA-PTX) at a molar ratio of 5.7:3.8:0.45:0.05, respectively, were prepared using the standard lipid film hydration method [3]. In brief, pre-determined chloroform aliquots of the lipids and PTX (0.5 mg/mL) were transferred to round bottom flask and a lipid film was obtained by evaporating the organic solvent under reduced pressure. Next, to promote the complete ionization of CHEMS molecules, an aliquot of NaOH solution (0.456 M) was added at a 1:1 molar ratio CHEMS:NaOH. The film was hydrated with NaCl 0.9% (w/v), followed by vigorous shaking in vortex. The vesicles were sonicated (20% amplitude) in an ice bath for 5 minutes using a high-intensity ultrasonic processor (R2D091109 model; Unique® Instruments, Indaiatuba, Brazil). The suspension were submitted to a centrifugation process (Sigma 4k-15 centrifuge, Sigma Laborzentrifugen GmbH, Osterode, Germany) at 3000 rpm at 4ºC for 10 minutes to eliminate non-entrapped PTX. Since the drug shown low water solubility, it

precipitate and a drug pellet is formed. The supernatant suspension represent the final and purified formulation. For the folate-coated liposomes, 0.05% of DSPE-PEG_{2000}-folate was added to the lipid film formation.

2.4 Physicochemical characterization

2.4.1 Mean diameter and zeta potential

The mean diameter of SpHL-DTPA-PTX and SpHL-DTPA-folate-PTX was determined by dynamic light scattering (DLS) at 25ºC and at a fixed angle of 173°, using Zetasizer NanoZS90 (Malvern Instruments, England). The Zeta potential of the samples was measured by DLS associated to the electrophoretic mobility using the same equipment. All the samples were analyzed after 10-fold dilution in filtered NaCl 0.9% (w/v) solution (cellulose ester membrane, 0.45 mM, Millipore). Data were expressed as the mean ± standard deviation (SD) of at least three different batches.

2.4.2 Drug Encapsulation Percentage

The percentage of drug encapsulation of PTX in SpHL-DTPA-PTX or SpHL-DTPA-folate-PTX was determined by high performance liquid chromatography (HPLC) based on the determination of PTX concentration in the liposomes before (non-purified liposomes) and after centrifugation (purified liposomes) [24]. The liposomal vesicles were disrupted using isopropanol in a volume ratio of 1:10 and later diluted in a mixture of acetonitrile:water (55:45 v/v). This dispersion was filtered through a 0.45 µm Millex HV filter (Millipore, Billerica, MA, USA) and injected in the chromatographic apparatus. The encapsulation percentage (EP) was calculated using the following equation and the data were expressed as the mean ± standard deviation of at least three different liposomal formulation measurements:

$$EP = \frac{[PTX]purifiedliposomes}{[PTX]nonpurifiedliposomes} x100$$

2.5 Radiolabeling procedure

A 0.250 ml aliquot of the SpHL-DTPA-PTX or SpHL-folate-DTPA-PTX was added to 200µg of $SnCl_2.2H_2O$ in acid solution (2 mg/ml) and the pH was adjusted for 7.4 in a sealed vial. An aliquot of 0.1 mL of $Na^{99m}TcO_4$ (37 MBq) was then added and the mixture was kept at room temperature for 15 min. ^{99m}Tc-PTX was prepared as reported by Monteiro and co-workers (2017) and it was used in this study as a comparative group with the liposomal preparations presented in this paper [26].

2.6 Radiochemical purity evaluation

Radiochemical purity analyses were performed by thin layer chromatography on silica gel (TLC-SG; Merck, Darmstadt, Germany) using acetone as mobile phase to quantify free $^{99m}TcO_4^-$. The radioactivity was determined by a gamma counter (Wallac Wizard 1470–020 Gamma Counter; PerkinElmer Inc., Waltham, Massachusetts, USA). The solution was purified from $^{99m}TcO_2$ using a 0.22 µm syringe filter, as previously described [23,24].

2.7 *In vitro* stability: Saline and plasma

TLC-SG was used to estimate the stability of ^{99m}Tc-SpHL-DTPA-PTX and ^{99m}Tc-SpHL-folate-DTPA-PTX in the presence of NaCl 0.9% (w/v), at room temperature, or plasma, at 37ºC. For plasma stability, 90 µl of the ^{99m}Tc-PTX solution were incubated with 1.0 ml of fresh mice plasma, under agitation, at 37°C. Radiochemical stabilities were determined on samples taken up at 1, 2, 4, 6, 8, and 24 h after incubation.

2.8 Pharmacokinetic Blood clearance

An aliquot of 100 µl of ^{99m}Tc-SpHL-DTPA-PTX or ^{99m}Tc-SpHL-folate-DTPA-PTX was administrated to healthy BALB/c female mice (n=7) through the tail vein. A small incision was made in the distal tail and blood samples (~20 µl each) were collected at 5, 10, 15, 30, 45, 60, 90, 120, 240, 360, 480 and 1440 min after administration. Each sample was weighted, and the associated radioactivity was determined in an automatic scintillation apparatus. The percentage of injected activity per gram (%ID/g) in each sample was determined. The data were plotted as a function of time, expressed as mean ± SD.

2.9 Biodistribution

Biodistribution studies were carried out in healthy female BALB/c mice (n=7). Aliquots of 3.7 MBq of ^{99m}Tc-PTX, ^{99m}Tc-SpHL-DTPA-PTX or ^{99m}Tc-SpHL-folate-DTPA-PTX were injected intravenously in the animals. At 4 and 8 h post-injection, mice were anesthetized with a mixture of xylazine (10 mg/kg) and ketamine (80 mg/kg). Liver, spleen, kidneys, stomach, heart, lungs, muscle, thyroid, and intestine were removed, and placed in pre-weighted plastic test tubes. The radioactivity was measured using an automatic gamma counter. A standard dose containing the same injected amount was counted simultaneously in a separate tube, which was defined as 100% radioactivity. The results were expressed as the percentage of injected dose per gram of tissue (%ID/g).

2.10 *In Vivo* Tumor Model

MDA-MB-231 cells were cultivated in DMEM supplemented with 10% (v/v) fetal bovine serum, penicillin (100 IU/ml), and streptomycin (100.0 µg/ml) and kept at 37°C in humidified air containing 5% CO_2. Cells were grown to confluence, then, harvested by trypsinization, centrifuged (5 min at 330 x *g*) and resuspended in 1.0 ml of DMEM. An aliquot of the cell suspension was stained with trypan blue (1:1) and counted in Newbauer chamber to determine cell viability.

An aliquot of 75 µl containing 5×10^6 cells in DMEM were suspended in 75 µl of Matrigel® and injected subcutaneously into the right thigh of female BALB/c nude mice (6-8 weeks) to established the human breast tumor xenograph [27]. Tumor cells were allowed to grow *in vivo* for 30 days and the animal was used for scintigraphic images.

2.11 Scintigraphic images

An aliquot of 18 MBq of ^{99m}Tc-PTX, ^{99m}Tc-SpHL-DTPA-PTX or ^{99m}Tc-SpHL-folate-DTPA-PTX was injected intravenously to each healthy female BALB/c nude mouse or MDA-MB-231 tumor-bearing female BALB/c nude mouse (n=7). Mice were anesthetized and horizontally placed under the collimator of a gamma camera (Mediso, Budapest, Hungary) coupled with a low-energy high-resolution collimator. Images were acquired at 4 and 8 h after injection using a 256 × 256 × 16 matrix size, with a 20% energy window set at 140 keV for a period of 300s

each. The same procedure was performed to tumor-bearing mice and images were acquired at 4 and 8 h post-administration (n=4).

2.12 Statistical analysis

Data were expressed as the mean ± standard deviation (SD). Normality and homogeneity of variance analysis were performed by D'agostino and Pearson and Bartlett's tests. Physical-chemical data were tested using the test *t* de student, while biodistribution data and the one-way analysis of variance (ANOVA) test followed by Tukey's test. A P-value less than 0.05 were considered to indicate a significant difference. All data were analyzed by GraphPad PRISM, version 5.00 software (GraphPad Software Inc., La Jolla, California, USA).

3 Results

3.1 Physicochemical characterization

SpHL-DTPA-PTX and SpHL-folate-DTPA-PTX showed a monodisperse size distribution, a neutral zeta potential and a similar encapsulation percentage (Table 1). These data support that both delivery systems presented suitable characteristics for intravenous administration.

Table 1 - Physicochemical characterization of liposomal systems (n=3).

Formulation	Diameter (nm)	PI	Zeta Potential (mV)	Encapsulation Percentage (%)	Drug load (mg/mL)
SpHL-DTPA-PTX	145 ± 3	0.232 ± 0.02	-0.34 ± 2.7	84 ± 1.5	0.42 ± 0.01
SpHL-folate-DTPA-PTX	152 ± 7	0.252 ± 0.01	-1.69 ± 0.8	86 ± 2.2	0.43 ± 0.01

The results were expressed as the mean ± standard deviation.

3.2 Radiochemical purity and *in vitro* stability

The radiolabeled yields for ^{99m}Tc-SpHL-DTPA-PTX and ^{99m}Tc-SpHL-folate-DTPA-PTX were 98.4 ± 1.1%and 98.0 ± 1.0%, respectively. $^{99m}TcO_2$ produced in the reaction was removed by

passing the system through sterile filters (pore diameter = 0.22μm) since this radiocolloid remains in the filter while $^{99m}TcO_4^-$ and the radiolabeled complexes are freely filtered [23,24]. ^{99m}Tc-SpHL-DTPA-PTX and ^{99m}Tc-SpHL-folate-DTPA-PTX showed high stability in saline and plasma, even after long periods (Figure 1). At 24 h post-incubation, in both media, the radiochemical purity was higher than 90% for both radiolabeled complexes, which indicates labeling stability between the ^{99m}Tc and DTPA.

Figure 1 - *In vitro* stability of ^{99m}Tc-SpHL-DTPA-PTX (A) and ^{99m}Tc-SpHL-folate-DTPA-PTX (B) as a function of time in presence of saline at room temperature (square) and plasma at 37°C (circle) (n=5).

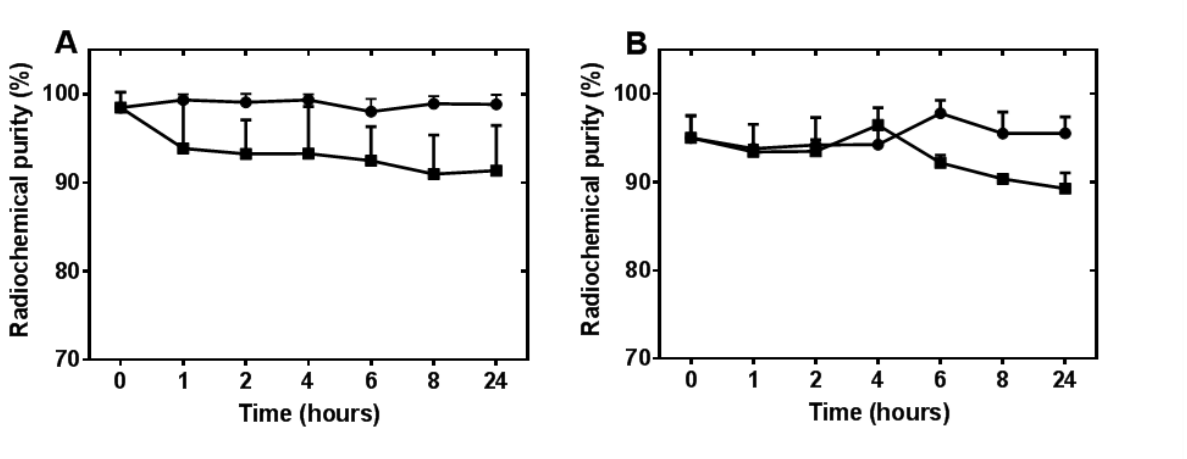

3.3 Pharmacokinetic Blood Clearance

After intravenous administration in healthy female BALB/c mice, blood levels of ^{99m}Tc-SpHL-DTPA-PTX and ^{99m}Tc-SpHL-folate-DTPA-PTX declined in a monophasic manner showing half-life of 400.1 and 54**1**.8 min, respectively. The areas under the curve (AUC) were also calculated for ^{99m}Tc-SpHL-DTPA-PTX and ^{99m}Tc-SpHL-folate-DTPA-PTX (1245.04 % ID·min^{-1} and 1637.68 % ID·min^{-1}, respectively).

3.4 Scintigraphic images and biodistribution studies

Scintigraphic images were acquired at 4 and 8 h after ^{99m}Tc-PTX, ^{99m}Tc-SpHL-DTPA-PTX or ^{99m}Tc-SpHL-folate-DTPA-PTX administration in healthy female BALB/c mice **(**Figure 2). Liver and spleen represent the major site of accumulation for all the evaluated complexes. Renal

excretion was also observed for all systems. In contrast to the liposomes, ^{99m}Tc-PTX showed a significant intestinal accumulation**.**

Figure 2 - Scintigraphic images obtained at 4 and 8 h post-injection of ^{99m}Tc-PTX (A), ^{99m}Tc-SpHL-DTPA-PTX (B) and ^{99m}Tc-SpHL-folate-DTPA-PTX (C) in healthy female BALB/c mice.

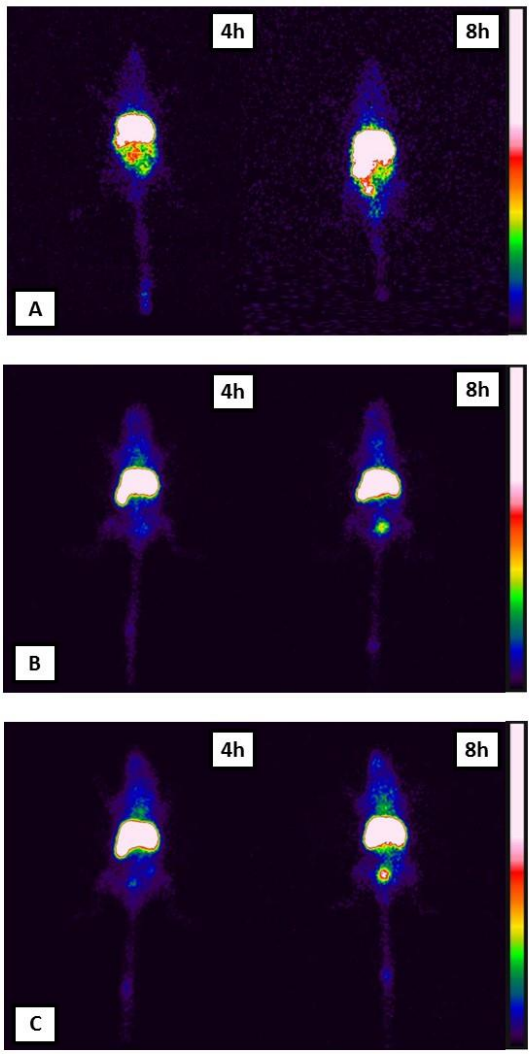

Biodistribution studies corroborate the findings in scintigraphic images (Figure 3). ^{99m}Tc-PTX, ^{99m}Tc-SpHL-DTPA-PTX and ^{99m}Tc-SpHL-folate-DTPA-PTX showed high uptake by the liver, spleen and kidneys and no significant accumulation was verified in other organs, such as stomach and thyroid, which indicates radiolabeled stability. As afore mentioned, ^{99m}Tc-PTX (Figure 3A) showed significant intestine uptake.

Figure 3 - Biodistribution profile obtained at 4 h (white bars) and 8 h (black bars) post-injection of ^{99m}Tc-PTX (A), ^{99m}Tc-SpHL-DTPA-PTX (B) and ^{99m}Tc-SpHL-folate-DTPA-PTX (C) in healthy female BALB/c mice. Bars represent the mean percentage of the injected dose per gram of tissue ± SD (n=7).

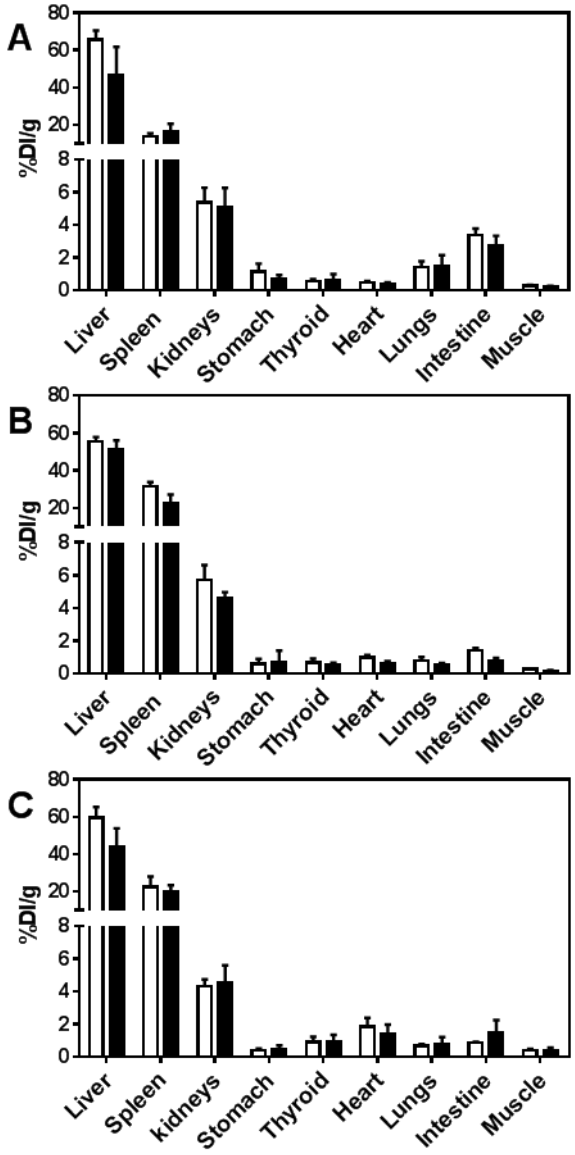

In order to reduce the number of animals used in this study, tumor-bearing mice were used only for imaging acquisition. Scintigraphic images provide information, in real time, of the whole body distribution of radiolabeled nanoparticles preventing the unnecessary use of a large amount of animals. Images were acquired at 4 and 8 h post-injection of ^{99m}Tc-PTX, ^{99m}Tc-SpHL-DTPA-PTX or ^{99m}Tc-SpHL-folate-DTPA-PTX in MDA-MB-231 tumor-bearing nude mice. The results showed the same biodistribution profile than those for healthy mice, indicating that the presence of the tumor tissue did not alter the distribution of the formulations.

In summary, high uptake was observed in liver, spleen, and kidneys (Figure 4). In addition, the tumor could be clearly seen after administrating ^{99m}Tc-SpHL-DTPA-PTX or ^{99m}Tc-SpHL-folate-DTPA-PTX. However, by injecting ^{99m}Tc-PTX, the tumor area was marginally visualized in the images**.** The tumor-to-muscle ratios confirm the higher accumulation for liposomal formulations than ^{99m}Tc-PTX (Figure 5). At 4 h post-injection, ^{99m}Tc-SpHL-folate-DTPA-PTX showed significant higher tumor-to-muscle ratios than the other complexes.

Figure 4 - Scintigraphic images obtained at 4 and 8 h post-injection of ^{99m}Tc-PTX (A), ^{99m}Tc-SpHL-DTPA-PTX (B) and ^{99m}Tc-SpHL-folate-DTPA-PTX (C) in xenographic tumor-bearing female BALB/c mice.

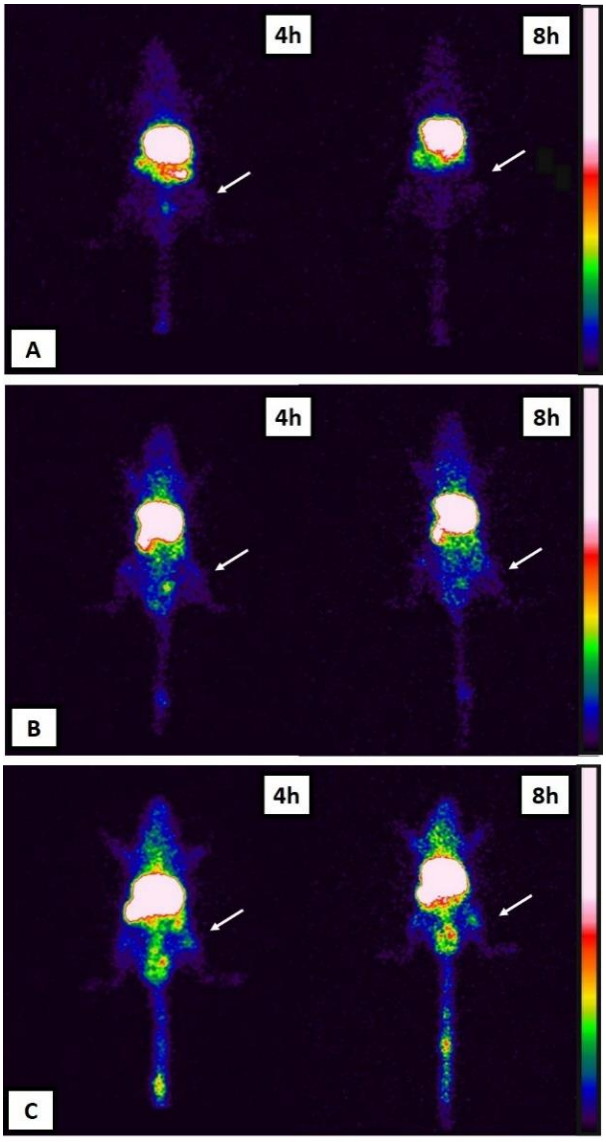

Figure 5. Tumor-to-muscle ratios determined by scintigraphic images at 4 and 8 h post-injection of ^{99m}Tc-PTX (white bars), ^{99m}Tc-SpHL-DTPA-PTX (gray bars) and ^{99m}Tc-SpHL-folate-DTPA-PTX (black bars) in xenographic tumor-bearing mice. Asterisks indicate significant difference (*p<0.05; ***p<0.001).

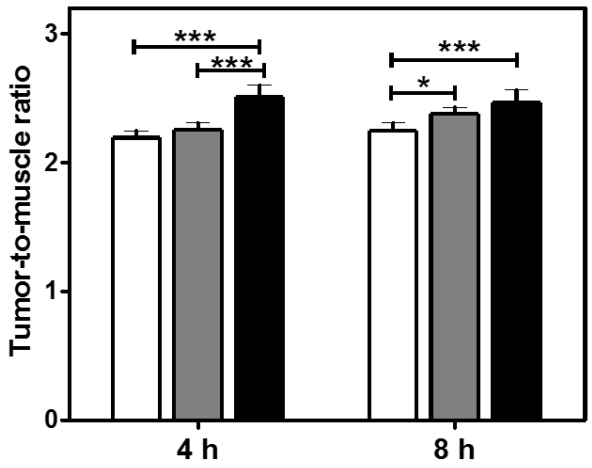

4 Discussion

Paclitaxel (PTX) is one of the most effective and potent antitumor drugs used in clinical oncology against a wide range of solid tumors, including metastatic breast cancer [6,8,10,26,28]. However, its low specificity can lead to an increased systemic toxicity, since the drug can act indiscriminately in tumor and healthy tissues. Serious hypersensitivity reactions, peripheral sensory neuropathy, and myelosuppression are the most commons side effects, which can limit its clinical application. Due to its poor water solubility, PTX is dispersed in a mixture of dehydrated ethanol and Cremophor EL® (1:1 v/v), that is also a toxic vehicle, and contributes to PTX toxicity [2,3,5,6,9-11]

Many efforts have been made to develop new strategies for cancer diagnosis and treatment that minimize dose-limiting toxicity [1,4,29,30]. Liposomes have emerged as an interesting alternative for drug delivery since this system can encapsulate both lipophilic and hydrophilic drugs. Additionally, liposomes can protect encapsulated drugs and improve treatment efficacy [6,12,13,28,29]. In this study, SpHL-folate-PTX was used to selectively deliver PTX into tumor, since i*n vitro* assays indicated that folate-coated strategy has dramatically improved the cytotoxicity of pH-sensitivity liposomes in comparison to either non-functionalized liposomes or micellar dispersion of PTX [3]. These encouraging results lead to further *in vivo* analysis seeking to understand the biodistribution profile, which is essential to evaluate the real contribution of the new targeted-formulation in achieving the tumor.

SpHL-PTX and SpHL-foalte-PTX have interesting characteristics that confers to the system specific abilities to accumulate in the tumor region, such as long-circulation, pH-sensibility and specific targeting to cell receptors. According to the American Pharmacopoeia [31], nanocarriers to be injected intravenously must be mean diameter equal or less than 500 nm, in order to guarantee the stability of an injectable lipid formulation. In addition, to prevent pulmonary embolism and microvasculature occlusion, the percentage concentration (w/v) of vesicles greater than 5 μm should be less than 0.05% of the total dispersed phase [32,33]. Besides that, the reduced particle size (≤ 500 nm) also favors passive targeting of liposomes allowing the extravasation and retention of nanostructures into tumors by EPR effect [34-37].

Our results by DLS showed that there is no difference between the size and PDI of both liposomal systems prepared. Reduced size vesicles and homogeneous distribution of liposomal systems prevent the occurrence of aggregation and fusion of the vesicles. In addition, particles ranging from 50-200 nm might be less uptaken by SMF cells after the systemic administration [38,39]. DLS associated to the electrophoretic mobility was used to determine surface charge of liposomes, SpHL-folate-PTX and SpHL-PTXshowed a zeta potential near to neutral. Similar results were previous obtained, and could be explained by the presence of PEG that generates a hydrophilic layer that impart liposome mobility. The presence of PEG is pivotal to protect the vesicles from fusion/aggregation and prevent opsonization [3,40-42]. Therefore, SpHL-folate-PTX and SpHL-PTX showed physicochemical characteristics that allow further *in vivo* studies.

^{99m}Tc-PTX was prepared using the methodology described by Monteiro et al. (2016, 2017) and was used as a comparative group with the liposomal preparations presented in these studies [3,16]. For liposome radiolabeling, the lipid DSPE-PEG_{2000}-DTPA was used since it is well known that ^{99m}Tc generates a stable complex with chelating agents, such as DTPA, for image purposes [23,41,43,44]. The results showed a high radiochemical purity and stability (over to 90%), up to 24 h after radiolabeling**.** Radiochemical purity above 90% is required since the presence of high amount of impurities leads to poor image quality, which might result in a biodistribution profile that no longer reflects the nanoparticle behavior [26,45].

^{99m}Tc-SpHL-DTPA-PTX and ^{99m}Tc-SpHL-folate-DTPA-PTX showed long blood circulation times that is important to confer more passages through the tumor area. Tumor vessels have been shown to have larger pores than the regular vasculature; consequently, particles in nanometric size, such as liposomes, are able pass through the walls of a vessel into the surrounding tissues, e.g. tumor [23,26,46].

Nanoparticles are extensively phagocytosed by macrophages present in the liver and spleen organs [25,26,46,47]. As predicted, the biodistribution studies showed high uptake in liver and

spleen for ^{99m}Tc-SpHL-DTPA-PTX and ^{99m}Tc-SpHL-folate-DTPA-PTX. The kidneys also showed a significant uptake, which indicates renal clearance of all complexes. Noteworthy, the low uptake in thyroid and stomach for ^{99m}Tc-SpHL-DTPA-PTX and ^{99m}Tc-SpHL-folate-DTPA-PTX confirms the high labeling stability showed by *in vitro* assays [46-49]. In addition, as previously described, ^{99m}Tc-PTX showed a substantial uptake by the intestines, suggesting that fecal route also contributes to the excretion of ^{99m}Tc-PTX [26].

The formulations evaluated in these studies showed a significant tumor uptake compared with the contralateral muscle in all timeframes. ^{99m}Tc-SpHL-DTPA-PTX and ^{99m}Tc-SpHL-folate-DTPA-PTX showed higher tumor-to-muscle ratio than ^{99m}Tc-PTX, at 8 h post-injection, indicating that longer circulation achieved by the liposomes leads to higher tumor accumulation. Interestingly, ^{99m}Tc-SpHL-folate-DTPA-PTX showed significant higher tumor-to-muscle ratio than ^{99m}Tc-SpHL-DTPA-PTX and ^{99m}Tc-PTX at 4 h after administration, suggesting that the folate-coating strategy can favor tumor accumulation in shorter time. The presence of folate on the liposome surface might contribute to the tumor uptake since MDA-MB-231 cells overexpress folate receptor on their membrane [49,50]. Therefore, ^{99m}Tc-SpHL-folate-DTPA-PTX showed better performance than ^{99m}Tc-SpHL-DTPA-PTX and ^{99m}Tc-PTX, since short time accumulation is interesting to both approaches, diagnosis and therapy. Imaging probes that quickly achieve higher signal-to-noise ratios are preferable and can ultimately lead to more optimal patient care. Additionally, nanoparticles that can deliver the drug through longer periods are adequate to guarantee sustained drug concentration in the tumor.

Therefore, our hypothesis is that^{99m}Tc-SpHL-folate-DTPA-PTX might enhance the drug concentration into the cytoplasmic of tumor cells, since the liposomes into endosomal vesicles (pH 5.0) will undergo destabilization or fusion with endosomal bilayer, releasing PTX directly in cytoplasm cell [3,14,37,51]. Moreover, folate will provide a cell-specific intracellular delivery, once cancer cells are known to overexpress a number of cell surface receptors, such as folate receptors [3,49,50]. Indeed, higher tumor accumulation was achieved by using folate-coated liposomes that might be interesting to improve antitumor efficacy.

In conclusion, liposomes showed adequate mean diameter and polidispersivity that allows intravenous administration. Moreover, ^{99m}Tc-SpHL-DTPA-PTX and ^{99m}Tc-SpHL-folate-DTPA-PTX showed high tumor uptake in scintigraphic images. Special emphasis should be given to ^{99m}Tc-SpHL-folate-DTPA-PTX that showed a sustained and higher tumor-to-muscle ratio than non-functionalized liposome. Therefore, results presented in this study indicate the feasibility of ^{99m}Tc-SpHL-folate-DTPA-PTX as a PTX delivery system to folate positive tumors.

Acknowledgements

The authors would like to thank Fundação de Amparo à Pesquisa do Estado de Minas Gerais (FAPEMIG-Brazil), Conselho Nacional de Desenvolvimento Científico e tecnológico (CNPq-Brazil), and Coordenação de Aperfeiçoamento de Pessoal de Nível Superior (CAPES-Brazil) for their financial support and scholarship.

Conflicts of interest

Authors declare that they have no conflicts of interest.

References

1. Safarzadeh E, Shotorbani SS, Baradaran B. Herbal medicine as inducers of apoptosis in cancer treatment. *Adv Pharm Bull.* 2014; 4:421-7.
2. Vanneman M, Dranoff, G. Combining immunotherapy and target therapies in cancer treatment. *Nat Rev.* 2012; 12:237-51.
3. Barbosa MV, Monteiro LOF, Carneiro G, et al. Experimental design of a liposomal lipid system: A potential strategy for paclitaxel-based breast cancer treatment. *Colloids Surf B: Biointerfaces.* 2015; 136:553-61.
4. Siegel RL, Miller KD, Jemal A. Cancer statistics, 2015. *CA Cancer J Clin*. 2015; 65:5–29.
5. Simpson GR, Relph K, Harrington K, et al. Cancer immunotherapy via combining oncolytic virotherapy with chemotherapy: recent advances. *Oncolytic Virother*. 2016; 5:1–13.
6. Koudelka S, Turánek J. Liposomal paclitaxel formulations. *J Controll Rel.* 2012; 163: 322-334.
7. Iwamoto T. Clinical application of drug delivery systems in cancer chemotherapy: review of the efficacy and side effects of approved drugs. *Biol Pharm Bull.* 2013; 36:715-8.
8. Chan JK, Brady MF, Person RT, et al. Weekly vs. every-3-week paclitaxel and carboplatin for ovarian cancer. *N Engl J Med.* 2016; 374:738-48.
9. Mielke S, Sparreboom A, Mross K. Peripheral neuropathy: A persisting challenge in paclitaxel-based regimes. *Eur J Cancer* 2006; 42:24-30.
10. Surapanemi MS, Das SK, DAS NG. Designing paclitaxel drug delivery systems aimed at improved patient outcomes: current status and challenges. *ISRN.* 2012; 1–15.
11. Yared JA, Tkaczuk KH. Update on taxane development: new analogs and new formulations. *Drug Des Dev Ther* 2012; 6:371-84.
12. Bertrand N, Wu J, Xu X, et al. Cancer nanotechnology: the impact of passive and active targeting in the era of modern cancer biology. *Adv Drug Deliv Rev.* 2014; 66:2-25.
13. Barbuti AM, Chen Z. Paclitaxel through the ages of anticancer therapy: exploring its role in chemoresistance and radiation therapy. *Cancers.* 2015; **7**: 2360-71.
14. Monteiro LOF, Lopes SCA, Barros ALB, et al. Phase behavior of dioleyphosphatidylethanolamine molecules in the presence of components of pH-sensitive liposomes and paclitaxel. *Colloids Surf B: Biointerfaces.* 2016; 144:276-83.
15. Yang A, Li J, Xu H, A study on antitumor effect of liposome encapsulated paclitaxel *in vivo* and *in vitro*. *Bulletin of Chinese Cancer*. 2006;15: 862-864.

16. Wang X, Song L, Li N, *et al*. Pharmacokinetics and biodistribution study of paclitaxel liposome in sprague-dawley rats and beagle dogs by liquid chromatography-tandem mass spectrometry. *Drug Res.* 2013; 63: 603–606.
17. Xu X, Wang L, Xu HQ, *et al*. Clinical comparison between paclitaxel liposome (Lipusu®) and paclitaxel for treatment of patients with metastatic gastric cancer. Asian Pac J Cancer Prev, 2013; 14: 2591-2594.
18. Yamashita Y, Egashira N, Masuguchi K, *et al*. Comparison of peripheral neuropathy induced by standard and nanoparticle albumin–bound paclitaxel in rats**.** J Pharmacol Sci. 2011; 117: 116-120.
19. Werner ME, Cummings ND, Sethi M, *et al*. Preclinical evaluation of Genexol-PM, a nanoparticle formulation of paclitaxel, as a novel radiosensitizer for the treatment of non-small cell lung cancer. Int J Radiat Oncol Biol Phys, 2013; 83:463–468.
20. Paik PK, James LP, Riely GJ, *et al*. A phase 2 study of weekly albumin-bound paclitaxel (Abraxane®) given as a two-hour infusion. Cancer Chemother Pharmacol, 2011; 1331-1337.
21. Lim WT, Tan EH, Toh CK, *et al*. Phase I pharmacokinetic study of a weekly liposomal paclitaxel formulation (Genexol-PM) in patients with solid tumors. Ann Oncol. 2010; 21: 382–388.
22. Feng L, Mumper RJ. A critical review of lipid-based nanoparticles for taxane delivery. *Cancer Letters* 2013; 334:157-175.
23. Oda CMR, Fernandes RS, Lopes SCA, et al. Synthesis, characterization and radiolabeling of polymeric nano-micelles as a platform for tumor delivering. *Biomed Pharmacother.* 2017, 89:268-75.
24. Barbosa MV, Monteiro LOF, Malagutti AR, et al. Comparative study of first-derivate spectrophotometry and high performance liquid chromatography methods for quantification of paclitaxel in liposomal formulation. *J Braz Chem Soc* 2015; 43: 1-6.
25. Fernandes RS, Silva JO, Lopes SVA, et al. Technetium-99m-labeled doxorubicin as an imaging probe for murine breast tumor (4T1 cell line) identification. *Nucl Med Commun.* 2016; 37:307-12.
26. Monteiro LOF, Fernandes RS, Castro LC, et al. Technetium-99m radiolabeled paclitaxel as an imaging probe for breast cancer in vivo. *Biomed Pharmacother.* 2017; 89:146-51.
27. Sinha A, Agarwal S, Parashar D, et al. Down regulation of SPAG9 reduces growth and invasive potential of triple-negative breast cancer cells: possible implications in targeted therapy. *J Exp Clin Cancer Res* 2013, 32:1-11.
28. Zhang D, Yang R, Wang S, et al. Paclitaxel: new uses for an old drug. *Drug Des Dev Ther* 2014; 8:279-84.
29. Laouini A, Jaafar-Maalej C, Limayem-Blouza I, Sfar S, Charcosset C, Fessi H. Preparation, Characterization and applications o liposomes: state of the art. *J Colloid Sci Biotechnol.* 2012; **1**:147-168.
30. Madni A, Sarfraz M, Rehman M, Ahmad M, Akhtar N, Ahmad S *et al*. Liposomal Drug Delivery: a versatile plataform for challenging clinical applications. *J Pharm Pharm Sci.* 2014;**17**:401-426.
31. USP 36-NF 34. *The United States Pharmacopoeia National Formulary*. Rockville: United States Pharmacopoeial Convention Inc.; 2016.
32. Driscoll DF. Lipid ingectable emulsions: pharmacopeial and safety issues. *Pharm. Res*. 2006; 23:1959-1969.
33. Hippalgaonkar K, Majundar S, Kansara V. Injectable lipid emulsions – Advancements opportunities and challenges. AAPS 2010; 11:1526-1540.

34. Matsumura Y, Maeda H. A new concept for macromolecular therapeutics in cancer chemotherapy: mechanism of tumoritropic accumulation of proteins and the antitumor agent smancs. Cancer Res. 1986; 46:6387-6392.
35. Meng S, Su B, Li W, *et al*. Enhanced antitumor effect of novel dual-targeted paclitaxel liposomes. *Nanotechnology*, v. 21, p. 415103, 2010.
36. Sawant RR, Torchilin VP. Challenges in development of targeted liposomal therapeutics. *AAPS***,** 2012; 14: 303-315.
37. Ferreira DS, Lopes SCA, Franco MS, *et al*. pH-sensitive liposomes for drug delivery in cancer treatment. *Ther Deliv* 2013;4:1-24.
38. Ulrich AS. Biophysical aspects of using liposomes as delivery vehicle. *Bioscience Reports* 2002; 22:129-150.
39. Yang T, Cui F, Choi M, *et al*. Liposome formulation of paclitaxel with enhanced solubility and stability. *Drug Deliv*. 2007; 14:308-313.
40. Woodle MC, Collins LR, Sponsler E, *et al*. Sterically stabilized liposomes: reduction in electrophorectic mobility but not electrostatic surface potencial. *Biophys. J.* 1992; 61: 902-910.
41. De Barros ALB, Andrade SF, Filho JDS, Cardoso VN, Alves RJ. Radiolabeling of low molecular weight D-galactose-based glycodendrimer with technetium-99-m and biodistribution studies. *J Radioanal Nucl Chem.* 2013; **298**:605-659.
42. Lopes SCA, Novais MVM, Teixeira CS, *et al*. Preparation, physicochemical characterization and cell viability evaluation of long-circulating and pH-sensitive liposomes containing ursolic acid. *Bio Med Res Int.* 2013; 1-7.
43. Varshney R, Sethi SK, Hazari PP, Chuttani K, Soni S, Milton MD *et al*. Synthesis of [DTPA-bis(D-ser)] chelate (DBDSC): An approach fo the design of SPECT radiopharmaceuticals based on technetium. *Curr Radiopharm.* 2012; **5**:348-355.
44. Zhu X, Li J, Hong Y, Kimura RH, Ma X, Liu H *et al*. 99mTc-labeled cysteine knot peptide targeting integrin □vβ6 for tumor SPECT imaging. *Mol Pharm.* 2014; **11**:1208-1217.
45. Fuscaldi LL, dos Santos DM, Pinheiro NGS, Araújo RS, de Barros ALB, Resende JM *et al*. Synthesis and antimicrobial evaluation of two peptide LyeTx I derivatives modified with the chelating agent HYNIC for radiolabeling with technetium-99m. *J Venom Anim Toxins incl Trop Dis.* 2016; **22**:1-8
46. Awasthi VD, Garcia D, Goins BA, Phillips V. Circulation and biodistribution profiles of long-circulating PEG-liposomes of various sizes in rabbits. *Int J Pharm.* 2003; **253**:121-132.
47. Barros ALB, Mota LG, Coelho MMA, Corrêa NCR, Góes AM, Oliveira MC *et al*. Bombesin encapsulated in long-circulating pH-sensitive liposomes as a radiotracer for breast tumor identification. *J Biomed Nanotechnol.* 2015; **11**:342-348.
48. Soares DCF, de Oliveira MC, de Barros ALB, Cardoso VN, Ramaldes GA. Liposomes radiolabeled with ^{159}Gd: in vitro cytotoxic antitumoral activity, biodistribution study and scintigraphic image in Ehrlich tumor bearing mice. *Eur J Pharm Sci.* 2011; **43**:290-296.
49. Loomis K, McNeely K, Bellamkonda RV. Nanoparticles with targeting, triggered release, and imaging functionality for cancer applications. *Soft Matter*. 2011; **7**:839-856.
50. Deshpande PP, Biswas S, Torchilin VP. Current trends in the use of liposomes for tumor targeting. *Nanomedicine.* 2013; **8**:1-32.
51. De Oliveira MC, Rosilio V, Lesieur P, *et al*. pH-sensitive liposomes as a Carrier for oligonucleotide in excess water. *Biophys Chem*. 2000;87:127-137.

4.3 Artigo 3: Paclitaxel-loaded folate-coated pH-sensitive liposomes enhance cellular uptake and antitumor activity

Autores: Liziane Monteiro, Renata Fernandes, Luciano de Castro, Diego dos Reis, Geovanni Cassali, Fernanda Evangelista, Adriano Sabino, Valbert Cardoso, Mônica Oliveira, André Luís de Barros, Elaine Leite.

Artigo submetido no periódico **Nanomedicine**.

Abstract

Aim: To evaluate *in vitro* and *in vivo* antitumor activity of PTX-loaded folate-coated and pH-sensitive liposomes (SpHL-folate-PTX) against breast tumor cell line.

Materials & Methods: Cellular uptake of the liposomes and PTX was evaluated. Apoptosis and cell cycle were analyzed by flow cytometry. *In vivo* antitumor activity was carried out in MDA-MB-231 tumor-bearing Balb/c nude female.

Results and Conclusions: Cellular uptake assay showed a high cell delivery of PTX by SpHL-folate-PTX, which leads to a superior cytotoxicity and activation of apoptosis pathways. SpHL-folate-PTX treatment induces an expressive increase of cells in G0/G1 phase. *In vivo* studies showed a higher efficacy of SpHL-folate-PTX treatment than free PTX and SpHL-PTX. Therefore, the data confirmed the potential of SpHL-folate-PTX for breast cancer therapy.

KeyWords: triple-negative breast cancer, paclitaxel, liposomes, pH-sensitivity, folate, antitumor activity, MDA-MB-231.

Summary points

- PTX-loaded folate-coated and pH-sensitive liposomes (SpHL-folate-PTX) present the ability to improve the concentration of PTX in the tumor tissue mediated by the folate receptors.
- The physicochemical analysis of the system demonstrated suitable characteristics for *in vivo* administration.
- Cellular uptake assay, *in vitro*, showed a higher delivery of PTX into the cells by SpHL-folate-PTX, resulting in a significantly higher cytotoxicity against MDA-MB-231 cells.
- SpHL-folate-PTX may inhibit the proliferation of tumor cell by blocking the G0/G1 phase, while PTX:Cr+ET and SpHL-PTX present the most of cells stopped at G2/M.
- Apoptosis was found out as the main cell death pathway after PTX treatments.
- Liposomal systems, with or without PTX, presented lower hemolysis levels than PTX:Cr+Et and Cr+Et, suggesting greater hemocompatibility.
- The encapsulation of PTX in SpHL-folate clearly improved the antitumor activity of the drug, since the inhibition of tumor growth was approximately 70% and 30% higher than PTX:Cr+Et and SpHL-PTX, respectively.
- Decreasing in the proliferative cells and increase of the apoptotic cells percentage were observed by immunohistochemical analyses after the SpHL-folate-PTX treatment.

1. Introduction

Paclitaxel (PTX) is a microtubule-stabilizing agent widely used to treat solid tumors such as breast, ovarian, prostate, non-small cell lung cancer, colon, Kaposi's sarcoma related to immunodeficiency syndrome (AIDS) and head and neck cancer [1-5]. This drug causes abnormal mitotic spindle assembly, chromosome segregation, and G0/G1 or G2/M cell cycle arrest inducing tumor cell death [2-4]. However, the use of this drug is impaired by its low aqueous solubility. The conventional PTX formulation (Taxol™) contains a high concentration of Cremophor EL® (polyethoxylated castor oil), a substance with expressive toxic effects including neurotoxicity, myelosuppression, and serious hypersensitivity reactions [3, 6-10]. Some formulations with PTX into different nanostructure systems have been approved for clinical applications such as Lipusu™ (conventional liposomal made up of phosphatidylcholine and phosphatidylglycerol), Abraxane™ (PTX albumin-bound nanoparticle formulation), and

Genexol-PM™ (polymeric micelles containing PTX). Although these nanoformulations have shown better responses compared to Taxol™, some studies have demonstrated enhanced risk for toxicity, especially in patients with altered metabolism, as well as low selectivity to tumor tissue [4,11-13].

Our group recently described the preparation of PTX-loaded folate-coated long circulating and pH-sensitive liposomes (SpHL-folate-PTX). This liposomal formulation is composed by dioleylphosphatidylethanolamine (DOPE), cholesterylhemisuccinate (CHEMS), distearoylphosphatidylethanolamine-polyethylene glycol$_{2000}$ (DSPE-PEG$_{2000}$), and distearoylphosphatidyl-ethanolaminepolyethyleneglycol$_{2000}$-folate (DSPE-PEG$_{2000}$-folate) at a molar ratio of 5.7:3.8:0.45:0.05, respectively [3,5,10,14]. This nanosized liposomal dispersion was stable at pH 7.4 but destabilized under acidic conditions (pH 5.0). The pH-sensitivity of this system was clearly evidenced by changes in the phase transitions of the structural lipid (DOPE), which is essential to release the drug at the cytoplasmic level [5,14]. *In vitro* studies showed the higher cytotoxic activity of SpHL-folate-PTX compared to non-functionalized liposome (SpHL-PTX) or PTX dispersed in a 1:1 blend of Cremophor EL® and dehydrated ethanol (PTX:Cr+Et) against MDA-MB-231, a human breast tumor cell line [3]. In addition, a high tumor uptake as well as a sustained and higher tumor-to-muscle ratio were obtained after intravenous administration, in tumor-bearing mice, of SpHL-folate-PTX radiolabeled with technetium (^{99m}Tc) compared to a formulation without folate functionalization. Altogether, these findings suggest that SpHL-folate-PTX can be potentially applied for the treatment of folate positive tumors.

Therefore, a proof-of-concept study was designed in order to demonstrate the feasibility of SpHL-folate-PTX to treat tumors. To attain this aim, liposomes were prepared and characterized. Cellular uptake and flow cytometry analyses were carried out to confirm cytotoxicity. Then, the in vivo antitumor activity of SpHL-folate-PTX was performed in a breast tumor model.

2. Material and Methods

2.1 Material

Paclitaxel was purchased from Quiral Quimica do Brasil S.A (Juiz de Fora, Brazil). DOPE and DSPE-PEG$_{2000}$ were purchased by Lipoid GmbH (Ludwigshafen, Germany). CHEMS, CremophorEL^{TM} and $SnCl_2.2H_2O$ were purchased from Sigma Chemical Company (St. Louis,

USA). Sodium chloride (NaCl) was purchased from Merck (Rio de Janeiro, Brazil). Acetonitrile HPLC grade was obtained from Fischer Scientific (New Jersey, USA). ^{99m}Tc was obtained from an alumina-based ^{99}Mo/^{99m}Tc generator. Water was purified using a Milli-Q apparatus (Millipore, Billerica, USA). All other chemicals and reagents used in this study were of analytical grade.

MDA-MB-231 (human breast adenocarcinoma) cell line was obtained from American Type Culture Collection (ATCC® HTB-26™) (Manassas, USA). Dulbecco's modified Eagle's medium (DMEM), fetal bovine serum, penicillin, and streptomycin were purchased from Gibco Life Technologies (Carlsbad, USA). Trypsin-EDTA solution (0.5%) and trypan blue were supplied by Sigma-Aldrich (São Paulo, Brazil). Matrigel was obtained from BD Biosciences (Bedford, MA). Female BALB/c mice (8-weeks old) were acquired from CEBIO-UFMG (Belo Horizonte, Brazil) and female BALB/c nude mice (6-weeks old) were supplied by IPEN-SP (São Paulo, Brazil). All animal studies were approved by the local Ethics Committee for Animal Experiments (CEUA/UFMG) under the protocol numbers 100/2013 and 292/2016.

2.2 Paclitaxel dispersion preparation

The micellar dispersion of PTX was prepared by dissolving 30.0 mg of the drug in 2.0 mL of a mixture of dehydrated ethanol:Cremophor EL™ (1:1 v/v) under vigorous stirring [10,15]. This dispersion was diluted in NaCl 0.9% (w/v) solution before intravenous injection.

2.3 Liposome Preparation

The liposomes were prepared by the lipid hydration method a lipid concentration of 40 mmol/L of DOPE, CHEMS, and DSPE-PEG$_{2000}$ (at a molar ratio of 5.7:3.8:0.5, respectively) [3,10,14]. Briefly, chloroform aliquots of the lipids and PTX (2.0 mg/mL) were transferred to a round bottom flask and the organic solvent was removed under reduced pressure. The resulting film was hydrated with a solution of NaOH (0.456M), in order to guarantee the complete ionization of CHEMS, and NaCl (0.9% w/v). The obtained vesicles were sequentially submitted to the high-intensity probe sonication (20% amplitude) for 5 minutes, in an ice bath, using a high-intensity ultrasonic processor (R2D091109 model; Unique® Instruments, Indaiatuba, Brazil). Free PTX was removed by centrifugation (HeraeusMultifage X1R Centrifuge, Germany) at 3000 rpm at 4ºC for 10 minutes. The empty liposomes (without drug) were also prepared as described above. For the folate-coated liposomes, 0.05% of DSPE-PEG$_{2000}$-folate was added to

the lipid film formation. When applicable, DSPE-PEG_{2000}-DTPA was also added to the liposome preparation. All preparations were stored at 4 °C.

2.4 Physicochemical characterization

The liposomes were characterized by their diameter, polydispersity index (PI), zeta potential, and encapsulation percentage (EP) of the drug. The diameter and PI of all liposomes formulations were determined by dynamic light scattering (DLS) at 25°C and at a fixed angle of 90°, using Zetasizer NanoZS90 (Malvern Instruments, England). Zeta potential was measured by DLS associated with the electrophoretic mobility using the same equipment. All the samples were analyzed after 10-fold dilution in previously filtered NaCl 0.9% (w/v) solution (cellulose ester membrane, 0.45 mM, Millipore). Data were expressed as the mean ± standard deviation (SD) of at least three different batches.

The EP of PTX in the liposomes was determined by high-performance liquid chromatography (HPLC) according to the method previously described [16].

2.5 MDA-MB-231 cell culture

The MDA-MB-231 cell line was cultivated in DMEM supplemented with 10% (v/v) fetal bovine serum, penicillin (100.0 IU/ml), and streptomycin (100.0 µg/ml) and kept at 37°C in humidified air containing 5% CO_2. Cells were grown to confluence, then, harvested by trypsinization, centrifuged (5 min at 330*g*) and resuspended in 1.0 ml of DMEM. Cell viable count was performed in a Newbauer hemocytometer using Trypan blue (1:1) dye exclusion method.

2.6 Cellular uptake of radiolabeled nanosystems and quantification of PTX

Cellular uptake study was performed according to the protocols previously described elsewhere [17,18]. Firstly, the preparations were radiolabeled with ^{99m}Tc according to the method previously reported [10,15]. MDA-MB-231 cells ($1.0x10^6$ cells), in culture medium, were incubated with 30 µL of PTX:Cr+Et, SpHL-PTX or SpHL-folate-PTX labeled with ^{99m}Tc at 37°C under stirring (Metabolic Bath Dubnoff MA-95/CF Marconi, Brazil). After 15, 30, 60 and 120 min, the suspension was centrifuged at 2000 rpm for 5 min at room temperature. The

radioactivity in the pellet and supernatant was determined in a gamma counter (n=5) and the percentage of uptake radiation was calculated according to the equation:

$$\%\text{Uptake} = \frac{\text{Amount of radioactivity (pellet)}}{\text{Amount of radioactivity (pellet+supernatant)}} \times 100$$

The intracellular PTX concentration was quantified by HPLC (n=5) according to the previous protocol reported with modifications [19]. Briefly, 1.0×10^6 MDA-MB-231 cells were incubated with a volume corresponding to 20.0 μg PTX (PTX total) of the PTX:Cr+Et, SpHL-PTX or SpHL-folate-PTX. The cells were kept at 37°C under stirring. After 15, 30, 60 and 120 min, the suspension was centrifuged at 2000 rpm for 5 min at room temperature. The pellet was washed with 1.0 mL of PBS to remove the non-uptake drug. Afterward, 1.0 mL of acetonitrile was added to the pellet and the preparation was taken to the ultrasonic bath for 5.0 minutes to lyse the cells and precipitate the protein. The samples were centrifuged at 5000 rpm for 15 min at room temperature and an aliquot of the supernatant was used for quantifying the intracellular PTX (PTX sample). The percentage of PTX uptake was calculated by using the following equation:

$$\%\text{Uptake of PTX} = \frac{[\text{PTX sample}]}{[\text{PTX total}]} \times 100$$

2.7 Cell Proliferation Assay

The antiproliferative effects were determined by the sulforhodamine B assay, based on the measurement of cellular protein content as previously described [20]. MDA-MB-231 cells were treated with different concentrations of PTX:Cr+Et; SpHL-PTX and SpHL-folate-PTX (ranged from 9.7 nM to 5000 nM) and their respective controls. Blank liposomes were diluted in the same way as PTX-loaded liposomes. After 48 h the inhibitory concentration (IC50) was defined as the concentration that inhibited cell proliferation by 50% when compared to that of the untreated controls.

2.8 Cell cycle and apoptosis analysis

Freshly prepared solutions of PTX:Cr+Et, SpHL-PTX, and SpHL-folate-PTX, at concentrations correspond to inhibitory concentration (IC50) of each treatment, were added to

MDA-MB-231 cells seeded in 12-well plates at a density of 2.0 x 10^5 cells per well and incubated for 24 h at 37ºC and 5% CO_2. After 48 h of incubation at 37ºC and 5% CO_2, the supernatant was removed and reserved. Then, the cells were washed twice with PBS buffer at pH 7.4. The cells were trypsinized and the reserved supernatant was added. Afterward, the resulting suspension was centrifuged for 5 min at 2000 rpm and resuspended in 1.0 ml of PBS buffer. Different samples of each treatment were used for evaluation of the apoptosis and cell cycle by flow cytometric analysis. The cells were incubated with 1.0 mL of ethanol at 4 °C for 30 minutes. Then, the samples were centrifuged for 5 min at 2000 rpm, resuspended in propidium iodine solution (50 g/mL), which was prepared in 0.1% sodium citrate plus 0.1% Triton X-100 and incubated at 4 °C for 20 min. A total of 50,000 events were recorded and the analysis was performed on a flow cytometer (LSR Fortessa BD Biosciences) according to the manufacturer's instruction.

For the quantification of cells undergoing apoptosis was used the Annexin V-FITC Apoptosis Detection Kit (BD Biosciences, USA). The cell samples were stained with 2.5 μL of FITC-conjugated Annexin-V plus 5 μL of PI solution for 10 min at room temperature and protected from the light. The cells were also analyzed using a flow cytometer (LSR Fortessa BD Biosciences), after acquiring 50,000 events per sample.

2.9 Hemolysis assay

Hemolysis assay was performed according to published procedures [21-23]. In brief, fresh female Swiss blood (8 weeks, 20.0 ± 2.0 g) was collected in tubes containing 10% w/v EDTA solution. The red blood cells (RBC) were separated by centrifugation at 3000 rpm for 10 min at room temperature (Heraeus Multifage X1R Centrifuge, Germany). RBC collected from the bottom were washed with NaCl 0.9% (w/v) until a colorless supernatant was obtained above the cell mass. The final pellet was diluted with NaCl 0.9% (w/v) solution to obtain a 4% (w/v) RBC concentration. The formulations evaluated were PTX:Cr+Et, SpHL-PTX, and SpHL-folate-PTX at concentrations 0.05, 0.1, and 0.5 mg/mL and their respective controls. The samples were incubated with an equal volume of 4% RBC suspension (n=5) for 1 h at 37 °C under agitation at 500 bpm (Metabolic Bath Dubnoff MA-95/CF Marconi, Brazil). After the incubation, the cell suspensions were centrifuged at 2000 rpm for 5 min and the supernatants absorbance was measured in a spectrophotometer (Evolution 201 UV-Visible Spectrophotometer Thermo Scientific, USA) at 540 nm. Deionized water and NaCl 0.9% (w/v)

were used as negative (NC) and positive (PC) controls, respectively. The percent hemolysis was calculated using the following equation:

$$\% \text{ hemolysis} = \frac{\text{SampleAbsorbance} - \text{NC Absorbance}}{\text{PC Absorbance} - \text{NC Absorbance}} \times 100$$

2.11 Antitumor activity

Female BALB/c nude mice (6-weeks old, 18.0 ± 2.0g) were kept under specific pathogen-free conditions in autoclaved plastic cages, and they had free access to autoclaved food and water. They were maintained in an area with a standardized light/dark cycle, temperature and relative humidity were also controlled. Aliquot of 75 µl containing 5×10^6 MDA-MB-231 cells in DMEM were suspended in 75 µl of Matrigel™ and injected subcutaneously into the right flank of mice [24]. Tumor cells were allowed to grow for 30 days. When the tumor volume reached approximately 100 mm^3, the animals were randomly divided into five experimental groups (six animals per group). Three different groups (PTX:Cr+Et; SpHL-PTX and SpHL-folate-PTX) received PTX at a dose of 7.5 mg/kg [25]. Other two control groups were treated with a vehicle solution Cr+Et or liposomes without PTX. The treatments were administered by intravenous route, every 4 days, in 6 administrations. The first day of treatment was considered day zero (D0) of the study. Antitumor activity was evaluated over a 50-day period and was based on the tumor volume and the tumor growth inhibition ratio determination, scintigraphic images of the tumor using the complex ^{99m}Tc-HYNIC-βAla-Bombesin$_{(7-14)}$, histomorphometric, and immunohistochemistry of the tumor tissue. This study was approved by the Ethics Committee on Animal Use (CEUA) from UFMG with the protocol number 100/2013.

2.11.4 Tumor volume and tumor growth inhibition ratio determination

The tumor volume (V) was evaluated twice a week by the measurements of two orthogonal diameters (d1and d2) with a slide caliper (Mitutoyo, MIP/E-103), where d1 and d2 were the smallest and the largest perpendicular diameters, respectively, and calculated as follows: $v = d1^2 x\ d2 \times 0.5$[26]. Tumor growth was monitored before the treatment (D0) and prior to the administration of each dose. Mice body weight was also monitored at the same time. At the end

of the experimental period (D50), the relative tumor volume (RTV) for each experimental group was determined as follows:

$$\% \text{ RTV} = \frac{\text{Tumor volume on day 50}}{\text{Tumor volume on day 0}}$$

The inhibition ratio (IR) was also calculated as follows:

$$\text{IR} = \frac{\text{mean RTV from each treatment}}{\text{mean RTV from the control group}} \text{ x } 100$$

2.10.2 Scintigraphic images

The scintigraphic images were obtained using ^{99m}Tc-HYNIC-□Ala-Bombesin$_{(7-14)}$, at D0, D35, and D50.To perform scintigraphic images, the animals received 37 MBq of ^{99m}Tc-HYNIC-βAla-Bombesin$_{(7-14)}$ by the intravenous route. At 4 hours after radiolabeled complex administration, the mice were anesthetized with a mixture of ketamine (60mg/kg) and xylazine(8 mg/kg) solution and horizontally placed under the collimator of a gamma camera (Mediso, Budapest, Hungary) coupled with a low-energy high-resolution collimator. Images were acquired at using a 256 × 256 × 16 matrix size, with a 20% energy window set at 140 keV for a period of 300s each [27]. The quantitative analyses of scintigraphic images were conducted on the determination of the radioactivity in the target area (tumor) and the non-target area (contralateral muscle). The intensity of the radiation emitted was quantified in pixels for each one of the delineated areas and the target to non-target ratio was calculated as follows:

$$\text{Ratio} = \frac{\text{Target to non-target ratio on D50}}{\text{Target to non-target ratio on D0}}$$

2.10.3 Histomorphometric analyses of the tumor

After obtaining scintigraphic images, the anesthetized mice were sacrificed by cervical dislocation on D50, and the tumor was removed and weighted. Then, the tumor tissue was fixed in formalin (10% w/v in phosphate-buffered saline, pH 7.4), embedded in paraffin blocks, sectioned into a 4 µm thickness, placed onto glass slides, and hematoxylin-eosin stained. The images of cross-sections were obtained for morphometric evaluation, and 15 fields per slide were examined using a 40× magnification in an optical microscope (final magnification = ×

1000). The images were captured with a microcamera (Spot Insight Color; SPOT Imaging Solutions, Sterling Heights, MI) attached to a microscope (Olympus BX-40; Olympus, Tokyo, Japan) and the SPOT® software, version 3.4.5. The percentage of the necrosis, neoplasia, inflammation, apoptosis and stroma areas was determined using a 25-point graticule.

2.10.4 Immunohistochemical analyses of the tumor

Histological sections with 4 µm thickness were stained using the avidin-biotinylated peroxidase complex (Dako K0690; K0690-HRP) with primary antibody anti-Ki67 from mouse (MIB-1, 1:100 v/v dilution; Dako) or polyclonal anti-cleaved caspase-3 antibody (Ab-4, 1:300, MarcaNeoMarkers), and 3′3-diaminobenzidine (DAB) as chromogen agent. Then, slides were counter-stained using Harris hematoxylin and subsequent evaluation by lighting microscopy. The images were captured using the Spot Insight Color microcamera attached to the Olympus BX-40 Microscope. Ki67 staining was considered positive when cells revealed a dark brown nuclear staining. The proliferative index was obtained by calculating the percentage of positive cells (immunostained) in a total of 500 tumor cells. To evaluate the apoptosis cell, the samples were immunostained with caspase-3 marker. Three images were obtained by the 20x objective and the number of labeled cells were counted.

2.11 Statistical Analyses

Statistical analyses were performed using GraphPadPrism 5.0 software. The normality and homogeneity of the variance analysis were verified by D'agostino and Pearson's and Bartlett's tests, respectively. The difference among experimental groups was tested using the one-way analysis of variance (ANOVA), followed by the Tukey's test. The hemolytic activity, tumor growth, and histomorphometric data were transformed. Differences were considered significant when p values were lower or equal to 0.05 ($P<0.05$).

3 Results

3.1 Physicochemical characterization

The physicochemical characteristics of the liposomal formulations are summarized in Table 1. The average diameter of SpHL was significantly smaller than SpHL-PTX and SpHL-folate-

PTX, which can be attributed to PTX introduction in the liposomal bilayer. The PDI values near 0.2 indicate monodispersed systems. Zeta potential values near to neutral range were observed for all systems. Finally, a high encapsulation efficiency of PTX was obtained (~ 90%) in both formulations, suggesting a strong interaction between drug and hydrocarbon chains of the lipids. Similar results were obtained in a previous study [3,10,14].

Table 1 -Physicochemical characterization of liposomal systems.

Formulation	Average Size ± SD(nm)	PI ± SD	Zeta Potential ± SD (mV)	Encapsulation Percentage (%)
SpHL	135 ± 5	0.216 ± 0.002	-2.3 ± 0.2	-
SpHL-PTX	159 ± 5[a]	0.231 ± 0.009	-4.0 ± 1.3	88± 3
SpHL-folate-PTX	155 ± 6[a]	0.238 ± 0.008	-3.65 ± 1.0	90± 4

[a]represents significant difference as compared with liposomal formulation without PTX. *P*-values equal or less than 0.05 were set as the level of significance (Tukey's test). Data are expressed as the mean ± standard deviation (n=3).

3.2 Cellular uptake of radiolabeled nanosystems and quantification of PTX

The radiolabeled yields for PTX:Cr+Et, SpHL-PTX, and SpHL-folate-PTX were 94.9 ± 0.2%; 97.8 ± 0.9% and 98.2 ± 1.2%, respectively. The results were similar than those previously obtained by our group [10,15]. Data of cellular uptake of the radiolabeled nanosystems as well as intracellular PTX percentage are shown in Figure 1A. Both liposomes showed similar cellular uptake throughout the experiment ($p>0.05$), while ^{99m}Tc-PTX:Cr+Et demonstrate higher uptake ($p<0.05$). Regarding PTX uptake (Figure 1B), it could be observed an increase of PTX concentration inside the cells over time for all formulations. At 15, 30, and 120 min SpHL-PTX and SpHL-folate-PTX showed a higher drug uptake than PTX:Cr+Et. Interestingly, at 120 min, SpHL-folate-PTX was able to provide a higher amount of PTX to the cell than the non-targeted liposome ($p<0.05$).

Figure 1 – Cellular uptake of radiolabeled nanosystems (A) and PTX (B) as a function of time. MDA-MB-231 cells were incubated with PTX-formulations. White, gray and black bars representPTX:Cr+Et; SpHL-PTX and SpHL-folate-PTX, respectively.

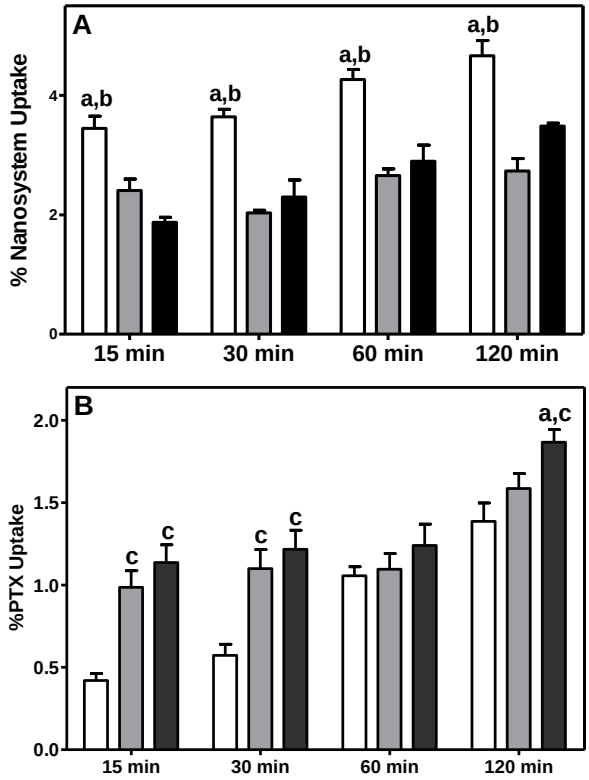

[a]indicates significant difference as compared to SpHL-PTX (p <0.05).
[b]indicates significant difference as compared to SpHL-folate-PTX (p <0.05).
[c]indicates significant difference as compared to PTX:Cr+Et (p <0.05).

3.3 Cell Proliferation Assay

The antiproliferative effects were determined in MDA-MB-231 cell line by the sulforhodamine B assay. It could be observed that the liposomal functionalization with folate promoted an expressive increase in cytotoxicity activity, since a significant reduction in cell viability was observed with the increase of PTX concentration when compared to PTX:Cr+Et and SpHL-PTX ($p<0.05$). The IC50 values determined for treatments associated with PTX were 1174.0 ± 107.5; 500.7 ± 24.4, and 22.5 ± 2.74 nM for the PTX: Cr+Et; SpHL-PTX, and SpHL-folate-PTX, respectively. The data determined in this assay were used to the apoptosis and cell cycle analyses. Blank liposomes did not show cytotoxicity at the doses evaluated.

3.4 Apoptosis analysis

Flow cytometry was used to evaluate the level of apoptosis for all formulations using FITC-Annexin V and PI label. As shown in Figure 2, the encapsulation of PTX into liposome bilayer did not compromise the drug cytotoxicity since an increased number of positive cells in apoptosis (four-fold) was observed for all formulations compared to the control group, indicating that the formulations were able to reduce cell proliferation.

Figure 2 – Analysis of cell death profile of MDA-MB-23 cells without treatment (a) and after the treatment with PTX:Cr+Et (b), SpHL-PTX (c), SpHL-folate-PTX (d) stained with propidium iodide (PI) and FITC-Annexin V.

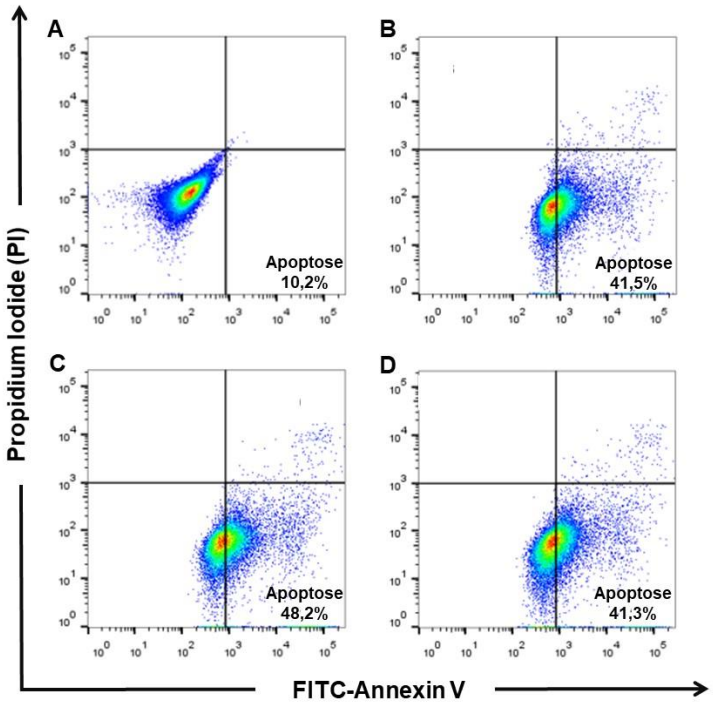

3.5 Cell cycle analyses

In order to confirm the observations suggested by apoptosis analysis, we investigated the DNA content of MDA-MB-231 cells after the different treatments. It is well established that apoptotic cells are characterized by DNA fragmentation and loss of nuclear DNA content. Since PI is able to bind DNA, we can evaluate the cellular DNA content by flow cytometric analysis. Thus, the effect of the PTX encapsulation into SpHL and SpHL-folate on the cell cycle of MDA-MB-231 after treatment with the 50% inhibitory concentration cells can be observed in Figure 3. A similar cell cycle profile was observed after PTX:Cr+Et and SpHL-PTX treatment, the majority

of cells were in G0/G1 phase of the cell cycle. On the other hand, a significant change was observed after the treatment with SpHL-folate-PTX. An expressive increase in the percentage of cells in G0/G1 and a simultaneous reduction of cells in G2/M were obtained when compared to PTX:Cr+Et and SpHL-PTX treatments.

Figure 3 – Percentage of cells in each phase distribution in MDA-MB-231 cells after treatment with PTX:Cr+Et, SpHL-PTX, SpHL-folate-PTX, and control. The results are expressed as percentage of positive events for each phase of the cell cycle.

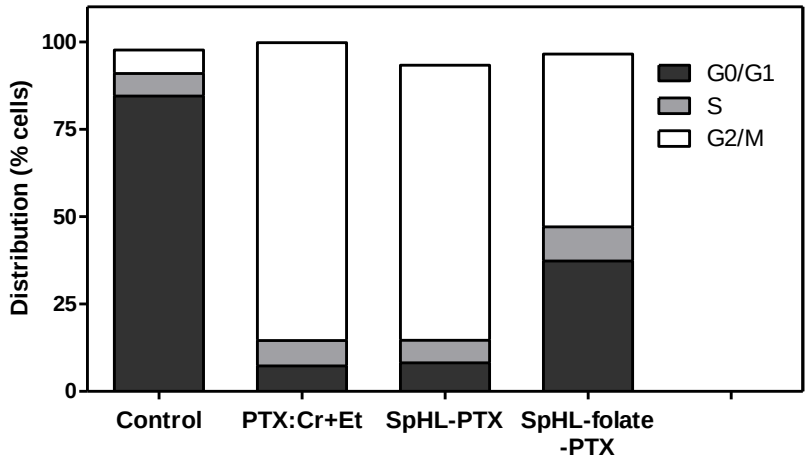

3.6 Hemolysis assay

Hemocompatibility profiles of formulations with or without PTX are shown in Figure 4. The high hemolytic ratios could be observed after incubation of RBC with Cr+Et control, mainly at a concentration of 0.50 mg/mL (13.5 ± 1.4%). On the other hand, the liposomal formulations were able to reduce significantly this effect. The highest hemolysis rate by liposomal formulations was 3.0 ± 0.1% at a concentration equal to 0.50 mg/ml. The PTX association in Cr + Et caused a significant deacrease in hemocompatibility compared to the vehicle at all tested concentrations, clearly indicating a dose-dependent relationship in hemolytic activity. In contrast, SpHL-PTX and SpHL-folate-PTX had a hemolysis rate significantly lower than PTX:Cr+Et at all evaluated concentrations, suggesting that liposomal systems are a safer option to carrier PTX. It is important to note that at the higher concentration (0.5 mg/mL) a significant difference was observed in the hemolytic ratio between SpHL-PTX and SpHL-folate-PTX.

Figure 4 – Hemolysis percentage after the treatment with Cr+Et; SpHL; PTX:Cr+Et; SpHL-PTX and SpHL-folate-PTX in different concentrations (n=5).

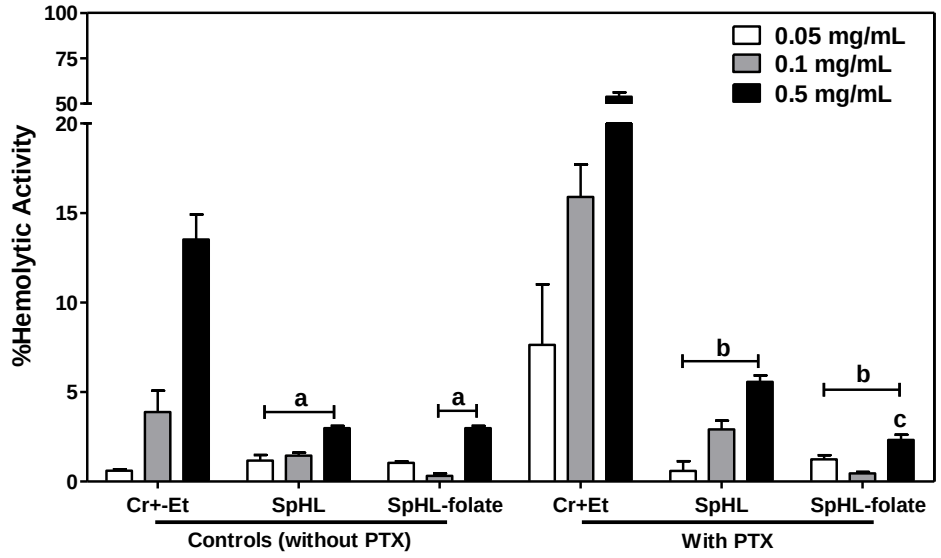

[a]indicates significant difference to Cr+Et ($p < 0.05$).
[b]indicates significant difference to PTX:Cr+Et ($p < 0.05$).
[c]indicates significant difference to SpHL-PTX ($p < 0.05$).

3.7 Antitumor activity

Figure 5A shows the tumor growth for all the evaluated groups over time. Both vehicles (Cr+Et and SpHL) were used as control groups. Expressive and similar ($p>0.05$) tumor growth was observed for the controls. By contrast, the tumor volume was significantly lower in mice treated with PTX in the different formulations at doses of 7.5 mg/kg compared to mice from the control group ($p<0.05$).No significant difference ($p>0.05$) was observed in the mean tumor volume of mice treated with SpHL-PTX and PTX:Cr+Et until 50 days after the first administration. On the other hand, the tumor growth in mice treated with SpHL-folate-PTX was lower than mice that received PTX:Cr+Et ($p < 0.05$). It is worth mentioning that no change could be observed in the tumor volume for 50 days after the first injection of SpHL-folate-PTX. In addition, a significant difference in the tumor volume between SpHL-PTX and SpH-folate-PTX was observed after the 20th day of evaluation, which coincides with the end of treatment. Concerning the tumor mass data (Figure 5B), the group treated with SpHL-folate-PTX showed the lowest tumor mass, which was significantly different from SpHL-PTX and PTX:Cr+Et groups ($p>0.05$).

Figure 5 –The panel A represents the antitumor effect and the panel B showed the tumor mass of SpHL-PTX, SpHL-folate-PTX, PTX:Cr+Et, and control groups, SpHL and Cr+Et administered by IV route, in BALB/c nude mice xenographic tumor-bearing (n=6). Values represent the mean ± SD.

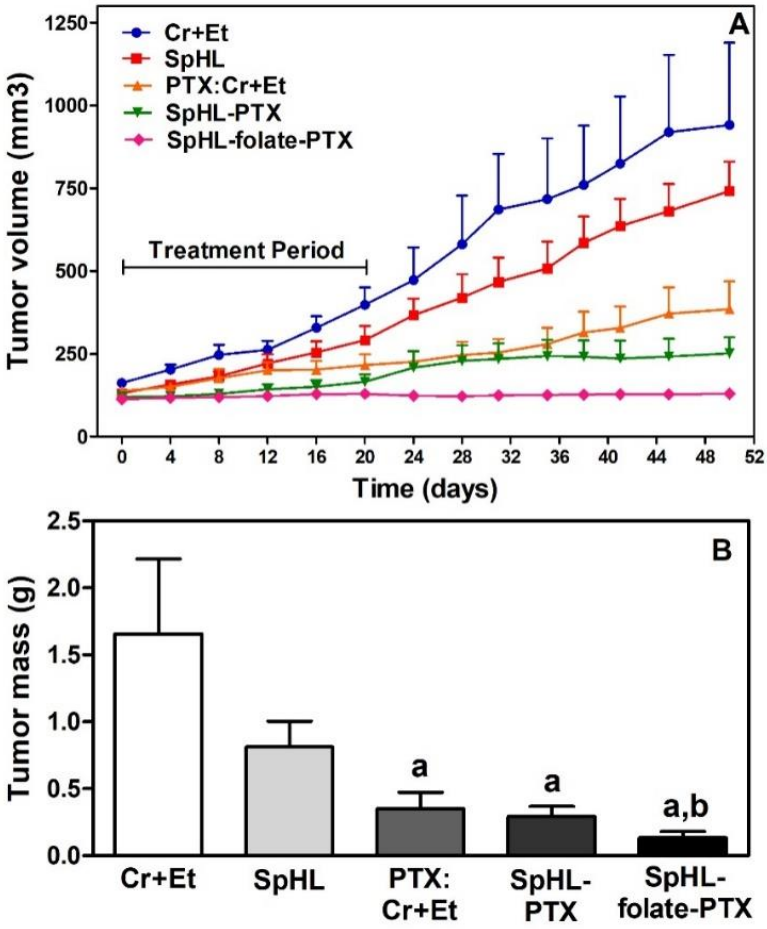

[a]indicates significant difference as comparedto Cr+Et ($p < 0.05$).
[b]indicates significant difference as comparedto SpHL ($p < 0.05$).

RTV and IR analyses corroborated the tumor volume data (Table 2).SpHL-PTX and SpHL-folate-PTX showed a significant difference compared to the controls groups. In addition, SpHL-folate-PTX was able to inhibit the growth by 80% while the inhibition observed to PTX:Cr+Et and SpHL-PTX were only 48% and 63%, respectively. These data suggest that the presence of folate in the formulation has an important role in the antitumor activity.

Table 2 -Relative tumor volume (RTV) and tumor growth inhibition ratio (IR) after administration of SpHL-PTX, SpHL-folate-PTX, PTX:Cr+Et, and control groups, SpHL and Cr+Et administered by IV route, in BALB/c nude mice xenographic tumor-bearing. Results expressed as the mean ± standard error.

Formulation	RTV	IR (%)
Cr+Et	5.8 ± 3.5	-
SpHL	5.8 ± 1.9	-
PTX:Cr+Et	3.0 ± 1.27	48
SpHL-PTX	2.1 ± 1.2[a]	63
SpHL-folate-PTX	1.1 ± 0.1[a,b]	80

RTV data were transformed by using the equation: y = log (variable)
[a]indicates significant difference as comparedto Cr+Et and SpHL($p < 0.05$).
[b]indicates significant difference as comparedto PTX:Cr+Et ($p < 0.05$)

3.7.1 Scintigraphic images

Antitumor efficacy was also evaluated by scintigraphic images using the radiotracer ^{99m}Tc-HYNIC-β-Ala-Bombesin$_{(7-14)}$ (Figure 6). From the images, the target/non-target ratios at the beginning (D0) and at the end of the treatment (D50) were determined (Table 3). Significant reduction of viable residual tumor mass after PTX treatments compared to control groups was observed ($p<0.05$).SpHL-folate-PTX group showed a decrease of 39% and 32% in residual tumor mass compared with the PTX:Cr+Et and SpHL-PTX group, respectively. These results are confirmed by the lower uptake of the radiopharmaceutical observed in the Figure 7D. Furthermore, this data are in agreement with those of tumor volume and mass, demonstrating the better performance ofSpHL-folate-PTX.

Figure 6 – Scintigraphic image of ^{99m}Tc-HYNIC-β-Ala-Bombesin$_{(7-14)}$in breast tumor-bearing mice 4 h after intravenous radiopharmaceutical administration at 50th of evaluation. The arrow indicates the tumor area. Images of SpHL group are similar to CR+Et group.

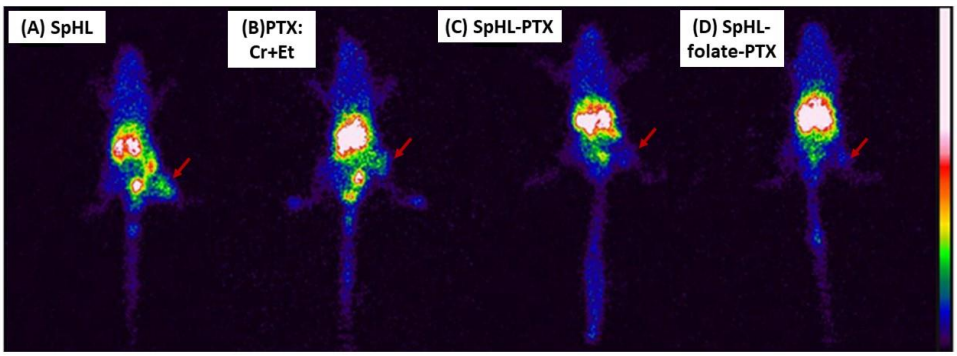

Table 3 - Target/non-target ratios after 4 hours of intravenous injection of the ^{99m}Tc-HYNIC-β-Ala-Bombesin$_{(7-14)}$ in breast tumor-bearing mice. Mean ± SD.

Formulation	Target/non-targetratio
Cr+Et	2.05 ± 0.01
SpHL	2.02 ± 0.01
PTX:Cr+et	1.40 ± 0.06[a]
SpHL-PTX	1.26 ± 0.03[a]
SpHL-folate-PTX	0.86 ± 0.03[a,b,c]

[a]indicates significant difference as comparedto Cr+Et and SpHL ($p < 0.05$).
[b]indicates significant difference as comparedto PTX:Cr+Et ($p < 0.05$).
[c]indicates significant difference as comparedto SpHL-PTX ($p < 0.05$).

3.7.2 Histopathological and histomorphometric analyses

Figure 7 shows the histological photomicrographs of the tumors of all tested groups. Macroscopically, the tumors presented a well-defined white neoplastic mass with an irregular surface. In the control groups, Cr+Et and SpHL, the tumor mass presented a rigid consistency, different from the PTX treated groups which showed a consistency more friable and markedly smaller that indicates a reduction in the tumor areas. All tumor mass exhibited inflammatory infiltrate predominantly in peritumoral regions with a predominance of mononuclear cells, besides a delicate fibrovascular stroma.

Figure 7–H&E-stained photomicrographs of tumor tissue extracted, 50 days after treatment, from mice receiving (A/B) Cr+Et, (C/D)PTX:Cr+Et, (E/F) SpHL, (G/H) SpHL-PTX and (I/J) SpHL-folate-PTX. The arrows indicate necrosis areas and asterisks show liquefiable necrosis regions. Yellow arrowheads (J) indicate peritumoral inflammatory infiltrate and black arrowheads (F) mitotic figure.

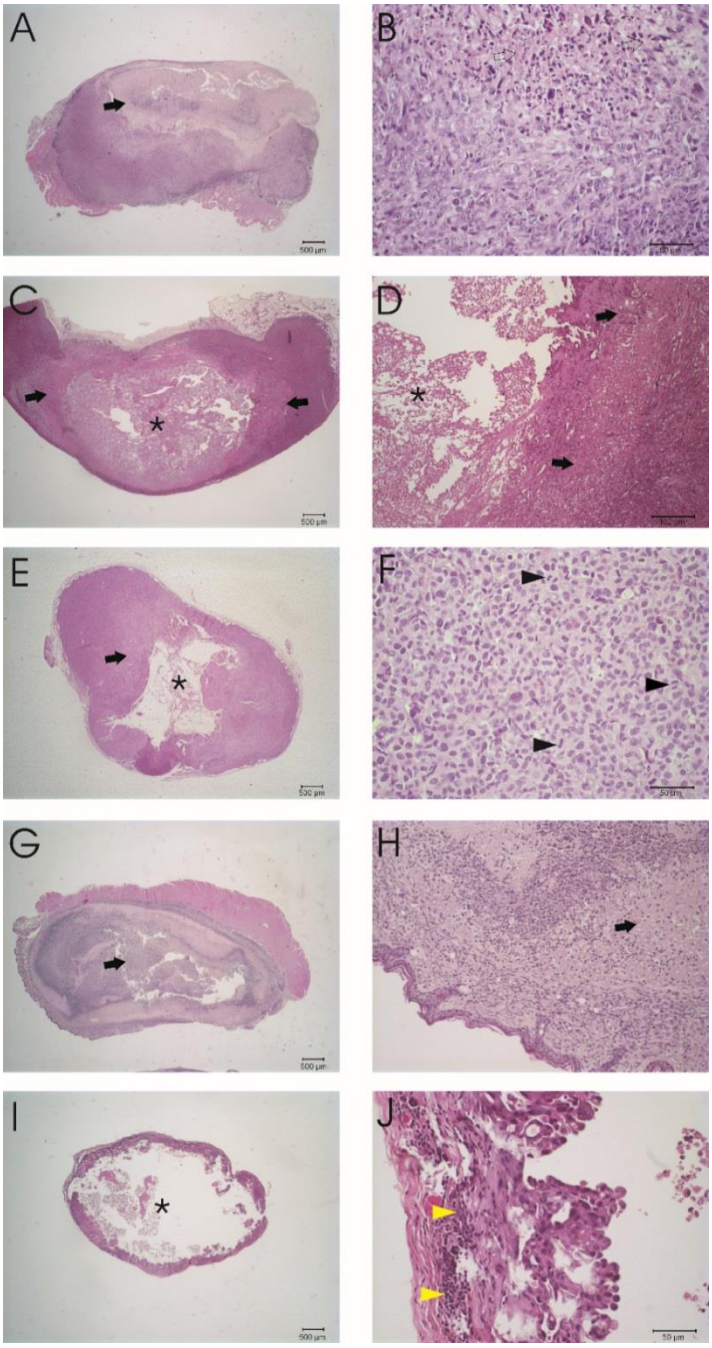

The Cr+Et treatment group (Figure 7A and 7B) presented cystic areas with the absence of liquid. Extensive areas of epithelial proliferation malignant in a solid arrangement with high

pleomorphism cellular and numerous mitosis figures, sometimes in a tubular organization were observed. The central of necrosis areas were composed of eosinophilic tissue, the pyknotic nucleus in karyorrhexis, often associated with a mononuclear inflammatory infiltrate. SpHL group showed similar findings, however, the cystic areas demonstrate the presence of liquid with amorphous and eosinophilic content, characteristic of liquefiable necrosis (Figure 8E).

In the PTX treatment groups, cystic areas with a clear and viscous liquid present with amorphous and eosinophilic content, compatible with liquefiable necrosis could be observed. The neoplastic cells presented high cellular pleomorphism, with acidophilic characteristics, a vacuolized cytoplasm, and a basophilic and condensate nucleus. In Figure 7C and 7D, it could be observed that the PTX:Cr+Et exhibited epithelial proliferation in a solid arrangement, sometimes with a tubular formation, delicate fibrovascular stroma and some mitotic figures. By contrast, the tumors of the animals treated with SpHL-PTX and SpHL-folate-PTX exhibited predominantly a tubular arrangement of the cells, with the papillary formation and rare mitotic figures.

Histomorphometric analyses of all tumors demonstrated neoplasia, necrosis, and inflammation. The percentage variation of these parameters is shown in Table 4.

Table 4 - Morphometric variables of the tumor 50 days after the administration of PTX:Cr+Et, SpHL-PTX, SpHL-folate-PTX, and control groups.

(%)	Cr+Et	SpHL	PTX:Cr+ET	SpHL-PTX	SpHLF-PTX
Neoplasia	49.4 ± 22.2	45.8 ± 28.5	27.6 ± 16.6	24.6 ± 5.9	15.9 ± 10.4
Necrosis	28.6 ± 28.9	34.8 ± 27.9	44.4 ± 21.6	66.0 ± 6.7	42.8 ± 23.8
Inflammation	8.0 ± 4.6	5.7 ± 4.6	10.8 ± 6.9	4.5 ± 5.0	23.4 ± 7.3
Apoptosis	0.7 ± 0.5	0.6 ± 0.8	0.5 ± 0.7	0.6 ± 0.6	0.5 ± 0.9
Stroma	11.6 ± 6.2	10.9 ± 11.5	12.0 ± 4.9	3.4 ± 2.3	17.0 ± 12.3

After the treatment with SpHL-folate-PTX a significant decrease in the percentage of neoplasia areas was observed compared with both control groups. On the other hand, this parameter was similar among groups treated with different PTX formulations ($p>0.05$). It was observed a significant increase of inflammation areas in the tumors of the group treated with SpHL-folate-PTX.

3.7.3 Immunohistochemical tumor analyses

All tumor tissue evaluated showed positive nuclear staining for Ki-67(Figure 8A). However, the expression was significantly higher in the control groups. Among the PTX-treated groups, reduced cellularity and a lower number of Ki-67 positive cells were verified in the tumor of mice treated with the SpHL-folate-PTX. On the other hand, no difference was detected between the PTX:Cr+Et and SpHL-PTX.

Figure 8 – (A) Percentage of Ki-67 positives cells in 500 cells of the tumor tissue evaluated 50 days after the administration, in tumor-bearing mice, of Cr+Et, SpHL, PTX:Cr+Et, SpHL-PTX,and SpHL-folate-PTX. (B) Caspase-3 positives cells present in the tumor tissue evaluated 50 days after the administration of Cr+Et, SpHL, PTX:Cr+Et, SpHL-PTX, and SpHL-folate-PTX in tumor-bearing mice. Values represent the mean ± SD (n=6).

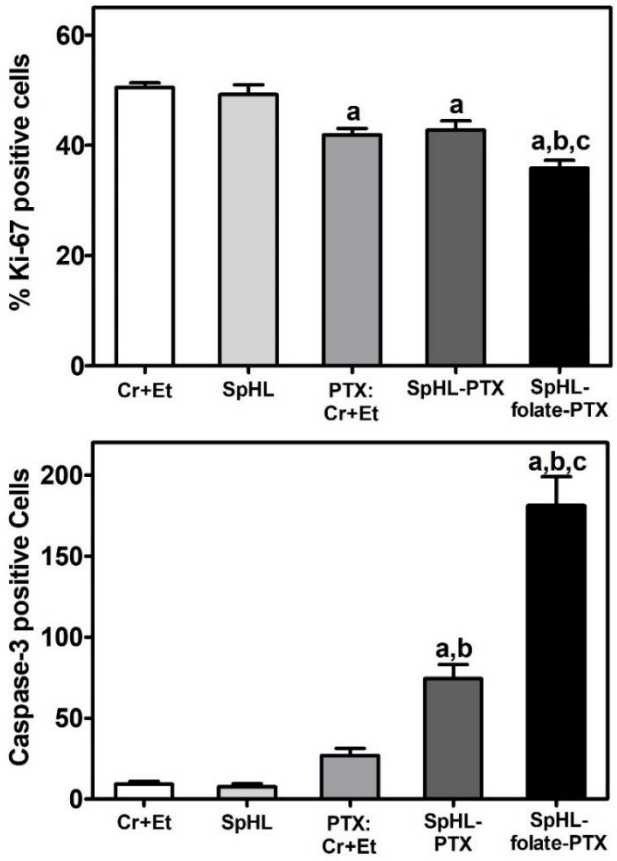

[a]indicates significant difference as compared to Cr+Et and SpHL (p <0.05).
[b]indicates significant difference as compared to PTX:Cr+Et (p <0.05).
[c]indicates significant difference as compared to SpHL-PTX (p <0.05).

The presence of apoptotic cells was evaluated by caspase-3 marker (Figure 8B).SpHL-folate-PTX treatment showed a number of apoptotic cells significantly higher than all the others groups evaluated ($p<0.05$). A significant difference was also observed for SpHL-PTX group compared to PTX:Cr+Et and control groups.

4 Discussion

The use of receptor-mediated drug delivery systems based on liposomes for cancer treatment has been a strategy often studied in order to increase the specificity and reduce the systemic toxicity of cytotoxic agents [18]. The superexpression of folate receptors in some solid tumors, such as breast cancer, has provided an interesting therapeutic target for treating this type of tumor [3,10,29,30]. Our group has already described the efficient incorporation of PTX in long-circulating and pH-sensitive liposomes functionalized with folate and their ability to promote an enhanced concentration of PTX the tumor tissue [3,10]. In order to evaluate whether this selective delivery of PTX into tumor may improve the therapeutic efficacy of PTX-based treatment, we presented herein investigations related to the *in vitro* and *in vivo* antitumor activity in a model of human MDA-MB-231 breast cancer cells.

Several studies have demonstrated that the physicochemical properties of nanocarriers, such as size, shape, surface charge are directly related to cellular uptake [31]. As can be observed in Table 1, all formulations showed suitable characteristics for *in vivo* administration. Among the evaluated parameters, it is well described that the mean diameter has a fundamental role in the cellular uptake since it is directly related to the endocytosis process [18,32]. The main endocytosis pathways to nanoparticles up to 50 nm and 100 nm are clathrin and caveolin-mediated, respectively, while macropinocytosis is the most important for particles with a diameter higher than 100 nm. In addition, the time required for the endocytosis process by the different transmembrane transporters may cause differences in the cellular uptake of the nanosystems[19,32,33]. Thus, the reduced uptake of the liposomal formulations compared to PTX:Cr+Et can be explained by the different phagocytosis pathways. However, the liposomes were able to carry a higher concentration of PTX into the cells, as can be seen in Figure 1. Similar results were obtained by Gu and co-workers (2012). In this way, the cytotoxicity of SpHL-folate-PTX against MDA-MB-231 tumor cells was significantly higher than that verified for PTX:Cr+Et and SpHL-PTX. This increase in the cytotoxicity observed after functionalization with folate might be explained by the higher uptake observed for this system mediated by its binding to the folate receptors presents on the membrane of MDA-MB-231

cells [3,10]. The set of results, PTX cellular uptake and cytotoxicity indicate that the insertion of the drug into folate-coated liposomes favors its cellular uptake, making the cells more susceptible to the PTX action.

Inside the tumor cells, the PTX binds to the β tubulin subunit and leads to the irreversible stabilization of the microtubules, resulting in the inhibition of cell division. PTX may inhibit the proliferation of the tumor cell by blocking G0/G1 or G2/M phases of the cell cycle, which is dependent on the drug concentration [1-5,35-37]. In the present study, a significant difference cell cycle-profile was observed after PTX encapsulation into folate-coated liposomes compared to PTX:Cr+Et and LpHS-PTX. This finding might be attributed to the different doses used in the treatment since the IC50 for each individual formulation had been selected in this assay. Previous studies have demonstrated that low-dose PTX induced G0/G1 cell cycle arrest in esophageal squamous cell carcinoma larynx carcinoma and ovarian cancer [38]. Consistently, the results of the present study demonstrated that 22.5nM (correspond to IC50 value) of PTX blocked G0/G1 phases of the cell cycle, dose-related to the treatment with SpHL-folate-PTX. The arrest in the G0/G1 phase suggests early detection of damage in genetic material, which gives the cells time to repair the critical damage before DNA replication occurs, avoiding the propagation of genetic lesions to progeny cells and activating the apoptotic pathway [39]. Thus, arresting tumor cells in G0/G1 can slow the proliferation of tumor cells and the induction of apoptosis may have more impact on growth and death of tumor cells.

As shown in Figure 2, apoptosis was confirmed as the main cell death pathway for all groups evaluated. There is evidence that PTX is able to induce apoptosis through the activation of bcl-2 and raf-1, induction of p53 and tumor necrosis factor expression, as well as activation of EGFR-tyrosine kinase complex [3,4,11,40]. Besides, studies have shown that the activation of caspases (caspase-3, caspase-9, caspase-8, and caspase-2) might be involved leading to nuclear fragmentation and phospholipids externalization [11,41,42].

Hemocompatibility was evaluated for PTX-loaded liposomes in order to assure the suitable characteristics for intravenous administration. It is known that many solvents as well as anticancer drugs such as Cremophor EL^{TM} and PTX, respectively, cause irreversible interaction and fusion with the membrane of the blood cells, leading to cell lyse [22,43-46]. Thus, the PTX-loaded liposome may be an alternative to overcome this toxic effect. According to the American Society for Testing and Materials (E2324-08), the nanoparticles that induce a hemolysis ratio less than5% are considered as non-toxic[46-47]. The liposomal systems, with or without PTX, presented lower hemolysis levels than PTX:Cr+Et and Cr:Et suggesting greater biocompatibility. This finding can be attributed to the presence of PEG that prevents the

interaction of nanocarrier with blood components and reduces the hemolysis ratio to values below 5.0%[46,48]. Similar results were previously reported [22,49].

Concerning the antitumor activity, the encapsulation of PTX in SpHL-folate clearly improved the antitumor activity of the drug (Figure 5 and Table 2). A significant difference in the tumor growth profile and the tumor mass of mice that received SpHL-folate-PTX compared to SpHL and Cr+Et could be verified. The inhibition of tumor growth for SpHL-folate-PTX was approximately 70% and 30% higher than PTX:Cr+Et and SpHL-PTX, respectively. This finding might be explained by the fact that SpHL-folate-PTX led to an increase of PTX cellular concentration due to the combination of active targeting and prolonged circulation proprieties, resulting in a significant antitumor effect. Since MDA-MB-231 cell lines have folate receptors in the cell membrane, an improved uptake mediated by these receptors may occur. On the other hand, different PTX treatments were not able to reduce the tumor volume showing the cytostatic action of this drug [1,2,4,6-8,13].

Despite the tumor volume measurement has been considered an important tool in the therapeutic efficacy evaluation, it is not the most accurate markers of efficacy. It is well-established the appearance of areas of edema, apoptotic, fibrotic, and necrotic tissue after treatment [50,51]. Consequently, tumor volume might not reflect the residual disease state. In this way, the acquisition of scintigraphic images allowed elucidating better the antitumor efficacy of treatments by labeling only viable tumor cells. The previous study has demonstrated the feasibility of ^{99m}Tc-HYNIC-β-Ala-Bombesin$_{(7–14)}$ as a functional diagnostic agent for MDA-MB-231 tumors [27]. Scintigraphic images analysis confirmed the significant reduction of viable residual tumor mass for the group treated with SpHL-folate-PTX. In addition, a substantial reduction of RTV after the treatment with SpHL-folate-PTX was observed (58.0%). These results corroborate the tumor volume measurements (Figure 5 and Table 2) and demonstrate that SpHL-folate-PTX was more effective to cut down on the RTV.

Microscopical analyses of the tumor showed that mice PTX treated had mass markedly lower than the control groups, corroborating the tumor volume data. On the other hand, no significant difference between the control groups was observed after histological analyses. Mice treated with the liposomal formulation showed tumors in a predominantly tubular arrangement, which suggests the presence of cells more homogeneous and a less aggressive tumor compared to the control group.

Significant changes in the percentage of neoplasia, necrosis, and inflammation areas were verified after the administration of PTX in different formulations, compared with the control group. Although the histological evaluation has shown extensive necrosis areas after SpHL-

folate-PTX treatment, a reduction of this parameter percentage was observed by histomorphometric analyses. This fact may be explained by the smaller tumor size associated with the presence of a significant peripheral inflammation area and a small number of neoplastic cells leading to diminished necrosis area calculated by histomorphometric analyses.

The extensive inflammatory areas were observed after PTX treatments, mainly for SpHL-folate-PTX. Previous studies have shown that PTX is able to increase IL-1β, TNF- α and T lymphocytes in different cell lines [52,53]. In this way, one hypothesis for the increased efficacy of SpHL-folate-PTX might be related to the higher cellular uptake of them that leads to a higher drug concentration inside the cells causing a pronounced inflammatory response against the tumor, which restricts its growth.

Furthermore, immunohistochemistry demonstrated that the SpHL-folate-PTX treatment reduced significantly the count of Ki-67 positive cells compared to other groups. This result corroborates the tumor volume data as well as scintigraphic images and histomorphometric data, suggesting an involvement ofPTX on the inhibition of cell proliferation. The presence of apoptotic cells, evaluated by caspase-3, was significantly higher for SpHL-folate-PTX than the other groups. This behavior is in agreement with the results obtained in the cell death profile analyses by flow cytometry (Table X). Although in vitro studies had shown a similar number of apoptotic cells of the group treated with PTX:Cr+Et and SpHL-folate-PTX, it is important to emphasize that the dose used to PTX:Cr+Et was 50-times higher than SpHL-folate-PTX. On the other hand, when similar doses of PTX were used in vivo studies the percentage of apoptotic cells was significantly higher in mice treated with SpHL-folate-PTX. Taken together these results suggest that SpHL-folate-PTX therapy was more effective to inhibit cell proliferation and breast cancer progression.

5 Conclusion

In conclusion, the results demonstrated that the folate-functionalized liposome was more effective in the delivery of PTX into tumor cells and, consequently, showed greater *in vivo* antitumor effectiveness. Since breast cancer, especially triple-negative breast cancer, shows aggressive behavior and high lethality, the data of the present study provide a new possibility of future clinical applications of SpHL-folate-PTX formulations in treatment against this type of cancer.

Acknowledgment

The authors would like to thank FAPEMIG, CAPES, CNPq, and LNLS (Campinas, Brazil) for their financial support. In addition, Liziane O. F. Monteiro is grateful to CAPES for providing a scholarship.

Conflicts of interest

Authors declare that they have no conflicts of interest.

References

Papers of special note have been highlighted as: *of interest; **of considerable interest.

1. Iwamoto T. Clinical application of drug delivery systems in cancer chemotherapy: review of the efficacy and side effects of approved drugs. Biol Pharm Bull., 36(5), 715-718, 2013.
2. Zhang D, Yang R, Wang S, Dong Z. Paclitaxel: new uses for an old drug. Drug. Des. Devel. Ther., 8, 279–284, 2014.
3. Barbosa MV, Monteiro LOF, Carneiro G, Malagutti AR, Vilela JMC, et al. Experimental design of a liposomal lipid system: A potential strategy for paclitaxel-based breast cancer treatment. Colloids Surf. B, 136, 553-561, 2015.

** Reports the development of long-circulating and pH-sensitive PEG-folate-coated containing PTX and demonstrate its higher encapsulation percentage and small size (next to 200 nm), besides to a more pronounced cytotoxic against MDA-MB-231 and MCF-7 cell lines.

4. Barbuti AM, Chen Z. Paclitaxel through the ages of anticancer therapy: Exploring its role in chemoresistance and radiation therapy. Cancers, 7(4), 2360-2371, 2015.
5. Monteiro LOF, Lopes SCA, Barros ALB, Magalhães-Paniago R, Malachias Â, Oliveira MC, et al. Phase behavior of dioleyphosphatidylethanolamine molecules in the presence of components of pH-sensitive liposomes and paclitaxel. Colloids Surf. B, 144, 276-283, 2016.

* By SAXS analyses, the findings clearly evidence the phase transition of DOPE molecules in the presence and absence of PTX indicating that the introduction of the drug in the system does not bring damage to the pH-sensitivity of SpHL-PTX.

6. Bertrand N, leroux JC. The journey of a drug-carrier in the body: an anatomo-physiological perspective. J. Controll. Release, 161, 152-163, 2012.

7. Koudelka S, Turánek J. Liposomal paclitaxel formulations. J. Controll. Release, 163, 322-334, 2012.
8. Surapaneni MS, Das SK, Das NG. Designing Paclitaxel Drug Delivery Systems Aimed at Improved Patient Outcomes: Current Status and Challenges. ISRN, 2012, 1-15, 2012.
9. Yuan X, Ji W, Chen S, Bao Y, Tan S, Lu S, et al. a novel paclitaxel-loaded poly(d,l-lactide-coglycolide)-Tween 80 copolymer nanoparticle overcoming multidrug resistance for lung cancer treatment. Int. J. Nanomed., 11, 2119–2131, 2016.
10. Monteiro LOF, Fernandes RS, Oda CMR, Lopes SC, Townsend DM, Cardoso VN et al. Paclitaxel-loaded folate-coated long circulating and pH-sensitive liposomes as a potential drug delivery system: a biodistribution study. Biomed. Pharmacother., 97, 489–495, 2018.

**A biodistribution study which indicates that folate presence will provide a cell-specific intracellular delivery, since a higher tumor-muscle ratio was observed after SpHL-folate-PTX intravenous administrate.

11. Videira MA, Arranja AG, Gouveia, LF. Experimental design towards an optimal lipid nanosystem: A new opportunity for paclitaxel-based therapeutics. Eur. J. Pharm. Sci., 49, 302-310, 2013.
12. Feng L, Mumper RJ. A critical review of lipid-based nanoparticles for taxane delivery. Cancer Lett., 334, 157-175, 2013.
13. Yared JA, Tkaczuk KH. Update on taxane development: new analogs and new formulations. Drug Des. Devel. Ther., 6, 371-384, 2012.
14. Monteiro LOF, Malachias A, Pound-Lana G, Magalhães-Paniago R, Mosqueira VCF, Oliveira MC, et al. Paclitaxel-loaded ph-sensitive liposome: new insights on structural and physicochemical characterization. Langmuir, 34(20), 5728-5737, 2018.

*Demonstrates the pH-sensitivity of SpHL-PTX evidenced by changes in the supramolecular organization of DOPE molecules at lower pH conditions. Furthermore, morphological and physicochemical characterization of SpHL-PTX evidenced the formation of nanosized dispersion suitable for intravenous administration.

15. Monteiro LOF, Fernandes RS, Castro LC, Cardoso VN, Oliveira MC, Townsend DM, et al. Technetium-99m radiolabeled paclitaxel as an imaging probe for breast cancer in vivo. Biomed. Pharmacother., 89, 146-151, 2017.
16. Barbosa MV, Monteiro LOF, Malagutti AR, Oliveira MC, Carvalho-Junior AD, Leite EA. Comparative study of first-derivate spectrophotometry and high performance liquid chromatography methods for quantification of paclitaxel in liposomal formulation. J. Braz. Chem. Soc., 43, 1-6, 2015.

17. Arbab AS, Koizumi K, Toyama K, Araki T. Uptake of Technetium- 99m-Tetrofo smin, Technetium-99m-MIBI and Thallium-201 in Tumor Cell Lines. J. Nucl. Med., 37(9), 1551-1556, 1996.
18. Paillard A, Hindré F, Vignes-Colombeix C, Benoit J, Garcion E. The importance of endo-lysosomal escape with lipid nanocapsules for drug subcellular bioavailability. Biomaterials, 31, 7542-7554, 2010.
19. Nie s, Hsiao WLW, Pan W, Yang Z. Thermoreversible Pluronic® F127-based hydrogel containing liposomes for the controlled delivery of paclitaxel: in vitro drug release, cell cytotoxicity, and uptake studies. Int. J. Nanomedicine, 6, 151–166, 2011.
20. Vichai V, Kirtikara K. Sulforhodamine B colorimetric assay for cytotoxicity screening. Nat. Protoc.. 1, 1112− 1116, 2006.
21. Li Y, Xiao K, Luo J, Xiao W, Lee JS, Gonik AM, et al. Well-defined, Reversible Disulfide Cross-linked Micelles for Ondemand Paclitaxel Delivery. Biomaterials, 32(27), 6633–6645, 2011.
22. Jain V, Swarnakar NK, Mishra PR, Verma A, Kaul A, Mishra AK, et al. Paclitaxel loaded PEGylated gleceryl monooleate based nanoparticulate carriers in chemotherapy. Biomaterials, 33(29), 7206-7220, 2012.
23. Zhang X, Huang Y, Zhao W, Chen Y, Zhang P, Li J, et al. PEG-Farnesyl Thiosalicylic Acid Telodendrimer Micelles as an Improved Formulation for Targeted Delivery of Paclitaxel. Mol. Pharm., 4(11),2807−2814, 2014.
24. Sinha A. Down regulation of SPAG9 reduces growth and invasive potential of triple-negative breast cancer cells: possible implications in targeted therapy. J. Exp. Clin. Cancer Res., 32, 1-11, 2013.
25. Meng S, Su B, Li W, Ding Y, Tang L, Zhou W, et al. MENG, S. *et al*. Enhanced antitumor effect of novel dual-targeted paclitaxel liposomes. Nanotechnology, 21, 415103, 2010.
26. Roland CL, Dineen SP, Lynn KD, Sullivan LA, Dellinger MT, Sadegh L, et al. Inhibition of vascular endothelial growth factor reduces angiogenesis and modulates immune cell infiltration of orthotopic breast cancer xenografts. Mol. Cancer Ther., 8(7), 1761-1771, 2009.
27. De Barros ALB, Mota LG, Ferreira CA, Corrêa NCR, Góes AM, de Oliveira MC, et al. ^{99m}Tc-labeled bombesin analog for breast cancer identification. J. Radioanal. Nucl. Chem., 2331-2338, 2012.

*Demonstrate that HYNIC-βAla-Bombesin(7–14) radiolabeled with technetium-99m can be considered as a candidate for the identification of bombesin-positive tumors, as MDA-MB-231 cancer cell line.

28. Olusanya TOB, Ahmad RRH, Ibegbu DM, Smith JR, Elkordy AA. Liposomal Drug Delivery Systems and Anticancer Drugs. Molecules, 23, 1-17, 2018.
29. Bertrand N, Wu J, Xu X, Kamaly, N, Farokhzad OC. Cancer nanotechnology: the impact passive and active targeting in the era of modern cancer biology. Adv. Drug. Deliv. Ver., 66, 2-25, 2014.
30. Marshalek JP, Sheeran PS, Ingram P, Dayton PA, Witte RS, Matsunaga TO. Intracellular delivery and ultrasonic activation of folate receptor-targeted phase-change contrast agents in breast cancer cells *in vitro*. J. Control. Release, 243, 69-77, 2016.
31. Yang MM, Wilson WR, Wua Z. pH-Sensitive PEGylated Liposomes for Delivery of an Acidic Dinitrobenzamide Mustard Prodrug: Pathways of Internalization, Cellular Trafficking and Cytotoxicity to Cancer Cells. Int. J. Pharm., 516, 323-333, 2017.
32. Salatin S, Maleki S, Yari KA. Effect of the surface modification, size, and shape on cellular uptake of nanoparticles. Cell. Biol. Int., 39, 881-890, 2015.
33. Cleal K, He L, Watson PD, Jones AT. Endocytosis, Intracellular Traffic and Fate of Cell Penetrating Peptide Based Conjugates and Nanoparticles. Curr. Pharm. Des., 2878-2894, 2013.
34. Gu Q, Xing JZ, Huang M, Zhang X, Chen J. Nanoformulation of paclitaxel to enhance cancer therapy. J. Biomater. Appl., 28(2), 298-307, 2012.
35. Schiff PB, Fant J, Horwitz SB. Promotion of microtubule assembly in vitro by taxol. Nature, 277, 665-667, 1979.
36. Lv C, Qu H, Zhu W, Xu K, Xu A, Jia B, et al.Low-Dose Paclitaxel Inhibits Tumor Cell Growth by Regulating Glutaminolysis in Colorectal Carcinoma Cells. Front. Pharmacol., 8, 1-10, 2017.
37. Li W, Zhu W, Lv C, Qu H, Xu K, Li H, et al. Low-dose paclitaxel downregulates MYC proto-oncogene bHLH transcription factor expression in colorectal carcinoma cells. Oncol. Lett., 15, 1881-1887, 2018
38. Yun T, Liu Y, Gao D, Linghu E, Brock MV, Yin D, et al. Methylation of CHFR sensitizes esophageal squamous cell cancer to docetaxel and paclitaxel. Genes Cancer, 6, 38-48, 2015.
39. Maroni LC, Silveira ACO, Leite EA, Melo MM, Ribeiro AFC, Cassali GD, et al. Antitumor effectiveness and toxicity of cisplatin-loaded long-circulating and pH-sensitive liposomes against Ehrlich ascitic tumor. Exp. Biol. Med., 237, 973–984, 2012.

40. Kopczynska E. Role of microRNAs in the resistance of prostate cancer to docetaxel and paclitaxel. Contemp. Oncol., 19(6), 423–427, 2015.
41. Grivicich I, Regner A, Rocha AB. Morte Celular por Apoptose. Rev. Bras. Cancerologia, 53(3), 335-343, 2007.
42. Jelínek M, Balušíková K, Kopperová D, Němcová-Fürstová V, Šrámek J, Fidlerová J, *et al*. Caspase-2 involved in cell death induction by taxanes in breast cancer cells. Cancer Cell Int., 13-42, 2013.
43. Krzyzaniak JF, Raymond DM, Yalkowsky SH. Lysis of human red blood cells 2: effect of contact time on cosolvent induced hemolysis. Int. J. Pharm., 152(2), 193-200, 1997.
44. Nornoo AO, Osborne DW, Chow DS. Cremophor-free intravenous microemulsions for paclitaxel: I: formulation, cytotoxicity and hemolysis. Int. J. Pharm, 349(1), 108-116, 2008.
45. Bertrand N, Leroux JC. The journey of a drug-carrier in the body: an anatomophysiological prespective. J. Control. Release, 161,152163, 2012.
46. Dobrovolskaia MA, Mcneil SE. Understanding the correlation between *in vitro* and *in vivo* immunotoxicity tests for nanomedicines. J. Controll. Release, 172(2),456-466, 2013.
47. ASTM E2524-08(2013), Standard Test Method for Analysis of Hemolytic Properties of Nanoparticles, ASTM International, West Conshohocken, PA, 2013, www.astm.org.
48. Bender EA, Adorne MD, Colomé LM, Abdalla DSP, Guterres SS, Pohlmann AR. Hemocompatibility of poly(ε-caprolactone) lipid-core nanocapsules stabilized with polysorbate 80-lecithin and uncoated or coated with chitosan. Int. J. Pharm., 426, 271-279, 2012.
49. Hong SS, Choi JY, Kim JO, Lee MK, Kim SH, Lim SJ. Development of paclitaxel-loaded liposomal nanocarrier stabilized by triglyceride incorporation. Int. J. Nanomedicine, 11, 4465-4477, 2016.
50. Kubota K. From tumor biology to clinical PET: A review of positron emission tomography (PET) in oncology. Ann. Nucl. Med., 15(6), 471–486, 2001.
51. Leite EA, Souza CM, Carvalho-Júnior AD, Coelho LG, Lana AM, Cassali GD, et al. Encapsulation of cisplatin in long-circulating and pH-sensitive liposomes improves its antitumor effect and reduces acute toxicity. Int. J. Nanomedicine, 7, 5259-5269, 2012.
52. Voloshin T, Alishekevitz D, Kaneti L, Miller V, Isakov E, Kaplanov I, et al. Blocking IL1β pathway following paclitaxel chemotherapy slightly inhibits primary tumor growth but promotes spontaneous metastasis. Mol. Cancer Ther., 14(6), 1385–1394, 2015.
53. Mitchison TJ, Pineda J, Shi J, Florian S. Is inflammatory micronucleation the key to a successful anti-mitotic cancer drug? Open Biol., 7, 1-9, 2017.

DISCUSSÃO GERAL

5. DISCUSSÃO GERAL

PTX é um potente agente antitumoral amplamente utilizado contra uma ampla variedade de tumores, incluindo câncer de mama metastático (GUCHELAAR *et al*., 1994; LIU, ZHANG, YAN, 2011; KOUDELKA e TURÁNEK, 2012; SURAPANEMI, DAS, DAS, 2012; ZHANG *et al*., 2014; CHAN *et al*., 2016; MONTEIRO *et al*., 2017). Entretanto, a baixa especificidade da formulação mais utilizada na clínica (Taxol®) pode ocasionar elevada toxicidade, uma vez que essa atua de forma indiscriminada em células saudáveis e células tumorais (MIELKE, SPARREBOOM, MROSS, 2006; SURAPANEMI, DAS, DAS, 2012; VANNEMAN e DRANOFF, 2012; YARED, TKACZUK, 2012; BARBOSA *et al*., 2015; SIMPSON *et al*., 2016). Nesse sentido, esforços vem sendo feitos no desenvolvimento de novas estratégias para o diagnóstico e tratamento do câncer, no intuito de minimizar os efeitos tóxicos das formulações atualmente disponíveis (LAOUINI *et al*., 2012; MADNI *et al*., 2014; SAFARZADEH, SHOTORBANI, BARADARAN, 2014; SIEGEL, MILLER, JEMAL, 2015; MONTEIRO *et al*., 2018b).

Lipossomas pH-sensíveis tem sido uma abordagem promissora para aumentar a eficácia terapêutica e especificidade de diversos fármacos antitumorais. Estes sistemas foram delineados para explorar o pH reduzido existente na matriz extracelular tumoral e, também, dentro das vesículas endossomais, condição que induz a desestabilização das vesículas lipossomais e liberação do conteúdo encapsulado no citoplasma celular (DE OLIVEIRA *et al*., 1998; FERREIRA *et al*., 2013; LOPES *et al*., 2013; MALLICK *et al*., 2014; STUBBS, MC SHEEHT, GRIFFITHS, 1999; FERREIRA *et al*., 2013; GOUBRAN *et al*., 2014; BARBOSA *et al*., 2015). Entretanto, sistemas lipossomais pH-sensíveis precisam ser estáveis no pH fisiológico dos fluidos corporais para permitir sua administração. Nesse contexto, a avaliação da organização estrutural dos lípides formadores da membrana lipossomal frente alterações no pH torna-se essencial para determinar a atividade antitumoral dos sistemas (DE OLIVEIRA *et al*., 1998; DE OLIVEIRA *et al*., 2000; MALLICK *et al*., 2014; MONTEIRO *et al*., 2016). Baseado nisso, a parte inicial desse estudo dedicou-se a avaliação das características físico-químicas e da organização supramolecular dos lipossomas pH-sensíveis em diferentes meios (NaCl 0,9% m/v, DMEM e DMEM com 10% SFB) em diferentes pH (7,4; 6,8 e 5,0) utilizando a técnica de SAXS.

Os resultados obtidos para o sistema lipossomal em NaCl 0,9% demonstraram a estabilidade dos LpHS e LpHS-PTX em pH fisiológico (7,4). Esse resultado pode ser confirmado pelos dados obtidos pela técnica de DLS, AF4-MALS-DLS e MET. O estudo revelou também, que o sistema sofreu desestabilização em condições ácidas, semelhantes àquelas encontradas na região tumoral (pH 6,8 e 5,0) (MONTEIRO *et al*., 2018b). Além disso, observou-se que a introdução do PTX na bicamada lipídica levou a um aumento significativo no tamanho das vesículas lipossomais e a alterações significativas na organização supramolecular do sistema. Contudo, sugere-se que a incorporação do antitumoral na bicamada lipídica não ocasionou alterações na pH-sensibilidade do sistema lipossomal. Esses resultados corroboram àqueles previamente apresentados por Barbosa e colaboradores (2015) que demonstraram a habilidade do LpHS-PTX em liberar 75,0% do conteúdo encapsulado em pH 5,0.

As análises dos sistemas lipossomais na presença dos constituintes de meio de cultura e do SFB foram realizadas no intuito de aproximar à condição de interação entre os LpHS e LpHS-PTX e os componentes dos fluidos biológicos (DE OLIVERA *et al*., 2000; SIMÕES *et al*., 2004, MONTEIRO *et al*., 2018b). Os dados demonstraram a formação de estruturas lipossomais mais organizadas, contudo, esse fato não alterou a pH-sensibilidade do sistema, uma vez que alterações na organização supramolecular do sistema foram observadas em meio ácido, até mesmo na presença de proteínas do soro fetal bovino. Resultados semelhantes foram previamente reportados por Silva e colaboradores (2011).

Aliado a isso, as análises morfológicas e físico-químicas do sistema demonstraram parâmetros adequados para administração intravenosa (LIU, HUANG, 1990; DRISCOLL, 2006; HIPPALGAONKAR, MAJUNDAR, KANSARA, 2010; USP, 2016). As técnicas de DLS, AF4-MALS-DLS e MET indicaram a presença de vesículas menores que 200 nm, com características de um sistema monodisperso. É interessante observar que, como anteriormente mencionado, o tamanho reduzido favorece o escape do SFM e a passagem dos lipossomas pelas fenestrações presentes no endotélio tumoral permitindo seu acúmulo nessa região devido ao efeito EPR, além de aumentar a estabilidade da formulação na presença de fluidos corporais (MATSUMURA, MAEDA, 1986; LIU, HUANG, 1990; VEMURI, RODES, 1995; DE OLIVEIRA *et al*., 1998; DE OLIVEIRA *et al*., 2000; ULRICH, 2002; MENG *et al*., 2010; SAWANT, TORCHILIN, 2012; FERREIRA *et al*., 2013; MONTEIRO *et al*., 2018b). O potencial zeta reportado, com valores próximos a neutralidade, pode ser atribuído à presença do DSPE-PEG_{2000} na composição do sistema lipossomal, que ocasiona a redução da mobilidade

eletroforética. Esse fato pode ser explicado pela barreira hidrofílica formada pelo PEG na superfície da nanopartícula, protegendo-a de processos como fusão, agregação e adesão de opsoninas plasmáticas, contribuindo assim para o aumento do tempo de circulação sanguínea do sistema avaliado (WOODLE *et al*., 1992; MIYATA, CHRISTI, KATAOKA, 2011; SOARES *et al*., 2011; LEITE *et al*., 2012; LOPES *et al*., 2013; WOLFRAM *et al*., 2014; BARBOSA *et al*., 2015; DE BARROS *et al*., 2015). Os resultados demonstrados para os LpHS-folato-PTX foram semelhantes aos apresentados para LpHS-PTX.

Uma vez que resultados prévios *in vitro* demonstraram que LpHS-folato-PTX foi capaz de entregar preferencialmente o PTX no interior das células tumorais indicando que a funcionalização da superfície lipossomal com moléculas de folato é uma estratégia efetiva para aumentar a citotoxicidade (BARBOSA *et al*., 2015), uma avaliação do perfil de captação intracelular *in vitro* bem como análise do ciclo celular foram conduzidos.

A análise do perfil de captação celular dessas nanopartículas demonstrou que, apesar da menor captação intracelular observada para LpHS-PTX e LpHS-folato-PTX quando comparada ao PTX:Cr+Et, os nanossistemas lipossomais foram capazes de carrear uma maior concentração de PTX para o interior das células. Uma vez no interior das células, o PTX se liga aos microtúbulos e leva a inibição do processo de divisão celular mediante bloqueio do ciclo celular nas fases G0/G1 ou G2/M, dependendo da concentração de PTX utilizada. Essas diferenças no perfil de ciclo celular foram observadas entre os diferentes grupos avaliados. Esse fato pode ser atribuído as diferentes doses utilizadas nessa avaliação, correspondentes a concentração inibitória que provoca morte de 50% das células (CI50) para cada formulação individualmente avaliada (SCHIFF *et al*., 1979; GUCHELAAR *et al*., 1994; OTHMAN *et al*., 2001; ALTMANN & GERTSH, 2007; SURAPANENI, DAS e DAS, 2012; ZHANG *et al*., 2014; BARBOSA *et al*., 2015; BARBUTI e CHEN, 2015; LV *et al*., 2017). Estudos mostram que o PTX é capaz de induzir o processo de morte celular por diferentes vias de ativação intracelulares (VIDEIRA, ARRANJA, GOUVEIA, 2013; BARBUTI, CHEN, 2015; KOPCZYNSKA, 2015). A avaliação dos tratamentos PTX:Cr+Et, LpHS-PTX e LpHS-folato-PTX confirmou o processo de apoptose como a principal via de morte das células avaliadas em todos os grupos. Entretanto estudos futuros são necessários para determinar com maiores detalhes as vias ativadas ao longo desse processo.

A fim de prosseguir com os estudos *in vivo*, almejando a administração intravenosa dos nanosistemas, avaliamos inicialmente a biocompatibilidade do sistema com os fluidos corporais. Como as hemácias são as células que se encontram em maior quantidade na corrente sanguínea, essas têm sido alvo de pesquisas para testes de toxicidade de diferentes formulações nanoestruturadas. De acordo com *American Society for Testing and Materials* (E2324-08) taxa hemolítica inferior a 5,0% caracteriza nanopartículas não tóxicas (DOBROVOLSKAIA *et al*., 2008; DASH *et al*., 2010; BENDER *et al*., 2012; JAIN *et al*., 2012; DOBROVOLSKAIA, MCNEIL, 2013). Nesse sentido, os resultados demonstraram que os sistemas lipossomais, carreando ou não o PTX, apresentaram baixos níveis de hemólise sugerindo maior biocompatibilidade dos componentes bem como maior capacidade em inibir a interação do PTX com as hemácias. Embora, a propriedade fusogênica da DOPE tenha um importante papel na interação com hemácias, alguns estudos sugerem que o revestimento da formulação com o PEG, um polímero hidrofílico, ocasiona uma redução da taxa de hemólise para valores inferiores a 5,0% (DOBROVOLSKAIA *et al*., 2008; BENDER *et al*., 2012). Portanto, esses resultados nos encorajaram a prosseguir com os estudos *in vivo* de avaliação da biodistribuição e da atividade antitumoral.

O perfil de biodistribuição *in vivo* foi avaliado no intuito de demonstrar a real contribuição da presença do folato no aumento da captação pelo tecido tumoral. Sabe-se que nanopartículas, em geral, são extensivamente fagocitadas pelas células do SFM. Esse fato explica os resultados de biodistribuição apresentados para os sistemas lipossomais em animais sadios, que demonstraram elevada captação em fígado e baço, além de uma captação renal significativa (LOOMIS, MCNEELY, BELLAMKONDA, 2011; DESHPANDE, BISWAS, TORCHILIN, 2012; AWASTHI *et al*., 2003; DE BARROS *et al*., 2015; FERNANDES *et al*., 2016; MONTEIRO *et al*., 2017). A partir das imagens cintilográficas obtidas em animais BALB/c nude acometidos por tumor de mama MDA-MB-231 foi possível observar que, no tempo de 4 h, LpHS-folato-PTX apresentou uma captação tumoral significativamente maior comparada ao PTX:Cr+Et e LpHS-PTX. Além disso, a captação tumoral foi superior à captação no músculo contralateral. Esses dados podem ser explicados pela presença do folato na superfície da vesícula aliada à propriedade de circulação prolongada conferida pela presença de DSPE-PEG_{2000}, as quais proporcionam aumento da especificidade e um maior acúmulo desse sistema na região tumoral ao longo tempo. Assim, em células tumorais que apresentam uma expressão aumentada de receptores de ácido fólico, como a linhagem MDA-MB-231, pode-se inferir que

a uma maior captação do nanossistema folatado permitirá alcançar concentrações intracelulares elevadas do fármaco na região tumoral de forma a garantir adequada atividade antitumoral.

Os resultados do estudo de atividade antitumoral corroboraram os dados de biodistribuição ao demonstrar uma redução expressiva no crescimento tumoral nos animais tratados com LpHS-folato-PTX em comparação ao PTX:Cr+Et ($p<0,05$). Entre as formulações lipossomais contendo PTX, diferença significativa no volume tumoral entre os grupos foi observada somente a partir do vigésimo dia de avaliação (após o final do tratamento). Vale mencionar ainda que, diferente do grupo tratado com LpHS-PTX e PTX:Cr+Et, o tratamento com LpHS-folato-PTX inibiu significativamente o crescimento tumoral, resultando praticamente na ausência de alteração desse parâmetro ao longo de todo período experimental ($p<0,05$). Dados de inibição do crescimento tumoral foram aproximadamente 1,7 e 1,3 vezes maiores para LpHS-folato-PTX do que aqueles apresentados para LpHS-PTX e PTX:Cr+Et, respectivamente. É interessante observar também que nenhum dos tratamentos utilizando o PTX foi capaz de reduzir o volume tumoral dos camundongos BALB/c nude fêmeas, demonstrando que o fármaco apresenta significativa ação citostática nas células tumorais (SCHIFF, FANT, HORWITZ, 1979; GUCHELAAR *et al.*, 1994; JORDAN, WILSON, 2004; ALTMANN, GERTSH, 2007; SURAPANENI, DAS, DAS, 2012).

Apesar da medida do volume tumoral ser uma importante ferramenta para avaliação da atividade terapêutica, sabe-se que esse parâmetro não reflete as características específicas das células tumorais, como áreas de tecido necrótico, apoptose, inflamação, além da presença de células tumorais viáveis (KUBOTA, 2001; LEITE *et al.*, 2012). Nesse sentido, imagens cintilográficas dos animais tratados foram obtidas no início e no final do tratamento. Além disso, análises histomorfométricas e imunohistoquímicas foram realizadas nos tecidos tumorais.

Estudos anteriores demonstraram a viabilidade do complexo ^{99m}Tc-HYNIC-β-Ala-Bombesina$_{(7–14)}$ como agente diagnóstico tumoral devido a sua afinidade pelas células MDA-MB-231 (DE BARROS *et al.*, 2012). Nesse sentido, os resultados utilizando este agente de identificação confirmaram a redução significativa da massa tumoral residual viável para o grupo tratado com LpHS-folato-PTX. Além disso, a redução do volume tumoral residual após os tratamentos com PTX:Cr + Et, LpHS-PTX e LpHS-folato-PTX foi de 31,7%, 38% e 58,0% em relação ao grupo controle, respectivamente. Estes resultados estão de acordo com os observados

na determinação do volume do tumor ao longo do tempo, demonstrando novamente o sistema lipossomal folatado como a melhor opção terapêutica.

As análises histológicas do tecido tumoral mostraram que os animais tratados com PTX apresentaram uma massa tumoral visivelmente menor que os grupos controle, dados que corroboram com os outros previamente apresentados. Além disso, animais tratados com as formulações lipossomais apresentaram uma organização das células tumorais predominantemente em arranjo tubular, sugerindo a formação de um tecido mais homogêneo com características menos agressivas quando comparadas ao grupo controle. É interessante notar que, após o tratamento com LpHS-folato-PTX uma redução significativa nas áreas de neoplasia bem como na contagem de células positivas para Ki-67 foi observada quando comparada aos grupos controle (LpHS e Cr+Et). Por outro lado, aumento significativo na porcentagem das áreas de inflamação foi observado nas amostras analisadas para esse mesmo grupo de tratamento. Este achado pode ser explicado pela capacidade do PTX em modular alguns marcadores de resposta inflamatória, como IL-1β, linfócitos T e TNF-α, levando ao aumento da resposta inflamatória nesse grupo (RICHES, CHAN, WINSTON, 1996; ALISHEKEVITZ *et al*., 2015; MITCHISON *et al*. 2017). Os dados demonstraram também uma porcentagem significativamente maior de células caspase-3 positivas, características de células em processo apoptótico. Embora pelos dados do estudo *in vitro* de citometria de fluxo tenha se observado taxas de apoptose semelhantes para o PTX:Cr+Et e LpHS-folato-PTX, uma dose 50 vezes maior foi utilizada para o tratamento com PTX:Cr+Et. Por outro lado, nos animais acometidos com tumor e tratados com doses semelhantes das diferentes formulações, observou-se taxas de apoptose mais elevadas no grupo LpHS-folato-PTX, sugerindo que maiores concentrações foram alcançadas no tecido tumoral e consequentemente melhor resposta terapêutica foi obtida.

O esquema apresentado na Figura 11 resume os resultados principais obtidos nesse estudo: 1) A formulação apresenta características físico-químicas adequadas para administração *in vivo*; 2) O sistema lipososmal apresenta-se estável em pH 7.4 nos diferentes meios avaliados, demonstrando a capacidade da formulação em manter sua integridade na circulação sanguínea; 3) Avaliação da biodistribuição *in vivo* demonstrou que a presença do folato ocasiona uma ligação sítio-específica às células MDA-MB-231, devido a preseca de receptores próprios em sua superfície, aumentando o acúmulo dos LpHS-folato-PTX na região tumoral; 4) Uma vez em contato com o pH 5,0 da região endossomal, estudos de organização estrutural

demonstraram a desestabilização da estrutura lipossomal e a liberação do conteúdo encapsulado; 5) Uma vez no citoplasma celular, o PTX se liga a subunidades β tubulin ocasionando a estabilização irreversível dos microtubulos, o que resulta em inibição do ciclo celular em G0/G1 culminando em morte celular por apoptose; 6) O conjunto de resultados obtidos, então, explicam a redução significativa do crescimento tumoral *in vivo* demonstrando a maior eficácia da formulação LpHS-folato-PTX, tornando-a uma alternativa promissora no tratamento de tumor de mama.

Figura 11 – Hipótese da atuação dos LpHS-folato-PTX *in vivo*. O sistema lipossomal, que apresenta paramêtros físico químicos adequados para uso endovenoso, após administrado se acumula no tecido tumoral devido a presença do folato em sua composição, ocasionada por uma ligação sítio-específica aos seus receptores presentes na superfície das células MDA-MB-231. Uma vez internalizados, os lipossomas se desestabilizam em contato com o pH 5,0 endossomal culminando na liberação do PTX no citoplasma celular, que por sua vez se liga aos microtúbulos, ocasionando morte celular por apoptose, resultando em aumento expressivo da atividade antitumoral.

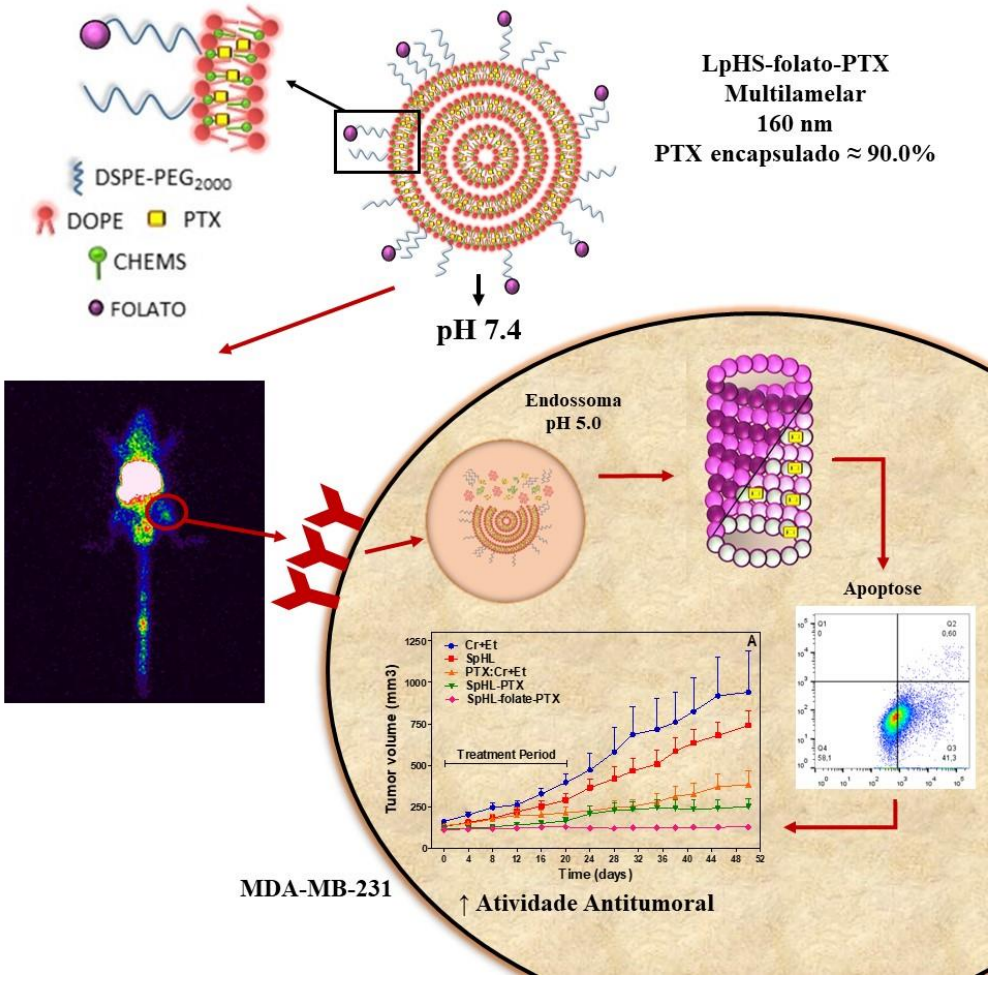

CONCLUSÃO

6. CONCLUSÃO

O presente estudo demonstrou que a inclusão da PTX nos lipossomas pH-sensíveis funcionalizados com folato resultou em um sistema com parâmetros adequados para administração intravenosa. Além disso, constatou-se a pH-sensibilidade do sistema em condições diversas, até mesmo em ambiente com características semelhante as condições fisiológicas, fato primordial para a eficácia terapêutica, uma vez que permite a desestabilização das vesículas lipossomais e a liberação do conteúdo encapsulado no citoplasma da célula tumoral.

Através dos estudos *in vivo* foi possível atestar, por meio de imagens contilográficas, um maior acúmulo dos LpHS-folato-PTX na região tumoral, o que pode ser explicado pela interação entre o folato presente no exterior da bicamada lipossomal e os receptores presentes na superfície das células tumorais, culminando em uma maior concentração de PTX dentro das células MDA-MB-231. Como o câncer de mama, especialmente o câncer de mama triplo negativo, apresenta comportamento agressivo e alta letalidade, pode-se concluir que a presença efetiva do PTX no interior das células favorece os efeitos apoptóticos do fármaco resultado em maior eficácia antitumoral. Assim, o conjunto de resultados apresentados no presente trabalho demonstram o potencial dos LpHS-folato-PTX para aplicação clínicas futuras em pacientes com tumores de mama triplo negativo no intuito de contornar problemas limitantes da terapia além de permitir um tratamento mais efetivo e específico.

Nesse sentido, a continuidade da investigação da efetividade da formulação LpHS-folato-PTX torna-se importante para o entendimento e otimização do sistema desenvolvido com intuito de aprimorar a formulação buscando o desenvolvimento de terapias antitumorais mais específicas e efetivas.

PERSPECTIVAS

7. PERSPECTIVAS

Com base nos resultados do presente estudo, pode-se propor algumas perspectivas, a saber:

- Investigação do mecanismo de ação dos LpHS-folato-PTX
- Avaliação da toxicidade *in vivo* dos LpHS-folato-PTX.

REFERÊNCIAS BIBLIOGRÁFICAS

REFERÊNCIAS BIBLIOGRÁFICAS

AGGARWAL, P., *et al*. Nanoparticle interaction with plasma proteins as it relates to particle biodistribution, biocompatibility and therapeutic efficacy. **Advanced Drug Delivery Reviews**, v. 61, p. 428-437, 2009.

AHN S.G. *et al*. Molecular Classification of Triple-Negative Breast Cancer. **Journal of Breast Cancer**, v. 19, p. 223-230, 2016.

ALISHEKEVITZ, L. *et al*. Blocking IL1β pathway following paclitaxel chemotherapy slightly inhibits primary tumor growth but promotes spontaneous metastasis. **Molecular Cancer Therapeutics**, v. 14, n. 6, p. 1385–1394, 2015.

ALLURI, P.; NEWMAN, L. Basal-like and Triple Negative Breast Cancers: Searching for Positives Among Many Negatives. **Surgical Oncology Clinics of North America**, v. 23, n. 3, p. 567–577, 2014.

ALMEIDA, V. L. *et al*. Câncer e agentes antineoplásicos ciclo-celular específico e ciclo-celular não específico que interagem com o DNA: uma introdução. **Química Nova**, p. 118-129, 2005.

ALTMANN, K. H., GERTSH, J. Anticancer drugs from nature- natural products as a unique source of new microtubule-stabilizing agents. **Royal Society of Chemistry**, p. 327-357, 2007.

ANDÒ, S. *et al*. The Multifaceted Mechanism of Leptin Signaling within Tumor Microenvironment in Driving Breast Cancer Growth and Progression. **Frontiers in Oncology**, v. 4, p. 1-6, 2014.

AWASTHI, V. D. *et al*. Circulation and biodistribution profiles of long-circulating PEG-liposomes of various sizes in rabbits. **International Journal of Pharmaceutics**, v. 253, p. 121-132, 2003.

ASTM E2524-08(2013), Standard Test Method for Analysis of Hemolytic Properties of Nanoparticles, ASTM International, West Conshohocken, PA, 2013, www.astm.org.

BALAZN, D. A.; GODBEY, W. T. Liposomes for use in gene delivery. **Journal of Drug Delivery**, p. 1-12, 2011.

BANGHAM, A. D.; STANDISH, M. M.; WATKINS, J. C. Diffusion of univalent ions across the lamellae of swollen phospholipids. Journal of Molecular Biology, v. 13, p. 238-252, 1965.

BARBOSA, M. V. *et al*. Experimental design of a liposomal lipid system: A potential strategy for paclitaxel-based breast cancer treatment. **Colloids and Surfaces B: Biointerfaces**, v. 136, p. 553-561, 2015.

BARBUTI, A. M.; CHEN, Z. Paclitaxel through the ages of anticancer therapy: Exploring its role in chemoresistance and radiation therapy. **Cancers**, v. 7, n. 4, p. 2360-2371, 2015.

BATISTA, C. M.; CARVALHO, C. M. B.; MAGALHÃES, N. S. S. Lipossomas e suas aplicações terapêuticas: estado da arte. **Revista Brasileira de Ciências Farmacêuticas**, v. 43, n. 2, p. 167-178, 2007.

BENDER, R. J.; GABHANN, M. F. Expression of VEGF and Semaphorin Genes Define Subgroups of Triple Negative Breast Cancer. **PLoS ONE**, v. 8, n. 5, 2013.

BERTRAND, N. *et al*. Cancer nanotechnology: the impact passive and active targeting in the era of modern cancer biology. **Advanced Drug Delivery Reviews**, v. 66, p. 2-25, 2014.

BRASILEIRO-FILHO, G.; PEREIRA, F. E. L.; GUIMARÃES, R. C. Distúrbios do Crescimento e da Diferenciação Celular. In: Brasileiro-Filho, G. Bogliolo Patologia. 7.ed. Rio de Janeiro: Guanabara Koogan, 2006. p. 175-236.

CARVALHO-JÚNIOR, A. D. *et al*. Preparation and cytotoxicity of cisplatin loaded liposomes. **Brazilian Journal Medical Biological Research**, v. 40, p. 1149-1157, 2007.

CHAN, J. K. *et al*. Weekly vs. every-3-week paclitaxel and carboplatin for ovarian cancer. **The New England Journal of Medicine**, v. 374, p. 738-748, 2016.

CHEN, Q. *et al*. Multi-center prospective randomized trial of paclitaxel liposome and traditional taxol in the treatment of breast cancer and non-small-cell lung. **Chinese Journal of Oncology**, v. 25; p. 190-192, 2003.

DASH, B. C. *et al*. The influence of size and charge of chitosan/polyglutamic acid hollow spheres on cellular internalization, viability and blood compatibility. **Biomaterials**, v. 31, n. 32, p. 8188-8197, 2010.

DE BARROS, A. L. B. *et al*. ^{99m}Tc-labeled bombesin analog for breast cancer identification. **Journal of Radioanalytical and Nuclear Chemistry**, p. 2331-2338, 2012.

DE BARROS, A. L. B. *et al*. Bombesin encapsulated in long-circulating pH-sensitive liposomes as a radiotracer for breast tumor identification. **Journal of Biomedical Nanotechnology**, v. 11, n. 2, p. 342-350, 2015.

DE OLIVEIRA, M. C. *et al*. pH-sensitive liposomes as a carrier for oligonucleotides: a physic-chemical study of the interaction between DOPE and 15-mer oligonucleotide in quasi-anhydrous samples. **Biochimica et Biophysica Acta**, v. 1372, p. 301-310, 1998.

DE OLIVEIRA, M. C. *et al*. pH-sensitive liposomes as a carrier for oligonucleotide in excess water. **Biophysical Chemistry**. v. 87, p. 127-137, 2000.

DESHPANDE, P. P.; BISWAS, S.; TORCHILIN, V. P. Current trends in the use of liposomes for tumor targeting. **Nanomedicine**, v. 8, p. 1-32, 2013.

DOBROVOLSKAIA, M. A. *et al*. Preclinical studies to understand nanoparticle interaction with the immune system and its potential effects on nanoparticle biodistribution. **Molecular Pharmaceutics**, v. 5, n. 4, p. 487-495, 2008.

DOBROVOLSKAIA, M. A.; MCNEIL, S. E. Understanding the correlation between *in vitro* and *in vivo* immunotoxicity tests for nanomedicines. **Journal of Controlled Release**, v. 172, n. 2, p. 456-466, 2013.

DONYAI, P.; SEWELL, G. J. Physical and chemical stability of paclitaxel infusions in different container types. **Journal of Oncology Pharmacy Practice**, v. 12, p. 211-222, 2006.

DRISCOLL, D. F. Lipid ingectable emulsions: pharmacopeial and safety issues. **Pharmaceutical Research**. v. 23, p. 1959-1969, 2006.

FADER, A. N.; ROSE, P. G. Abraxane for the treatment of gynecologic cancer patients with severe hypersensitivity reactions to paclitaxel. **International Journal of Gynecological Cancer**, v. 19, n. 7, p. 1281-1283, 2009.

FENG, L. MUMPER, R. J. A critical review of lipid-based nanoparticles for taxane delivery. **Cancer Letters**, v. 334, p. 157-175, 2013.

FERNANDES, R. S. *et al*. Technetium-99m-labeled doxorubicin as an imaging probe for murine breast tumor (4T1 cell line) identification. **Nuclear Medicine Communications**, v. 37; p. 307-312, 2016.

FERREIRA, D. S. *et al*. pH-sensitive liposomes for drug delivery in cancer treatment. **Therapeutic delivery**, v. 4, p. 1-24, 2013.

FOUAD, Y. A.; AANEI, C. Revisiting the hallmarks of cancer. **American Journal of Cancer Research**, v. 7, n. 5, p. 1016-1036, 2017.

FOULKES, W. D.; SMITH, I. E.; REIS-FILHO, J. S. Triple-Negative Breast Cancer. **The New England Journal of Medicine**, v. 363, p. 1938–1948, 2010.

FRÉZARD, F. *et al*. Lipossomas: propriedades físico-químicas e farmacológicas, aplicações na quimioterapia à base de antimônio. **Química Nova**, v. 28, p. 511-518, 2005.

GABIZON, A. *et al*. Long-circulating liposomes for drug delivery in cancer therapy: a review of biodistribution studies in tumor-bearing animals. **Advanced Drug Delivery Reviews**, v. 24; p. 337-344, 1997.

GELDERBLOM, H. *et al*. Cremophor EL: the drawbacks and advantages of vehicle selection for drug formulation. **European Journal of Cancer**, v. 37, p. 1590-1598, 2001.

GENTILE, E. *et al*. Liposomal chemotherapeutics. **Future Oncology**, v. 9, p. 1849–1859, 2013.

GORNSTEIN, E; SCHWARZ, T. L. The paradox of paclitaxel neurotoxicity: Mechanisms and unanswered questions. **Neuropharmacology**, v. 76, p. 175-183, 2014.

GOUBRAN, H. A. *et al*. Regulation of tumor growth and metastasis: the role of tumor microenvironment. **Cancer Growth and Metastasis**, v. 7, p. 9-18, 2014.

GUCHELAAR, H, J. *et al*. Clinical, toxicological and pharmaceutical aspects of the antineoplastic drug taxol: a review. **Clinical Oncology**, v. 4, p. 40-48, 1994.

HANAHAN, D. WEINBERG, R. Hallmarks of Cancer: The Next Generation. **Cell,** v. 144, p. 646-674, 2012.

HENNENFENT, K.; GOVINDAN, R. Novel formulations of taxanes: a review. Old wine in a new bottle? **Annals of Oncology**, v. 17, p. 735-749, 2006.

HIPPALGAONKAR, K.; MAJUNDAR, S.; KANSARA, V. Injectable lipid emulsions – Advancements opportunities and challenges. **American Association of Pharmaceutical Scientists**, v. 11, p. 1526-1540, 2010.

HLATKY, L.; HAHNFELDT, P. Beyond the cancer cell: progression-level determinants highlight the multiscale nature of carcinogenesis risk. **Cancer Research**, p. 659-664, 2014.

HOYER, K. Paclitaxel. **Clinical Journal of Oncology Nursing**, v. 4, p. 51-52, 2000.

HUANG, Y. *et al*. A novel hydrolysis-resistant lipophilic folate derivative enables stable delivery of targeted liposomes in vivo. **International Journal of Nanomedicine**, v. 9, p. 4581–4595, 2014.

INCA - Instituto Nacional do Câncer José Alencar Gomes da Silva – Ministério da Saúde. Estimativa 2018: Incidência de Câncer no Brasil. Disponível em: < http://www.inca.gov.br/estimativa/2018/casos-taxas-brasil.asp>. Acesso em 02 de agosto de 2018.

IWAMOTO, T. Clinical application of drug delivery systems in cancer chemotherapy: review of the efficacy and side effects of approved drugs. **Biological and Pharmaceutical Bulletin**, v. 36, n. 5, p. 715-718, 2013.

JAIN, V. *et al*. Paclitaxel loaded PEGylated gleceryl monooleate based nanoparticulate carriers in chemotherapy. **Biomaterials**, v. 33, n. 29, p. 7206-7220, 2012.

JENA, J. A Study on Natural Anticancer Plants. **International Journal of Pharmaceutical and Chemical Sciences**, v. 1, n. 1, p. 365-368, 2012.

JIAO, Q. *et al*. The latest progress in research on triple negative breast cancer (TNBC): risk factors, possible therapeutic targets and prognostic markers. **Journal of Thoracic Disease**, v. 6, n. 9, p. 1329–1335, 2014.

JORDAN, M. A.; WILSON, L. Microtubules as a target for anticancer drugs. **Nature Reviews Cancer**, v. 4, p. 253-265, 2004.

KENNY, L. M.; ABOAGYE, E. O.; PRICE, P. M. Positron emission tomography imaging of cell proliferation in oncology. **Clinical Oncology**, v. 16, p. 176-185, 2004.

KLIBANOV, A. L. *et al*. Amphipathic polyethyleneglycols effectively prolong the circulation time of liposomes. **Federation of European Biochemical Societies**, v. 268, p. 235-237, 1990.

KOUDELKA, S.; TURÁNEK, J. Liposomal paclitaxel formulations. **Journal of Controlled Release**, v. 163, p. 322-334, 2012.

KOPCZYNSKA, E. Role of microRNAs in the resistance of prostate cancer to docetaxel and paclitaxel. **Contemporary Oncology**, v. 19, n. 6, p. 423–427, 2015.

KUBOTA, K. From tumor biology to clinical PET: A review of positron emission tomography (PET) in oncology. **Annals Nuclear Medicine**, v. 15, n. 6, p. 471–486, 2001.

LASIC, D. D. Novel application of liposomes. **Trens en Biotechnology**, v. 16, p. 307-321, 1998.

LAOUINI, A. *et al*. Preparation, Characterization and applications o liposomes: state of the art. **Journal of Colloid Science and Biotechnology**, v. 1, p. 147-168, 2012.

LEBERT, J. M. *et al*. Advances in the systemic treatment of triple-negative breast cancer. **Current Oncology**, v. 25, p. 142-150, 2018.

LEITE, E. A. *et al*. Encapsulation of cisplatin in long-circulating and pH-sensitive liposomes improves its antitumor effect and reduces acute toxicity. **International Journal of Nanomedicine**, v. 7, p. 5259-5269, 2012.

LIM, W. T. *et al*. Phase I pharmacokinetic study of a weekly liposomal paclitaxel formulation (Genexol-PM) in patients with solid tumors. **Annals of Oncology**, v. 21, p. 382–388, 2010.

LIU, D.; HUANG, L. pH-Sensitive, plasma-stable liposomes with relatively prolonged residence in circulation. **Biochimica et Biophysica Acta,** v. 1022, p. 348-354, 1990.

LIU, G. X.; FANG, G. Q.; XU, W. Dual Targeting Biomimetic Liposomes for Paclitaxel/DNA Combination Cancer Treatment. **International Journal of Molecular Sciences**, v. 15, p. 5287–5303, 2014.

LIU, Y.; ZHANG, B.; YAN, B. Enabling anticancer therapeutics by nanoparticle carriers: the delivery of paclitael. **International Journal of Molecular Sciences**, v. 12, p. 4395-4413, 2011.

LOOMIS, K.; MCNEELEY, K.; BELLAMKONDA, R. V. Nanoparticles with targeting, triggered release, and imaging functionality for cancer applications. **Soft Matter**, v. 7, p. 839-856, 2011.

LOPES, S. C. A *et al*. Preparation, physicochemical characterization and cell viability evaluation of long-circulating and pH-sensitive liposomes containing ursolic acid. **BioMed Research International**, v. 2013, p. 1-7, 2013.

LV, C. *et al*. Low-Dose Paclitaxel Inhibits Tumor Cell Growth by Regulating Glutaminolysis in Colorectal Carcinoma Cells. **Frontiers in Pharmacology**, v. 8, p. 1-10, 2017.

MAEDA, H. *et al*. Tumor vascular permeability and the EPR effect macromolecular therapeutics: a review. **Journal of Controlled Release**, v. 65, p. 271-284, 2000.

MADNI, A. *et al*. Liposomal Drug Delivery: a versatile plataform for challenging clinical applications. **Journal of Pharmacy & Pharmaceutical Sciences**, v. 17, p. 401-426, 2014.

MALLICK, S.; CHOI, J. S. J. Liposomes: Versatile and Biocompatible Nanovesicles for Efficient Biomolecules Delivery. **Nanoscience and Nanotechnology**, v. 14, p. 755-765, 2014.

MANCINI, P. *et al*. Standard of Care and Promising New Agents for Triple Negative Metastatic Breast Cancer. **Cancers**, v. 6, n. 4, p. 2187–2223, 2014.

MARKMAN, M. Managing taxane toxicities. **Support Care Cancer**, v. 11, p. 144-147, 2003.

MATSUMURA, Y., MAEDA, H. A new concept for macromolecular therapeutics in cancer chemotherapy: mechanism of tumoritropic accumulation of proteins and the antitumor agent smancs. **Cancer Research**, v. 46, p. 6387-6392, 1986.

MAYER, L. D.; JANOFF, A. S. Optimizing combination chemotherapy by controlling drug ratios. **Molecular Interventions**, v. 7, n. 4, p. 216-223, 2001.

MENG, S. *et al*. Enhanced antitumor effect of novel dual-targeted paclitaxel liposomes. **Nanotechnology**, v. 21, 2010.

MIELKE, S.; SPARREBOOM, A.; MROSS, K. Peripheral neuropathy: A persisting challenge in paclitaxel-based regimes. **European Journal of Cancer**, v. 42, p. 24-30, 2006.

MINCHOM, A; AVERSA, C.; LOPEZ, J. Dancing with the DNA damage response: next-generation anti-cancer therapeutic strategies. **Therapeutic Advances in Medical Oncology**, v. 10, p. 1–18, 2018.

MITCHISON, J. *et al*. Is inflammatory micronucleation the key to a successful anti-mitotic cancer drug? **Open Biology**, v. 7, p. 1-9, 2017.

MONTEIRO, L. O. F. *et al*. Phase behavior of dioleyphosphatidylethanolamine molecules in the presence of components of pH-sensitive liposomes and paclitaxel. **Colloids and Surfaces B: Biointerfaces**, v. 144, p. 276-283, 2016.

MONTEIRO, L. O. F. *et al*. Technetium-99m radiolabeled paclitaxel as an imaging probe for breast cancer in vivo. **Biomedicine Pharmacotherapy**, v. 89, p. 146-151, 2017.

MONTEIRO, L. O. F. *et al*. Paclitaxel-loaded folate-coated long circulating and pH-sensitive liposomes as a potential drug delivery system: a biodistribution study. **Biomedicine and Pharmacotherapy**, v. 97, p. 489–495, 2018a.

MONTEIRO, L. O. F. *et al*. Paclitaxel-loaded ph-sensitive liposome: new insights on structural and physicochemical characterization. Langmuir, v. 34, n. 20, p. 5728-5737, 2018b.

MUFAMANDI, M. S. *et al*. A review on composite liposomal technologies for specialized drug delivery. **Journal of Drug delivery**, v. 2011, p. 1-19, 2011.

MIYATA, K.; CHRISTI, R. J.; KATAOKA, K. Polymeric micelles for nano-scale drug delivery. **Reactive and Functional Polymers**. v. 71, p. 227–234, 2011.

NOGUEIRA, E. *et al*. Design of liposomal formulation for cell targeting. **Colloids Surf B Biointerfaces**, v. 136, p. 514-526, 2015.

OLUSANYA, T. O. B. *et al*. Liposomal Drug Delivery Systems and Anticancer Drugs. **Molecules**, v. 23, n. 4, p. 1-17, 2018.

OTHMAN, T. *et al*. Hyperthermic enhancement of the apoptotic and antiproliferative activities of paclitaxel. **Pharmacology**, v. 62; p. 208–212, 2001

PAIK, P. *et al*. A phase 2 study of weekly albumin-bound paclitaxel (Abraxane®) given as a two-hour infusion. **Cancer chemotherapy and pharmacology**, p. 1331-1337, 2011.

PAUWELS, E. K. J. *et al*. FDG accumulation and tumor biology. **Nuclear Medicine & Biology**, v. 25, p. 317-322, 1998.

PERCHE, F.; TORCHILIN, V. Recent trends in multifunctional lipossomal nanocarriers for enhanced tumor targeting. **Journal of Drug Delivery**, p. 1-32, 2013.

PFLAUM, J.; SCHLOSSER, S.; MULLER, M. p53 family and cellular stress responses in cancer. **Molecular and Cellular Oncology**, v. 4; p 1-15, 2014.

PRAT, A. *et al*. Molecular characterization of basal-Like and non-basal-like triple-negative breast cancer. **The Oncologist**, v. 18, p. 123–133, 2013.

PRIOR, I. A.; LEWIS, P. D.; MATTOS, C. A comprehensive survey of *ras* mutations in cancer. **Cancer Research**, v. 72, p. 2457-2467, 2012

REDDY, T. J. A.; ALLAGADDA, V. M.; LEAMON, C. P. Targeting Therapeutic and Imaging Agents to Folate Receptor Positive. **Current Pharmaceutical Biotechnology**, v. 6, p. 131-150, 2005.

RIAZ, M. K. *et al*. Surface functionalization and targeting strategies of liposomes in solid tumor therapy: A review. **International Journal of Molecular Sciences**, v. 19, p. 1-27, 2018.

RICHES, D. W.; CHAN, E. D.; WINSTON, B. W. TNF-αinduced regulation and signalling in macrophages. **Immunobiology**, v. 195, p. 477–490, 1996.

ROBBINS, S. L.; COTRAN, R. S. Patologia: Bases patológicas das doenças, 7. ed. Rio de Janeiro: Editora Elsevier, 2005.

ROWINSKY, E. K.; DONEHOWER, M. D. Paclitaxel (Taxol). **The New England Journal of Medicine**, v. 332, p. 1004-1014, 1995.

SAFARZADEH, E., SHOTORBANI, S. S., BARADARAN, B. Herbal medicine as inducers of apoptosis in cancer treatment. **Advanced Pharmaceutical Bulletin**, v. 4, p. 421-427, 2014.

SAPRA, P.; ALLEN, T. M. Ligand-targeted liposomal anticancer drugs. **Progress Lipid Research**, v. 42, p. 439- 462, 2003.

SAWANT, R. R.; TORCHILIN, V. P. Challenges in development of targeted liposomal therapeutics. **The American Association of Pharmaceutical Scientists Journal**, v. 14, p. 303-315, 2012.

SCHIFF, P. B. FANT, J. HORWITZ, S. B. Promotion of microtubule assembly in vitro by taxol. **Nature**, v. 277, p. 665-667, 1979.

SIEGEL, D. P. Inverted micellar intermediates and the transitions between lamelar, cubic, and inverted hexagonal lipid phases-II. Implications membrane-membrane interactions and membrane fusion. **Biophysical Journal**, v. 49, p. 1171-1183, 1986.

SIEGEL, R. L.; MILLER, K. D.; JEMAL, A. Cancer Statistics, 2016. **Cancer Journal Clinicians**, v. 66, p. 7-30, 2016.

SIMÕES S. *et al*. On the formulation of pH-sensitive liposomes with long circulation times. **Advanced Drug Delivery Reviews,** v. 56, p. 947-965, 2004.

SHAILESH. S. *et al*. Liposomes: a review. **Journal of Pharmacy Research**, v. 2, p. 1163-1167, 2009.

SHAH, K. *et al*. Acute non-ST elevation myocardial infarction following paclitaxel administration for ovarian carcinoma: A case report and review of literature. **Journal of Cancer Research and Therapeutics**, v. 8, p. 442-444, 2012.

SHAH, R.; ROSSO, K.; NATHANSON, S. D. Pathogenesis, prevention, diagnosis and treatment of breast cancer. **World Journal of Clinical Oncology**, v. 5, n. 3, p. 283-298, 2014.

SHAJAHAN-HAQ, A. N.; CHEEMA, M. S.; CLARKE, R. Application of metabolomics in Drug Resistance Breast Cancer Research. **Metabolites**, v. 5, p. 100-118, 2015.

SILVA, S. M. L. *et al*. Study of the structural organization of cyclodextrin-DNA complex loaded anionic and pH-sensitive liposomes. **Chemical Physics Letters**, v. 506, p. 66-70, 2011.

SIMPSON, G. R. *et al*. Cancer immunotherapy via combining oncolytic virotherapy with chemotherapy: recent advances. **Oncolytic Virotherapy**. v. 5, p. 1-13, 2016.

SNYDER, J. P. The microtubule-pore gatekeeper. **Nature Chemical Biology**, p. 81-82, 2007.

SOARES, D. C. F. *et al*. Liposomes radiolabeled with ^{159}Gd: in vitro cytotoxic antitumoral activity, biodistribution study and scintigraphic image in Ehrlich tumor bearing mice. **European Journal of Pharmaceutical Sciences**, v. 43, p. 290-296, 2011.

STUBBS, M.; Mc SHEEHY, P. M. J.; GRIFFITHS, R. Causes and consequences of acidic pH in tumors: a magnetic resonance study. **Advances in Enzyme Regulation**, p. 13-30, 1999.

SURAPANENI, M. S.; DAS, S. K.; DAS, N. G. Designing Paclitaxel Drug Delivery Systems Aimed at Improved Patient Outcomes: Current Status and Challenges. **International Scholarly Research Network**, v. 2012, p. 1-15, 2012.

TELES, R. H. G; MORALLES, H. F.; COMINETTI, M, R. Global trends in nanomedicine research on triple negative breast cancer: a bibliometric analysis. **International Journal of Nanomedicine**, v. 13; p. 2321-2336, 2018.

TOMAO, F. *et al*. Triple-negative breast cancer: new perspectives for targeted therapies. **OncoTargets and Therapy**, v. 8, p. 177–193, 2015.

TONG, C. W. S. *et al*. Recent Advances in the Treatment of Breast Cancer. **Frontiers in Oncology**, v.8, p. 1-10, 2018.

TORCHILIN, V. P. Multifunctional nanocarriers. **Advanced Drug Delivery Reviews**, v. 64, p. 302-315, 2012.

TURNER, N. C.; REIS-FILHO, J. S. Tackling the Diversity of Triple-Negative Breast Cancer. **Clinical Cancer Research**, v. 19, n. 23, p. 6380-6388, 2013.

UEHARA, I; TANAKA, N. Role of p53 in the Regulation of the Inflammatory Tumor Microenvironment and Tumor Suppression. **Cancers**, v. 10, n. 7, p. 1-13, 2018.

ULRICH, A. S. Biophysical aspects of using liposomes as delivery vehicle. **Bioscience Reports**, v. 22, 129-150, 2002.

USP 36-NF 34. *The United States Pharmacopoeia National Formulary*. Rockville: United States Pharmacopoeial Convention Inc.; 2016.

VANNEMAN M.; DRANOFF, G. Combining immunotherapy and target therapies in cancer treatment. **Nature Reviews**, v. 12, p. 237-251, 2012.

VEMURI, S.; RHODES, C. T. Preparation and characterization of liposomes as therapeutic delivery systems: a review. **Pharmaceutica Acta Helvetiae**, v. 70, p. 95-111, 1995.

VIDEIRA, M. A.; ARRANJA, A. G.; GOUVEIA, L. F. Experimental design towards na optimal lipid nanosystem: A new opportunity for paclitaxel-based therapeutics. **European Journal of Pharmaceutical Sciences**, v. 49, p. 302-310, 2013.

WANG, X. *et al*. Pharmacokinetics and biodistribution study of paclitaxel liposome in sprague-dawley rats and beagle dogs by liquid chromatography-tandem mass spectrometry. **Drug Research**, v. 63, p. 603–606, 2013.

WANG, M.; THANOU, M. Targeting nanoparticles to cancer. **Pharmacological Research**, v. 62, p. 90-99, 2010.

WATANABE, K.; KANEKO, M.; MAITANI, Y. Functional coating of liposomes using a folate–polymer conjugate to target folate receptors. **International Journal of Nanomedicine**, v. 7, p. 3679–3688, 2012.

WERNER, M. E. *et al*. Preclinical evaluation of Genexol-PM, a nanoparticle formulation of paclitaxel, as a novel radiosensitizer for the treatment of non-small cell lung cancer. **International Journal of Radiation Oncology, Biology and Physics**, v. 83, n. 3, p. 463–468, 2013.

WESTBROOK, K.; STEARNS, V. Pharmacogenomics of breast cancer therapy: An update. **Pharmacology & Therapeutics**, v. 139, p. 1–11, 2013.

WOLFRAM, J. *et al*. Shrinkage of pegylated and non-pegylated liposomes in serum. **Journal of the Brazilian Chemical Society**, v. 114, p. 1-15, 2014.

WOZNIAK, K. M. *et al*. Sustained accumulation of microtubule-binding chemotherapy drugs in the peripheral nervous system: correlations with time course and neurotoxic severity. **Cancer Research**, v. 76, n. 11, p. 3332-3339, 2016.

WOODLE, M. C. *et al*. Sterically stabilized liposomes: reduction in electrophorectic mobility but not electrostatic surface potencial. **Biophysical Journal**, v. 61, p. 902-910, 1992.

XU, X. *et al*. Clinical comparison between paclitaxel liposome (Lipusu®) and paclitaxel for treatment of patients with metastatic gastric cancer. **Asian Pacific Journal of Cancer Prevention**, v. 14, p. 2591-2594, 2013.

YADAV, B. S. *et al*. Systemic treatment strategies for triple-negative breast cancer. **World Journal of Clinical Oncology**, v. 5, n. 2, p. 125-133, 2014.

YAMASHITA, Y. *et al*. Comparison of peripheral neuropathy induced by standard and nanoparticle albumin–bound paclitaxel in rats**. Journal of Pharmacological Sciences**, v. 117, p. 116-120, 2011.

YANG, A.; LI, J.; XU, H. A study on antitumor effect of liposome encapsulated paclitaxel in vivo and in vitro. **Bulletin of Chinese Cancer**, v. 15, p. 862-864, 2006.

YANG, C. H.; HORWITZ, S. B. Taxol®: The First Microtubule Stabilizing Agent. **International Journal of Molecular Sciences**, v. 18, n. 8, p. 1-11, 2017.

YARED, J. A.; TKACZUK, K. H. Update on taxane development: new analogs and new formulations. **Drug Design, Development and Therapy**, v. 6, p. 371-384, 2012.

YERSAL, O.; BARUTCA, S. Biological subtypes of breast cancer: Prognostic and therapeutic implications. **World Journal of Clinical Oncology**, v. 5, n. 3, p. 412–424, 2014.

ZHANG, D. *et al*. Paclitaxel: new uses for an old drug. **Drug Design, Development and Therapy**, v. 8, p. 279-284, 2014.

ZHANG, L. *et al.* Androgen Receptor, EGFR, and BRCA1 as Biomarkers in Triple-Negative Breast Cancer: A Meta-Analysis. **BioMed Research International**, p. 1-12, 2015.

ZHANG, X. *et al.* PEG-Farnesyl Thiosalicylic Acid Telodendrimer Micelles as an Improved Formulation for Targeted Delivery of Paclitaxel. **Molecular Pharmaceutics**, n. 11, p. 2807−2814, 2014.

ZHAO, G.; RODRIGUEZ, B. L. Molecular targeting of liposomal nanoparticles to tumor microenvironment. **International Journal of Nanomedicine**, v. 8, p. 61–71, 2013.

ZYLBERBERG, C.; MATOSEVIC, S. Pharmaceutical liposomal drug delivery: A review of new delivery systems and a look at the regulatory landscape. **Drug Delivery**, v. 23, p. 3319–3329, 2016.

ANEXOS

ANEXOS

Artigos científicos publicados a partir desse trabalho de tese de doutorado:

Artigo 1. Publicado no periódico Langmuir

MONTEIRO, L. O. F., et al. Paclitaxel-loaded ph-sensitive liposome: new insights on structural and physicochemical characterization. Langmuir, v. 34, n. 20, p. 5728-5737, 2018.

LANGMUIR Article
Cite This: *Langmuir* 2018, 34, 5728–5737 pubs.acs.org/Langmuir

Paclitaxel-Loaded pH-Sensitive Liposome: New Insights on Structural and Physicochemical Characterization

Liziane O. F. Monteiro,[†] Ângelo Malachias,[‡] Gwenaelle Pound-Lana,[§] Rogério Magalhães-Paniago,[‡] Vanessa C. F. Mosqueira,[§] Mônica C. Oliveira,[†] André Luís B. de Barros,[∥] and Elaine A. Leite*[,†]

[†]Departamento de Produtos Farmacêuticos, Faculdade de Farmácia, [‡]Departamento de Física, Instituto de Ciências Exatas, and [∥]Departamento de Análises Clínicas, Faculdade de Farmácia, Universidade Federal de Minas Gerais, Av. Antônio Carlos, 6627, 31270-901 Belo Horizonte, Minas Gerais, Brazil

[§]Laboratório de Desenvolvimento Galênico e Nanotecnologia, Universidade Federal de Ouro Preto, Campus Universitário Morro do Cruzeiro, 35400-000 Ouro Preto, Minas Gerais, Brazil

ABSTRACT: A long-circulating and pH-sensitive liposome containing paclitaxel (SpHL-PTX) was recently developed by our group. Once in an acidic environment, for example, tumors, these liposomes undergo destabilization, releasing the encapsulated drug. In this way, the aim of this study was to evaluate the molecular and supramolecular interactions between the lipid bilayer and PTX in similar biological environment conditions. High-sensitivity analyses of SpHL-PTX structures were obtained by the small-angle X-ray scattering technique combined with other techniques such as dynamic light scattering, asymmetric flow field-flow fractionation, transmission electron microscopy, and high-performance liquid chromatography. The results showed that PTX incorporation in the liposomal bilayer clearly leads to changes in supramolecular organization of dioleoylphosphatidylethanolamine (DOPE) molecules, inducing the formation of more ordered structures. Changes in supramolecular organization were observed at lower pH, indicating that pH sensitivity was preserved even in the presence of fetal bovine serum proteins. Furthermore, morphological and physicochemical characterization of SpHL-PTX evidenced the formation of nanosized dispersion suitable for intravenous administration. In conclusion, a stable nanosized dispersion of PTX was obtained at pH 7.4 with suitable parameters for intravenous administration. At lower pH conditions, the pH sensitivity of the system was clearly evidenced by changes in the supramolecular organization of DOPE molecules, which is crucial for the delivery of PTX into the cytoplasm of the targeted cells. In this way, the results obtained by different techniques confirm the feasibility of SpHL as a promising tool to PTX delivery in acidic environments, such as tumors.

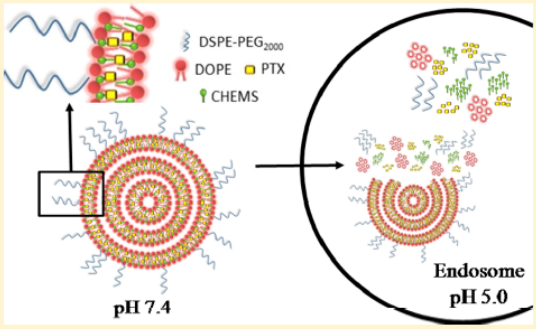

Artigo 2. Publicado no periódico Biomedicine and Pharmacotherapy

MONTEIRO, L. O. F. *et al*. Paclitaxel-loaded folate-coated long circulating and pH-sensitive liposomes as a potential drug delivery system: a biodistrution study. **Biomedicine & Pharmacotherapy,** v. 97, p. 489–495, 2018**.**

Biomedicine & Pharmacotherapy 97 (2018) 489–495

Contents lists available at ScienceDirect

Biomedicine & Pharmacotherapy

journal homepage: www.elsevier.com/locate/biopha

Original article

Paclitaxel-loaded folate-coated long circulating and pH-sensitive liposomes as a potential drug delivery system: A biodistribution study

Liziane O.F. Monteiro[a], Renata S. Fernandes[a], Caroline M.R. Oda[a], Sávia C. Lopes[a], Danyelle M. Townsend[b], Valbert N. Cardoso[c], Mônica C. Oliveira[a], Elaine A. Leite[a], Domenico Rubello[d,*], André L.B. de Barros[c,**]

[a] Department of Pharmaceutical Products, Faculty of Pharmacy, Universidade Federal de Minas Gerais, Belo Horizonte, Minas Gerais, Brazil
[b] Department of Drug Discovery and Pharmaceutical Sciences, Medical University of South Carolina, USA
[c] Department of Clinical and Toxicological Analyses, Faculty of Pharmacy, Universidade Federal de Minas Gerais, Belo Horizonte, Minas Gerais, Brazil
[d] Department of Nuclear Medicine, Santa Maria della Misericordia Hospital, Rovigo, Italy

ARTICLE INFO

Keywords:
Breast cancer
Scintigraphic images
MDA-MB-231 tumor
Paclitaxel
pH-sensitive liposomes
Folate

ABSTRACT

A range of antitumor agents for cancer treatment is available; however, they show low specificity, which often limit their use. Recently, we have reported the preparation of folate-coated long-circulating and pH-sensitive liposomes (SpHL-folate-PTX) loaded with paclitaxel (PTX), an effective drug for the treatment of solid tumors, including breast cancer. The purpose of this study was to prepare and characterize SpHL-PTX and SpHL-folate-PTX radiolabeled with technetium–99 m (^{99m}Tc). Biodistribution studies and scintigraphic images were performed after intravenous administration of ^{99m}Tc-PTX, ^{99m}Tc-SpHL-PTX and ^{99m}Tc-SpHL-folate-PTX into healthy and tumor-bearing mice. High radiochemical purity (> 98%) and *in vitro* stability (> 90%) were achieved for both liposome formulations. The pharmacokinetic properties of ^{99m}Tc-SpHL-DTPA-PTX and ^{99m}Tc-SpHL-folate-DTPA-PTX decreased in a monophasic manner showing half-life of 400.1 and 541.8 min, respectively. Scintigraphic images and biodistribution studies showed a significant uptake in liver, spleen and kidneys, demonstrating these routes as way for excretion. At 8 h post-injection, the liposomal tumor uptake was higher than ^{99m}Tc-PTX. Interesting, 4 h after administration, the liposome folate coated showed higher tumor-to-muscle ratio than ^{99m}Tc-SpHL-DTPA-PTX and ^{99m}Tc-PTX. In conclusion, the liposomal systems, showed high tumor uptake by scintigraphic images, especially the ^{99m}Tc-SpHL-folate-DTPA-PTX that showed a sustained and higher tumor-to-muscle ratio than non-functionalized liposome, which indicate its feasibility as a PTX delivery system to folate positive tumors.

Artigo 3. Publicado no periódico Biomedicine and Pharmacotherapy

MONTEIRO, L. O. F. *et al*. Technetium-99m radiolabeled paclitaxel as an imaging probe for breast cancer in vivo. **Biomedicine & Pharmacotherapy**, v. 89, p. 146-151, 2017.

Biomedicine & Pharmacotherapy 89 (2017) 146–151

Available online at ScienceDirect www.sciencedirect.com

Elsevier Masson France EM|consulte www.em-consulte.com/en

Original article

Technetium-99 m radiolabeled paclitaxel as an imaging probe for breast cancer *in vivo*

Liziane O.F. Monteiro[a], Renata S. Fernandes[a], Luciano C. Castro[a], Valbert N. Cardoso[b], Mônica C. Oliveira[a], Danyelle M. Townsend[c], Alice Ferretti[d], Domenico Rubello[d,*], Elaine A. Leite[a], André L.B. de Barros[b,*]

[a] Department of Pharmaceutical Products, Faculty of Pharmacy, Universidade Federal de Minas Gerais, Belo Horizonte, Minas Gerais, Brazil
[b] Department of Clinical and Toxicological Analyses, Faculty of Pharmacy, Universidade Federal de Minas Gerais, Belo Horizonte, Minas Gerais, Brazil
[c] Department of Drug Discovery and Pharmaceutical Sciences, Medical University of South Carolina, USA
[d] Department of Nuclear Medicine, Molecular Imaging, Radiology, Neuro Radiology, Medical Physics, Clinical Laboratory, Microbiology & Pathology, Santa Maria de la Misericordia Hospital, Rovigo, Italy

ARTICLE INFO

Article history:
Received 31 January 2017
Accepted 3 February 2017

Keywords:
Breast cancer
Scintigraphic images
Biodistribution profile
4T1 tumor
Paclitaxel

ABSTRACT

The high incidence and mortality of breast cancer supports efforts to develop innovative imaging probes to effectively diagnose, evaluate the extent of the tumor, and predict the efficacy of tumor treatments while concurrently and selectively delivering anticancer agents to the cancer tissue. In the present study we described the preparation of technetium–99 m (^{99m}Tc)-labeled paclitaxel (PTX) and evaluated its feasibility as a radiotracer for breast tumors (4T1) in BALB/c mice. Thin Layer Chromatography (TLC) was used to determine the radiochemical purity and *in vitro* stability of ^{99m}Tc-PTX. PTX micelles showed a unimodal distribution with mean diameter of 13.46 ± 0.06 nm. High radiochemical purity (95.8 ± 0.3%) and *in vitro* stability (over than 95%), up to 24 h, were observed. Blood circulation time of ^{99m}Tc-PTX was determined in healthy BALB/c mice. ^{99m}Tc-PTX decays in a one-phase manner with a half-life of 464.3 minutes. Scintigraphic images and biodistribution were evaluated at 4, 8 and 24 h after administration of ^{99m}Tc-PTX in 4T1 tumor-bearing mice. The data showed a significant uptake in the liver, spleen and kidneys, due to the importance of these routes for excretion. Moreover, high tumor uptake was achieved, indicated by high tumor-to-muscle ratios. These findings indicate the usefulness of ^{99m}Tc-PTX as a radiotracer to identify 4T1 tumor in animal models. In addition, ^{99m}Tc-PTX might be used to follow-up treatment protocols in research, being able to provide information about tumor progression after therapy.